

**AN EXPERIMENTAL INVESTIGATION OF AN INDUCTIVELY  
COUPLED DISCHARGE AT LOW PRESSURE**

**A thesis for the degree of  
PHILOSOPHIAE DOCTOR**

**Presented to  
DUBLIN CITY UNIVERSITY**

**By  
BARRY COONAN B.Sc.  
School of Physical Sciences  
DUBLIN CITY UNIVERSITY**

**Research Supervisor: Dr. Michael B. Hopkins**

**External Examiner: Dr. A. Holmes**

**September 1995**

**Declaration**

I hereby certify that this material, which I now submit for assessment on the programme of study leading to the award of Philosophiae Doctor is entirely my own work and has not been taken from the works of others save and to the extent that such work has been cited and acknowledged within the text of my work.

Signed: \_\_\_\_\_  
Barry Coonan

## **Acknowledgements**

I would like to thank everyone who helped during my work in the Plasma Physics lab. I would especially like to thank Dr. Mike Hopkins for his encouragement and advice throughout my postgrad. I would also like to thank Dr. Kevin Mellon for his help during my first year at the lab and to Dr. Will McColl for his advice with the inductively coupled plasma project.

I could not have got as far as I have without the help of the technicians in the department, especially Des Lavell, John Brosnan and Alan Hughes. I would like to thank the secretaries, Marion and Bridie, and everyone in the Plasma lab, Sam, Catherine, Deirdre, Ruth, Audrey, P.J., Jim, Seamus, Kieran and Oliver for the helpful and informative discussions. Thanks to all my fellow postgrads for making my stay in DCU a lot of fun.

Thanks also to Karine for her encouragement. Finally I would especially like to thank my parents and family and friends for all their support for the past four years.

## Contents.

Table of figures	vii
Abstract	x

### Chapter One: Introduction to plasma physics.

1.1 Introduction.	1
1.2 Plasma parameters.	3
1.2.1 Debye Shielding and Debye length.	3
1.2.2 Plasma frequency.	4
1.2.3 Electron and ion temperature.	4
1.2.4 Plasma potential and floating potential.	5
1.3 Collisions.	6
1.3.1 Elastic collisions.	6
1.3.2 Inelastic collisions.	7
1.4 Diagnostic techniques.	9
1.4.1 Radiation emission spectroscopy.	9
1.4.2 Laser diagnostic techniques.	10
1.4.3 Interferometry techniques.	11
1.4.4 Electrostatic probe techniques.	12
1.4.5 Electric and magnetic field measurement.	13
1.5 Plasma modelling.	14
1.6 Outline of proposed research.	15

### Chapter Two: Inductively coupled plasmas.

2.1 Introduction.	20
2.2 Applications and types of ICP.	20
2.3 Electrical characteristics of the ICP: transformer model	22
2.4 Plasma heating of the ICP.	25
2.4.1 Discharge initiation.	26
2.4.2 Ohmic heating.	27
2.4.3 Collisionless heating.	29

2.5 Electron kinetics in the ICP.	34
2.5.1 The distribution function and Boltzmanns equation	34
2.6 Kinetic modelling of the ICP.	38
2.6.1 The local model.	38
2.6.2 Introduction to the non-local model.	41
2.6.3 Non-local model.	41

### **Chapter Three: Plasma diagnostic techniques.**

3.1 Introduction	48
3.2 RF electrical measurements.	48
3.2.1 The power meter.	48
3.2.2 RF voltage probe.	50
3.3.3 RF current probe.	52
3.3 RF parameter measurement.	54
3.3.1 RF power measurement.	54
3.3.2 Determination of the electrical characteristics of the antenna and plasma.	55
3.4 Plasma parameter diagnostics.	56
3.4.1 Magnetic field probe.	56
3.5 The Langmuir probe.	57
3.5.1 Introduction	57
3.5.2 Theory of probe operation.	57
3.5.3 Langmuir probe plasma parameter measurement.	61
3.5.4 EEDF measurement	62
3.5.5 Langmuir probes in RF plasmas.	63
3.5.6 The tuned probe.	65
3.3.9 Probe diagnostic hardware.	68
3.4 Conclusion	69

### **Chapter Four: ICP parameter measurement.**

4.1 Introduction.	72
-------------------	----

4.2 Experimental system.	72
4.4.1 The discharge chamber.	72
4.4.2 RF design considerations and the RF circuit.	74
4.2.3 The antenna.	78
4.3 External electrical measurements.	80
4.3.1 RF voltage and current measurements.	80
4.3.2 Load impedance measurements.	81
4.4 Plasma parameter measurements in Argon: fixed position.	83
4.4.1 Electron and ion density.	83
4.4.2 Plasma potential and electron temperature.	86
4.5 Plasma parameter measurements in Hydrogen: fixed position	87
4.5.1 Electron and ion density measurements.	87
4.5.2 Plasma potential and electron temperature.	89
4.6 Radial measurements in Argon.	95
4.6.1 Electron density measurements.	95
4.6.2 Plasma potential and electron temperature.	95
4.6.3 Radial EEDF measurements.	96
4.7 Conclusions.	96

## **Chapter Five: Experimental investigation of low pressure heating in an ICP.**

5.1 Introduction.	99
5.2 Detection of the electron current in the plasma.	100
5.3 Skin depth measurements.	103
5.4 Plasma resistance measurements.	108
5.5 Discussion and conclusions.	111

## **Chapter Six: Measurements of electron kinetics in an ICP.**

6.1 Introduction.	116
6.2 Results of measurements taken in the background plasma.	119
6.2.1 EEDF measurements.	119

6.2.2 Space-charge potential measurements.	120
6.3 Results of measurements taken in the current (azimuthal) direction.	123
6.3.1 EEDF measurements.	123
6.3.2 Space-charge potential measurements.	126
6.4 Discussion of the local and non-local characteristics observed in the plasma in the azimuthal direction.	126
6.5 Conclusions.	128

## **Chapter Seven: Conclusions and suggestions for future work.**

7.1 Summary of work and conclusions.	131
7.2 Suggestions for future work.	132

## Table of Figures.

1.1 Double probe.	12
1.2 Typical emissive probe characteristic.	12
2.1 ICP semiconductor etch device.	21
2.2 ICP with immersed antenna for negative ion production.	21
2.3 An ICP used as a laser flashlamp.	22
2.4(a) Equivalent circuit of the ICP antenna and plasma.	23
2.4(b) Transformed ICP circuit using circuit analysis.	23
2.5 Azimuthal and longitudinal electric fields.	26
2.6 Development of space-charge and electrostatic field at ends of antenna.	26
2.7 Electron current and skin depth.	31
2.8 Comparison of collisionless and Ohmic surface resistances for a 4eV plasma	33
2.9 Comparison of collisionless and classical skin depths for a 4eV 10mTorr plasma	33
2.10 Volume in phase space, $dx dy dz$ .	34
2.11 Diagram of electric field and velocity orientation.	37
2.12 Sketch of EEDF under local kinetic conditions.	40
2.13 Schematic of space-charge potential.energy profile.	41
2.14 Sketch of EEDF of total energy under non-local kinetic conditions, and potential energy profile.	43
3.1 RF power meter circuit diagram.	49
3.2 RF voltage probe circuit diagram.	51
3.3 RF probe calibration setup.	51
3.4 Rogowski coil and one loop of coil.	52
3.5 Rogowski coil shielding	53
3.6 Magnetic field probe.	56
3.7 Ideal probe characteristic.	58
3.8 Comparison of dc and RF distorted I-V characteristic.	65

3.9 Probe circuit diagram including plasma.	66
3.10 Tuned probe.	67
4.1 ICP experimental setup with antenna.	73
4.2 Effect of RF on current carrying conductor cross-section.	75
4.3(a) Maximum power circuit.	77
4.3(b) RF circuit to be matched.	77
4.3(c) RF circuit with matching unit.	77
4.4(a) RF voltage (rms) measured at antenna at pressures from 1mTorr to 20mTorr	79
4.4(b) RF current (rms) measured at antenna at pressures from 1mTorr to 20mTorr	79
4.5(a) Load resistance measurements (ohms) Antenna resistance is 1.7ohms.	82
4.5(b) Load reactance measurements (ohms). Antenna reactance is 162ohms.	82
4.6 Sheath radii at electron and ion saturation.	83
4.7 Argon electron density measurements.	84
4.8 Argon ion density measurements.	84
4.9 Argon plasma potential measurements (V).	85
4.10 Argon electron temperature measurements (eV).	85
4.11 Ionisation cross-section of Argon and Hydrogen.	87
4.12 Hydrogen electron density measurements.	88
4.13 Hydrogen ion density measurements.	88
4.14 Hydrogen plasma potential measurements.	90
4.15 Hydrogen electron density measurements.	90
4.16 Radial electron density measurements in Argon at 5mTorr, 10mTorr and 20mTorr.	91
4.17 Radial plasma potential measurements in Argon at 5mTorr, 10mTorr and 20mTorr.	92
4.18 Radial electron temperature measurements in Argon at 5mTorr, 10mTorr and 20mTorr.	93
4.19 Radial EEDF measurements in Argon at 5mTorr, 10mTorr and 20mTorr	94

5.1 Disc probe and probe orientations used.	99
5.2 2mTorr 100W directional EEDF scan.	101
5.3 10mTorr 100W directional EEDF scan.	102
5.4 Plot of expected electric field profiles in a 20mTorr plasma.	105
5.5 Magnetic field probe measurements taken over a range of powers at 5mTorr.	105
5.6 Plot of least squares fit to measured data at 75W un a 20mTorr plasma.	106
5.7 Measured skin depths with predicted classical and collisionless values at 5, 10 and 20mTorr.	107
5.8 Argon resistance measurements values with normalised predicted values from collisional theory	109
5.9 Helium resistance values with normalised predicted values from collisional theory	109
5.10 Total collision cross sections of Argon and Helium.	111
6.1 3mTorr 100W EEDF measurements in the longitudinal direction.	117
6.2 10mTorr 100W EEDF measurements taken in the longitudinal direction	117
6.3 Measured and expected space-charge potential profiles at 3mTorr in the longitudinal direction.	118
6.4 Measured and expected space-charge potential profiles at 10mTorr in the longitudinal direction.	118
6.5 3mTorr 100W EEDF measurements in the aazimuthal direction.	124
6.6 10Torr 100W EEDF measurements in the aazimuthal direction.	124
6.7 3mTorr 100W measured and expected space-charge potential measurements.	125
6.8 10mTorr 100W measured and expected space-charge potential measurements.	125

**Abstract.**

Inductively Coupled Plasmas are an important type of radio frequency discharge. The plasma is electrodeless and characterised by high plasma densities at low pressures. The ICP is ideal for semiconductor processing where one requires an isotropic and uniform plasma with a sufficient plasma density at low pressure. The ICP also allows for independent biasing of the substrate being processed.

In this thesis an ICP with an internal antenna is characterised with the basic plasma parameters being measured as a function of input power, pressure and position within the plasma. The diagnostics used include a tuned Langmuir probe, magnetic field probe and RF current and voltage probes. The phenomena of low pressure heating in the discharge is investigated with reference to a collisionless heating mechanism. This heating mechanism is a warm plasma effect, the electrons sample the applied electric field for a time less than one RF cycle, otherwise they gain no net energy. Electron kinetics in the plasma are studied with the investigations based on the local and non-local models of electron kinetics. The local model predicts an electron energy distribution function in equilibrium with the local induced RF field, while the non-local model predicts that there is one EDF of total energy valid across the width of the discharge.

## Chapter 1. Introduction to plasma physics.

### 1.1 Introduction.

At room temperature in any gas there is a non-zero population of ionised particles present given by the Saha equation [1],

$$n(\text{cm}^{-3}) \approx n_a^{1/2} \frac{(2m_e T)^{3/4}}{h^{3/2}} \exp\left(\frac{-U_i}{2T}\right) \quad 1.1$$

where  $n$  is the number of ions or electrons present,  $n_a$  the neutral species population,  $T$  the gas temperature in eV,  $U_i$  is the ionisation potential of the gas in eV and  $h$  is Planck's constant. It is only when the charged particle concentration is such that the long range Coulomb forces restrict the particle motion that one can call the gas a plasma. Ionised gases have been known for over a century and in fact make up more than 99% of the known universe [2]. On earth natural plasmas are quite rare, occurring in the ionosphere and as lightning, as the high temperatures required cannot be readily obtained. These temperatures are found in the sun where energy is released from continuous thermonuclear fusion reactions. The temperatures present are so great that colliding Hydrogen atoms, Deuterium or Tritium, fuse together to form Helium and release large amounts of energy.



It was the possibility of inducing this reaction on earth which caused a resurgence of interest in plasma physics in the 1950's. Two methods were attempted to achieve nuclear fusion: laser heating of a deuterium and tritium pellet causing it to implode and fusion to occur, and secondly magnetically confining a dense plasma in a tokamak device at a sufficiently high temperature to allow fusion to occur [3,4]. Both technologies are still being developed.

Since the revival of interest in plasma physics, the field has expanded greatly to influence many areas of modern technology and has great potential in the future [5]. Computer chip manufacture has been revolutionised since plasma processing was introduced with smaller, cheaper and more powerful components being manufactured [6].

Film deposition, from thin film deposition used in magnetic recording disks to anti-corrosion coatings for machine parts, are now plasma based technologies [7,8]. In the areas of lighting and electronic displays, plasmas are likely to have an increasingly important role [9,10].

Coupled with the wide variety of plasma applications are the number of different types of discharge source [11]. Fluorescent and neon lamps are examples of dc discharges, (although they operate at 50Hz) where the discharge is sustained by the electrostatic field between two electrodes present in the discharge tube. The main radiation output occurs in the positive column of both discharges [9]. Filament driven discharges are plasma sources which are powered by electrons emitted and accelerated from a heated filament. The filament is usually biased negatively with respect to the discharge chamber to encourage electron flow from the filament to the plasma [12]. Plasmas can also be produced by applying high frequency electric fields. Using high frequency electric fields one can produce electrodeless discharges which can be cleaner and more reliable than plasmas where the powering electrodes are subject to particle bombardment by the plasma. High frequency sources include the ICP source used in this project, RF capacitive discharges [13] and microwave produced plasmas [14].

Considering the breakthroughs in plasma based manufacturing techniques, it is surprising to note the limited knowledge of some basic plasma phenomena and plasma chemistry. Plasma surface interactions, low pressure discharge heating and negative ion generation are just some important areas of plasma physics not fully understood. In order to increase our knowledge of plasma behaviour numerous diagnostic techniques have been developed [15-17]. Each technique allows one or more plasma parameters to be measured. The techniques range from microwave interferometry and plasma emission spectroscopy to laser plasma interaction and electrostatic probes. A brief review of some diagnostic techniques is given in section 1.4.

Computer modelling of plasmas has become increasingly important in recent years. Faster computers and workstations allow the complex behaviour of plasmas to be analyzed. Results from computer models can be compared with results found on real plasmas and sometimes interesting plasma phenomena are found firstly in computer models and then confirmed in experimental work. There are several categories of modelling popular today dealing with microscopic and macroscopic discharge behaviour.

These techniques are introduced in section 1.5.

An important aspect of plasma physics which dominates plasma behaviour is interparticle collisions. There are two main classes of collisions; elastic and inelastic collisions. Ionisation collisions are important inelastic collisions which are needed to initiate a plasma in the first place, and in order to sustain a plasma the ionisation rate must balance ion losses. A brief survey of plasma collisions is presented in section 1.3. The basic characteristics associated with plasmas, such as the plasma potential, are detailed in section 1.2.

## 1.2 Plasma parameters.

Plasma parameters are attributes of plasmas which allow the particular discharge to be analyzed and compared with other plasmas. These characteristics arise from the basic nature of the plasma, it is a collection of interacting charged and uncharged particles. It is assumed that there are equal numbers of positively charged and negatively charged particles in the plasma; it is said to be quasi-neutral. Due to the quasi-neutrality of the system the plasma is also assumed to be field free. The most basic plasma parameters is the electron and ion density since it is the presence of these particles which defines the plasma state.

### 1.2.1 Debye shielding and Debye length.

When a charged conductor is placed into a plasma it attracts oppositely charged particles and repels like charged particles. Thus a region of oppositely charged particles develops around the conductor which prevents the conductor electric field penetrating into the quasi-neutral plasma. This phenomena is known as Debye shielding and the depth of the charge imbalance around the conductor is known as a Debye length. The Debye length is calculated from a solution of Poissons equation,

$$\nabla^2\phi = -\frac{e}{\epsilon_0}(n_i - n_e) \quad 1.3$$

and is related to electron temperature and density,

$$\lambda_d = \left[ \frac{\epsilon_0 k T_e}{e^2 n_e} \right]^{1/2} \quad 1.4$$

One description of the plasma, called the plasma approximation, demands that the number of charged particles within a Debye sphere (a sphere one Debye length in radius) must be much greater than one. Also to preserve the quasi-neutrality property of the plasma, the plasma size must be much greater than the Debye sphere.

### 1.2.2 Plasma frequency.

The plasma is made up of interacting charged particles which are moving around at thermal velocities when not subject to external forces. When a force is applied or the plasma is perturbed in some way the plasma tries to compensate and preserve quasi-neutral and field free conditions. The time scale at which the plasma can react to these changes is related to the plasma frequency. Consider a plasma in equilibrium with all particles having zero kinetic energy. If an electron is displaced from its position it will immediately try to regain it. When the electron reaches its original location it has a finite velocity and continues past this position until its kinetic energy goes to zero. Thus in the absence of damping forces the electron oscillates about this position. The frequency of this oscillation is related to the plasma frequency,  $\omega_p$ , and is given by,

$$\omega_p = \left( \frac{ne^2}{\epsilon_0 m_e} \right)^{1/2} s^{-1} \quad 1.5$$

where  $n$  is the electron or ion density and  $m_e$  the electron or ion mass. As the ion mass is usually much greater than the electron mass, the electron plasma frequency is much greater than the ion frequency and it is usually the electron frequency which is quoted for a particular plasma.

### 1.2.3 Electron and ion temperature.

As stated above extremely high temperatures are required to initiate, and in the case of non-equilibrium (such as laboratory plasmas), to sustain a plasma. Average electron temperatures can be higher than 20,000K but because the thermal conductivity

of the electrons is so low, plasmas can be sustained in metal discharge chambers without melting the chamber walls. The electron temperature is related to the electron energy,  $E_e$ , and speed,  $u$ , by,

$$E_e = \frac{1}{2} m_e \bar{u}_e^2 = \frac{3}{2} k T_e \quad 1.6$$

where  $T_e$  the electron temperature. For convenience the electron temperature is usually stated in terms of electron volts, one electron volt being approximately 11,600K. This temperature can be used to characterise the velocity or energy distribution of electrons in a plasma. The electrons in a plasma in thermodynamic equilibrium, for example, can be described by a Maxwellian distribution at an average electron temperature,  $T_e$ ,

$$f(u) = n_e \left( \frac{m_e}{2\pi k T_e} \right)^{3/2} \exp \left[ \frac{-m_e u^2}{2k T_e} \right] \quad 1.7$$

where  $v$  is the electron speed. Equation 1.7 may also be used to represent the ions in a plasma where the electron temperature and mass is replaced by the ion temperature and mass.

The energies of individual particles can change when collisions occur; in inelastic collisions between ions and electrons, ions generally gain energy at the expense of electrons (superelastic collisions are an exception to this where an excited atom and electron collide, the atom de-excites and the electron gains energy). The particle temperatures can vary from region to region in the plasma itself. There may be more high energy electrons near the electrodes of an RF discharge than in the bulk plasma, due to the presence of high electric fields. This feature is particularly obvious in measurements taken in this project, near the powering antenna (chapter 5).

#### 1.2.4 Plasma potential and floating potential.

From the discussion above a detailed description of the plasma is emerging. It is a field free quasi-neutral collection of particles moving randomly at velocities determined by their individual temperatures and masses,

$$u_{thermal} = \left( \frac{8kT}{\pi m} \right)^{1/2} \quad 1.8$$

One might expect that the electrons, with their much greater thermal velocities, would leave the plasma and migrate to the discharge walls leaving ions and neutrals behind. In fact initially this is what happens. As the electrons move away from the centre of the discharge they leave an excess ion population behind. Thus a positive space charge develops which begins to retard the electron losses. A steady state is reached when the space charge is such that the numbers of electrons and positive ions leaving the plasma are equal. The potential of the bulk plasma is now known as the plasma potential. The plasma potential, which is related to electron and ion temperature and density, can give an insight into the dynamics of the plasma.

When an isolated conductor is placed in a plasma it is subject to the random flux of particles in the plasma. As the electron flux dominates other particle fluxes, electrons are more likely to reach the conductor surface and so they charge the conductor negatively. As the conductor begins to charge negatively it starts to retard the electron flux to its surface and attract positive species. A point is soon reached when the retarded electron flux and the attracted positive ion flux to the conductor surface are equal. The potential at which the conductor now sits is known as the floating potential.

### **1.3 Collisions.**

As stated previously, there are two main categories of collisions occurring in plasmas, that is elastic and inelastic collisions. In the former the internal energies of the colliding particles do not change, but in the latter internal energies do change. A knowledge of both is required to gain a fuller understanding of discharge physics. Elastic collisions effect the conductivity, mobility, diffusion coefficients and the shape of the EEDF (electron energy distribution function). Inelastic collisions are important as they dictate the electron and ion populations, electron temperatures and even radiation output.

#### **1.3.1 Elastic collisions.**

Elastic collisions can occur between all types of particles and at all particle energies. The maximum energy transfer in an elastic collision between an electron and

neutral particle in a plasma is given by,

$$\Delta E = 2 \frac{m_e}{M_n} E_{electron} \quad 1.9$$

where  $E_{electron}$  is the kinetic energy of the colliding electron and  $M_n$  is the mass of the neutral particle. The quantity  $2m_e/M_n$  is known as the momentum transfer coefficient. Since the electron mass is much less than the neutral particle mass, the energy transfer resulting from such a collision is small.

For charged particle collisions, such as electron-ion collisions, the effect of the particle electric fields becomes important. These collisions are known as Coulomb collisions and they have more and more influence on discharge characteristics as the degree of ionization increases. The effect of the Coulomb collisions between electrons is to thermalize the electron energy distribution function i.e. the energy distribution function becomes more like a Maxwellian distribution characterised by one unique temperature as the rate of electron-electron collisions increases.

### 1.3.2 Inelastic collisions.

Inelastic collisions can only occur between plasma particles if the energy transferred is sufficient to excite the electrons of one of the colliding particle i.e. to change the internal energy of the particle. Depending on the amount of energy transferred the inelastic collisions can take several forms and for every collision type there is a possible reverse process. From the conservation of energy principle in an inelastic collision one can write,

$$\frac{1}{2}m_1v_1 + \frac{1}{2}m_2v_2 = \frac{1}{2}m_1u_1 + \frac{1}{2}m_2u_2 + \Delta E \quad 1.10$$

where  $v_{1,2}$  and  $u_{1,2}$  represent the initial and final velocities of the colliding particles and  $\Delta E$  the net change in the internal particle energy as a result of the collision. If  $\Delta E > 0$  the collision is known as a collision of the first kind and when  $\Delta E < 0$  the collision is known as a collision of the second kind. An excitation collision is an example of a collision of the first kind, whereas a de-excitation collision is an example of a collision of the second kind.

Excitation, ionisation and recombination are three main inelastic collisions

involving electrons and neutral atoms, but collisions can of course occur between atoms, molecules and ions. Fifteen reactions are quoted by Cherrington [18], but there are more. Only the most common inelastic collision types will be described here.

Ionisation.  $X + e \rightarrow X^+ + 2e$

This reaction can only occur when the electron energy is greater than the energy required to remove the most loosely bound electron from the atom (the ionisation energy). This differs from gas to gas, but for Argon the threshold energy for ionisation collisions is approximately 15.7eV. The electron released in the reaction can itself, if it gains sufficient energy from the powering electric field, cause further ionisation reactions. In order to sustain any plasma the charged particle losses must be balanced by gains due to ionisation. Ionisation can also occur if the atom is subject to photon of energy greater than the ionisation energy. This process is known as photoionisation.

Excitation.  $X + e \rightarrow X^* + e$

Excitation can occur at lower energies than ionisation; in Argon the threshold energy is approximately 11.5eV. It involves the raising of the internal energy of the atom to an excited state, denoted by  $X^*$ . An electron is promoted to a higher level within the atom corresponding to the energy absorbed by the atom. An excited atom can be more easily ionised than a ground state atom due to its increased internal energy. A metastable state is formed if the internal electron is promoted to a level where a transition back to a ground state is unlikely. The metastables can have lifetimes of over 1mS and therefore are more likely to undergo a subsequent collision, either being ionised or further excited for example, before they undergo radiative relaxation back to their ground state.

Recombination.  $X^+ + A + e \rightarrow X + A$

This collision process is basically the reverse process to ionisation. Due to energy and momentum conservation requirements it is a three body process. The third body, A, can be a gas atom, electron or even chamber wall. The process can also occur when a positive and negative ion collide and an electron is exchanged resulting in two neutral atoms. A third possible process occurs when an electron and ion combine and the excess energy is released as a photon. This type of collision reaction is known as radiative

recombination.

Relaxation.  $X^* \rightarrow X + h\nu$

This process is a reverse of the excitation collision described above. The energy released in this collision is equal to the internal energy lost by the atom. It is this reaction which is the main contribution to the discharge glow. The frequency of the emission is dependent on the energy level of the excited electron and its original position.

Other collision processes.

Dissociation is a collision process confined to molecules where the energy of the colliding electron is sufficient to break the inter-atom bond. The result is two atomic species which can be both neutral, or in the case of dissociative ionisation, can be charged.

Electron attachment collisions where negative ions are formed, are important processes for some applications, such as neutral beam injection for fusion plasma heating [19,20]. For this application a density of negative hydrogen or deuterium atoms are required. For the reaction to occur more easily the hydrogen or deuterium molecule should be in an excited state and an electron can attach itself in a process known as dissociative attachment.



## 1.4 Diagnostic techniques.

In order to investigate the behaviour of any discharge one needs to determine the basic plasma parameters described in section 1.2. There are a wide variety of techniques developed to determine plasma characteristics, some specifically designed to measure a single plasma parameter while others can be used to measure several. Some common techniques are discussed in this section.

### 1.4.1 Radiation emission spectroscopy.

This is a broad field of diagnostic techniques where the electromagnetic radiation emitted by the discharge is observed. The technique is useful in reactive plasmas, very dense plasmas (such as fusion plasmas) and weak plasmas as it is non-intrusive; the

discharge being investigated is unperturbed. It can be divided into the broad areas of optical, ultraviolet and X-ray spectroscopy [21-23]. Spectroscopy involves the study of the radiation output by the plasma which usually results from particle de-excitation and recombination processes (X-ray radiation can occur when electrons undergo rapid de-acceleration i.e. when they are scattered by large charged particles; Bremsstrahlung radiation). The frequency of light output is dependent on the electronic transition made in the atom or molecule and using a monochromator one can target the process of interest to investigate its behaviour under different conditions.

Stark broadening of spectral emission lines is a method used to determine electron concentrations in plasmas [16]. Broadening of the spectral lines can occur when photons from emitting ions are in collision with electrons, thus disturbing the wavelength of the emitted radiation. The greater the number of electrons present the more collisions there will be resulting in an increased broadening of the spectral output.

Doppler broadening can also occur to spectral emissions from discharges [16]. This results from the random motion of the radiating particle in the plasma. If the particle is moving away from the observer the frequency of the radiation will be slightly lower, and if it is moving towards the observer the opposite case holds. This effect is most evident at high plasma temperatures where particle velocities are high.

#### **1.4.2 Laser diagnostic techniques.**

Lasers have proven an important plasma diagnostic and there are several techniques based on the interaction of a laser beam and plasma. Photodetachment is used to measure negative ion populations, especially important in neutral beam generation sources which require efficient negative hydrogen ion generation [24,25]. The principle of operation is very simple. A laser beam is fired into the plasma and along the axis of a positively biased electrostatic probe placed in the discharge. If the photon energy is sufficient ( $> .75\text{eV}$ , the electron affinity of a Hydrogen negative ion), the electron leaves the Hydrogen negative ion and is detected by the probe. Thus the excess electron current detected by the probe will be due to photodetachment of negative ions. To insure correct operation of the system the laser beam intensity should be strong enough so that all negative Hydrogen ions in the laser path lose their electrons and the photon energy is low enough so that photoionisation does not occur. The relation between negative ion density

$n_e$  and probe current during the laser pulse,  $I_e + \Delta I_e$  is then,

$$n_e = n_e \frac{\Delta I_e}{I_e} \quad 1.12$$

Laser induced fluorescence is a useful method in determining particular particle concentrations in plasmas [26,27]. The electronic state of the species of interest is deliberately changed by the input laser pulse and the resulting relaxation of the particle causes it to produce its own radiation; it fluoresces. The intensity of this emitted radiation at an angle to the laser pulse is related to the particle density in the path of the laser beam.

### 1.4.3 Interferometry techniques.

Microwave and optical interferometry are used for electron concentration measurements in plasmas and are based on the measurement of the refractive index of the discharge [13,28],

$$\mu = 1 - \left( \frac{\omega_p^2}{\omega^2} \right) \quad 1.13$$

where  $\omega_p$  is the plasma frequency and  $\omega$  the frequency of the microwave or optical beam (this assumes the microwave frequency,  $\omega$ , is much greater than the electron neutral collision frequency,  $\nu_m$ ). In microwave interferometry a microwave beam is split into two equal path lengths, one beam is sent through the discharge region, then the two are recombined and the phase difference measured. This phase difference,  $\Delta\phi$ , is related to the average electron density along the microwave beam path by,

$$\frac{1}{n_e} = \frac{2\epsilon_0 m_e c \omega \Delta\phi}{e^2 L} \quad 1.14$$

where  $L$  is the length of the beam path through the plasma. The microwaves cannot pass through the discharge if the electron density is too large, as the plasma frequency becomes greater than the microwave frequency and refractive index becomes less than zero,

$$\left( \frac{n_e e^2}{\epsilon_0 m_e} \right)^{\frac{1}{2}} > \omega$$

1.15

where the right hand side of equation 1.15 is the plasma frequency. A similar procedure is followed is optical interferometry.

#### 1.4.4 Electrostatic probe techniques.

Almost all the above techniques are non-intrusive (laser photodetachment requires an electrostatic probe to be positioned within the discharge). Electrostatic probes on the other hand require the presence of a conductor in the plasma region. If care is not taken the plasma can be perturbed, but these probe techniques can allow measurement of local discharge conditions. The Langmuir probe, described in detail in section 3.5, is a common diagnostic technique which can allow measurement of many local plasma parameters. There are variations on the basic Langmuir probe, such as the double probe and emissive probe. The double probe can be used when a reference electrode, like a metallic chamber wall, is not available (figure 1.1) [29]. This can occur in glass walled toroidal RF discharges for example. It consists of two probes which can have a bias placed on them

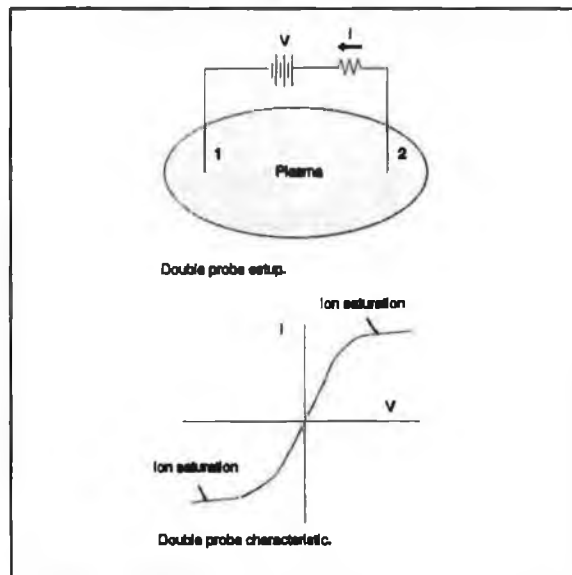


Figure 1.1. Double probe.

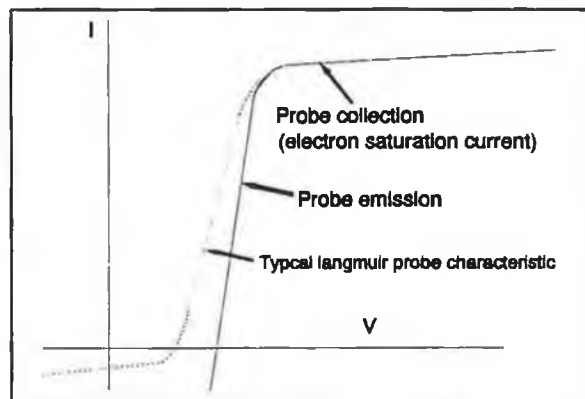


Figure 1.2. Typical emissive probe characteristic.

with respect to each other,

$$V = V_1 - V_2 \quad 1.16$$

If the voltage on both probes is equal then no current is collected by the circuit and both probes sit at the floating potential. If a bias is then placed between the two, the more positive probe will begin to draw more electrons and the more negative probe collects less electrons. If the potential between the probes is large enough the negative probe will collect no electrons but just the ion saturation current and the probe characteristic will saturate. From double probe measurements ion density and electron temperature can be calculated.

The emissive probe is a heated probe biased with respect to the plasma and hot enough to thermionically emit electrons [30]. When the probe is biased below the plasma potential the probe emits electrons, but when the bias is raised above the plasma potential the probe collects a saturation current of plasma electrons. The transition between the emission and collection regime occurs at the plasma potential (figure 1.2).

#### **1.4.5 Electric and magnetic field measurement.**

In many discharges a knowledge of the electromagnetic fields in the discharge can provide evidence for the plasma heating mechanism and give clues to plasma kinetics. Plasma sheath heating is considered an important heating mechanism in capacitive low pressure discharges and information on sheath potentials is desirable. In ICPs details of the penetration of the electromagnetic fields from the antenna is required for a fuller understanding of the discharge operation. The magnetic field probe [2,31], described in section 3.4, is used in this project to investigate the relation between field penetration in the discharge and the plasma discharge conditions. This field penetration is described by skin depth theory which can have a different form depending on the ratio of collision frequency to RF driving frequency in the discharge i.e. the gas pressure conditions (chapter 5). There are several methods used to determine the electric field in plasmas such as electron beam probe techniques [32,33]. Electron beam techniques involve firing an electron beam through the region of interest and recording the beam deflection which is related to the electric field present.

## 1.5 Plasma modelling.

Plasma modelling techniques have become more sophisticated in recent years with the advent of faster and more powerful computers [34,35]. Plasma models are very important in the development of an understanding of basic discharge behaviour. The simulations can be used to verify behaviour observed experimentally and also new phenomena can be found from modelling results leading to experiments to verify these findings. As the actual plasma is made up of large numbers of particles it is not possible to follow the actions of individual particles. Therefore simplifications and assumptions about certain aspects of the discharge are often made. Some models deal with average discharge characteristics while others make assumptions about discharge parameters, such as assuming Maxwellian velocity distributions.

In global or volume averaged models the energy and particle balance equations are solved for a particular plasma [36]. The energy and particle balance equations involve equating power absorbed by the plasma with the power used in collision processes and in losses to discharge walls. From the model one can predict particle densities and temperatures for different input powers, pressures and gas types.

The fluid model employs continuity and momentum conservation equations to calculate the behaviour of plasma particles [37]. The discharge is considered to be a conducting fluid of electrons and ions, thus avoiding the need to calculate the behaviour of individual particles. This model can be used to calculate plasma parameters, such as particle densities, temperatures and plasma potential.

Particle in cell Monte Carlo models provide information on particle kinetics by following individual particles which represent electrons, ions or neutrals [38,39]. This is achieved by integrating the equations of motion of the individual particles and solving Poissons equation for the resulting assembly on a mesh representing the discharge space. The model includes a Monte Carlo treatment of inter-particle collisions. The calculations, solving the equations of motion and then solving Poissons equation, is repeated many times until consistent results are obtained. This technique provides information on plasma parameters such as electron temperatures, densities and electron energy distribution functions.

Kinetic models are based on solving Boltzmanns equation for the plasma of interest [40]. The electric field in the plasma is calculated using Poissons equation. From

a solution of the Boltzmann equation one can obtain the particle velocity distribution function, which gives information on various process rates in the discharge such as ionisation and excitation rates, as well as average plasma parameters such as average velocities and particle temperatures.

Circuit models such as the transformer model described in section 2.3 employ an electrical circuit to approximate the discharge [41]. The discharge in an ICP can be treated as a one turn secondary of a transformer, the primary being the antenna. The procedure is straightforward and allows one to gain an insight into the electromagnetic interaction between the plasma and power source. In this project the transformer model predicted a drop in load inductance when the plasma is fired, an effect which was measured experimentally.

### **1.6 Outline of proposed research.**

The low pressure ICP, the operation of which is being investigated in this project, is a relatively new technology in the semiconductor industry. It is likely to become important over existing technologies in the field of semiconductor processing as it holds advantages over current systems. It can produce high plasma densities efficiently ( $> 10^{11}\text{cm}^{-3}$ ), at low pressures with relatively low plasma potentials. It also allows independent biasing of substrates which can allow control of etch rates etc. There are some areas of the discharge physics still not fully understood such as the low pressure heating mechanism.

As the ICP can obviously be operated at low pressures ( $< 10\text{mTorr}$ ), a low pressure heating mechanism must exist. A heating process was proposed by Turner [42] and this was a motivation for an experimental investigation of the subject. Using directional langmuir probes, magnetic field probes and resistance measurements a survey of low pressure heating was carried out and the results presented in chapter 5.

An in-depth characterisation of the system was carried out and the results presented in chapter 4. Radial and fixed position measurements were taken at various powers and pressures. The principle characteristics of the ICP were recorded, the high charged particle densities and low plasma potentials. Using RF current and voltage probes the electrical characteristics of the discharge were also investigated. The switch between a capacitively and inductively dominated heating mechanism, which occurs at

low power and pressure, was clearly noted.

The electron kinetics in the ICP were studied and the results presented in chapter 6. Characteristics expected for a low pressure discharge, non-local kinetics, were found but evidence for the presence of local kinetic effects were also noted. The reason for these results is open to interpretation and one proposed explanation is also given in this chapter.

An overall discussion and conclusion of results from this project are made in chapter 7. There is still much research to be carried out in this field and some proposed areas for continued research are pointed out.

## References.

- [1] Golant, Zhilinsky, Sakharov and Brown, *Fundamentals of plasma physics*, Wiley (1990).
- [2] N. A. Krall and A. W. Trivelpiece, *Principles of plasma physics*. McGraw-Hill (1973).
- [3] T. Kammash, *Fusion reactor physics: principles and technology*. Ann-Arbour Science, Michigan USA (1975)
- [4] J. J. Duderstadt and G. A. Moses, *Inertial confinement Fusion*. Wiley (1982)
- [5] J. L. Shohet. IEEE Trans. Plasma Sci. **19** (1991) 725.
- [6] B. Graves. IEEE Trans. Plasma. Sci. **22** (1994) 31.
- [7] H. Ehrich, B. Hasse, M. Mausbach and K. G. Muller. IEEE Trans. Plasma Sci. **18** (1990) 895.
- [8] E. Lugscheider and T. Weber. IEEE Trans. Plasma Sci. **18** (1990) 991.
- [9] J. T. Dakin. IEEE Trans. Plasma Sci. **19** (1991) 991.
- [10] A. Sobel. IEEE Trans. Plasma Sci. **19** (1991) 1032.
- [11] F. F. Chen. IEEE Trans. Plasma Sci. **23** (1995) 20.
- [12] K. N. Mellon. PhD. Thesis. Dublin City University, 1993.
- [13] R. A. Doyle. PhD. Thesis. Dublin City University, 1994.
- [14] G. Ciavola, S. Gammino, G. Raia and J. Sura. Rev. Sci. Instrum. **65** (1994) 1110.
- [15] P. E. Stott. Rep. Prog. Phys. **55** (1992) 1715.
- [16] R. H. Huddlestone and S. L. Leonard, *Plasma diagnostic techniques*. Academic Press, New York. (1965)
- [17] I. H. Hutchinson, *Principles of plasma diagnostics*. Cambridge Press.
- [18] B. E. Cherrington, *Gaseous Electronics and Gas Lasers*. Pergamon Press, (1979)
- [19] J. M. Wadehra. Appl. Phys. Lett. **35** (1979) 917.
- [20] J. R. Hiskes, A. M. Karo, M. Bacal, A. M. Bruneteau and W. G. Graham. J.

Appl. Phys **53** (1982) 3469.

[21] A. T. Young, P. Chen, K. N. Leung, L. Pan, D. Ponce and G. C. Stutzin. Rev. Sci. Instr. **65** (1994) 1416.

[22] R. Flohr and A. Piel. Phys. Rev. Lett. **70** (1993) 1108.

[23] F. Tochikubo and T. Makabe. Meas. Sci. Technol. **2** (1991) 1133.

[24] K. N. Mellon, B. P. Coonan and M. B. Hopkins. J. Phys. D: Appl. Phys. **27** (1994) 2480.

[25] M. Bacal and G. W. Hamilton. Phys. Rev. Lett. **42** (1979) 1538.

[26] A. Brockhaus, Y. Yuan and J. Engemann. J. Vac. Sci. Technol. A. **13** (1995) 400.

[27] S. W. Reeve and W. A. Weimer. J. Vac. Sci. Technol. A. **13** (1995) 359.

[28] L. J. Overset and M. B. Hopkins. J. Appl. Phys. **74** (1993) 4323.

[29] E. O. Johnson and E. Malter. Phys. Rev. **80** (1950) 58.

[30] E. Mravlag and P. Krumm. Rev. Sci. Instrum. **61** (1990) 2164.

[31] J. Hopwood, C. R. Guarnieri, S. J. Whitehair and J. J. Cuomo. J. Vac. Sci. Technol. A. **11** (1993) 147.

[32] R. P. Stein. Phys. Rev. **89** (1953) 134.

[33] R. Warren. Phys. Rev. **98** (1995) 1650.

[34] A. T. Drobot, *Computer Applications in Plasma Science and Engineering*. Springer-Verlag, New York, (1991).

[35] G. G. Lister. J. Phys. D. Appl. Phys. **25** (1992) 1649.

[36] C. Lee and M. A. Lieberman. J. Vac. Sci. Technol. A. **13** (1995) 368.

[37] R. A. Stewart, P. Vitello and D. B. Graves. J. Vac. Sci. Technol. B. **12** (1994) 478.

[38] C. K. Birdsall. IEEE Trans. Plasma. Sci. **19** (1991) 65.

[39] M. J. Kushner. J. Appl. Phys. **54** (1983) 4958.

[40] W. Nicholas, G. Hitchon, T. J. Sommerer and J. E. Lawler. IEEE Trans. Plasma.

Sci. **19** (1991) 113.

[41] R. B. Piejak, V. A. Godyak and B. M. Alexandrovich. Plasma Sources Sci. Technol. **1** (1992) 179.

[42] M. M. Turner. Phys. Rev. Lett. **71** (1993) 1844.

## **Chapter 2 : Inductively Coupled Plasmas.**

### **2.1 Introduction.**

The ICP is a type of electrodeless discharge; a discharge which is not in physical contact with the source of the powering electric field. Electrodeless discharges were first demonstrated in 1884 by Hittorf [1]. It was Babat in the 1940's who distinguished between inductive and capacitive electrodeless discharges which he classed as being H-type and E-type discharges respectively [2].

In the E-type discharge the conduction current of electrons and ions is not closed and the plasma is excited by an applied electrostatic field. Most of the applied voltage drop occurs near the electrodes resulting in a high sheath voltages.

The H-type discharge is excited by an applied radiofrequency (RF) electric field and the conduction current in the plasma is closed. The resulting sheath voltages are low, of the order of the mean energy of electrons (as with a dc plasma) [3]. The high electrostatic fields present in the capacitive discharge are not present in the ICP which results in lower ion energies and therefore reduced ion losses to the walls as compared to a capacitive discharge. Lower ion losses means that the ICP can efficiently provide a high density discharge for a given energy input.

### **2.2 Applications and types of ICP.**

The ICP has found uses in many areas of technology in recent years and particular applications can rely on specific configurations of the basic ICP [4].

Microchip manufacture is based on semiconductor etching and film deposition. Plasmas have been found to be more advantageous than previously used wet chemical techniques. Features as small as  $.25\mu\text{m}$  can now be etched meaning that more components can be fitted into smaller areas resulting in faster and cheaper microchips [5].

The ICP displays characteristics ideal for semiconductor processing [6-11]. The high plasma densities achievable mean high ion fluxes to surfaces and therefore increased etching or deposition. The substrate can be biased allowing the etch and deposition rates to be controlled independently of the discharge power, unlike the capacitive discharge where the etch and deposition rates are related to the input power. The biasing of the

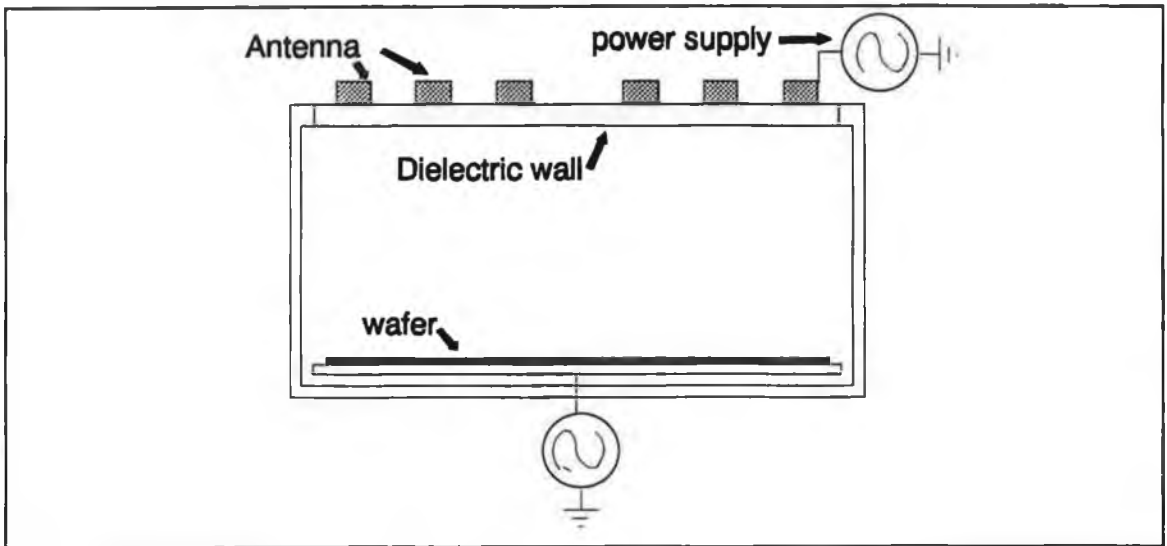


Figure 2.1: ICP semiconductor etch device.

semiconductor wafer can reduce substrate damage due to energetic ions compared with capacitive reactors. The ICP is also easily scaled up to high discharge diameters allowing larger wafers to be processed [12].

Neutral beam sources for the heating of future fusion plasmas require high density H or D beams with low impurity fraction (.2%). An ICP can be used to produce the positive or negative ion density required [13-15]. This prototype of ICP is powered using an external antenna or an insulated antenna immersed in the discharge as shown in figure 2.2. The ICP is operated at powers of tens of kilowatts and typical extracted beams are

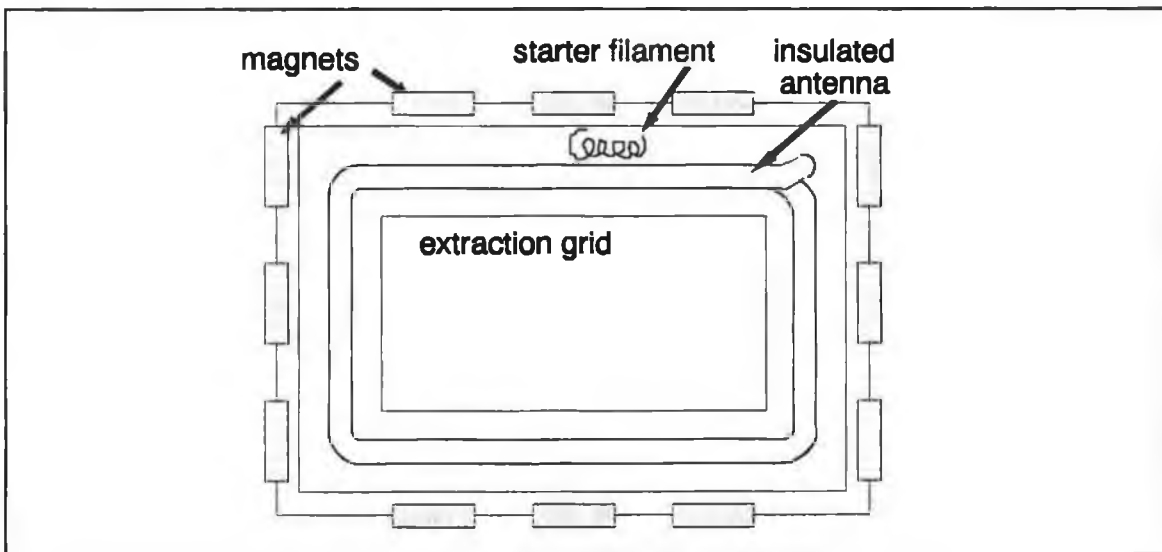


Figure 2.2: ICP with immersed antenna for H/D<sup>+</sup> production.

up to  $250\text{mA}/\text{cm}^2$  over  $100\text{cm}^2$ . This system is easy to use, reliable, clean and has potentially a much longer lifetime compared with filament driven negative ion sources.

ICP's have considerable potential in the area of lighting for the reasons stated above and also the fact that the resulting discharge is efficient and intense with high light output [16,17]. A recent innovation is the use of an inductively powered flashlamp to pump a laser crystal (Figure 2.3). The flashlamp can completely surround the laser crystal thus improving the flashlamp efficiency.

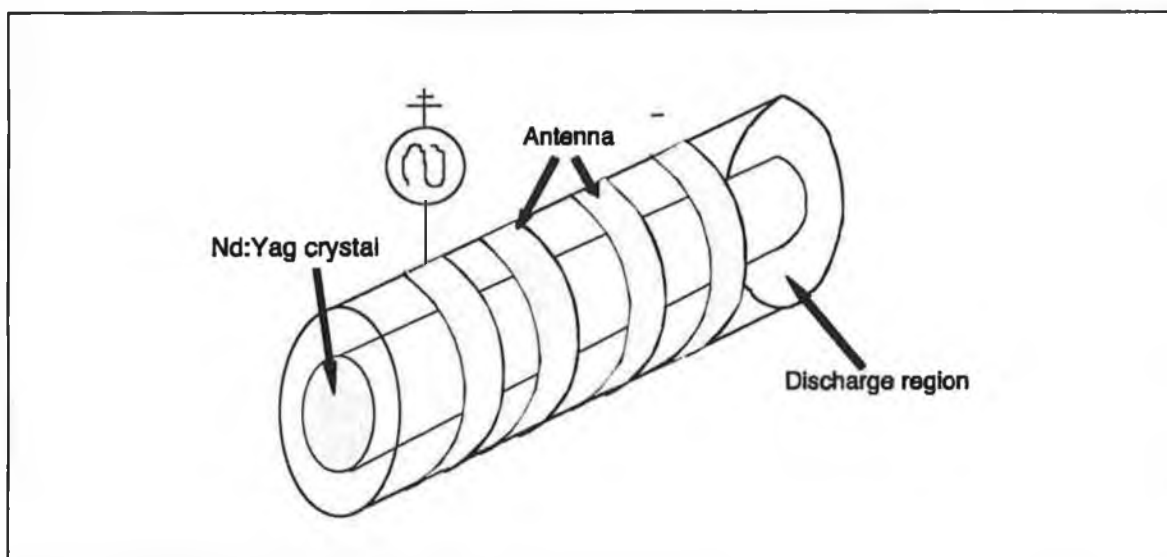


Figure 2.3: An ICP used as a laser flashlamp.

Plasma torches are ICP with an antenna surrounding a quartz tube through which a gas flows. Although there have been considerable advances in plasma torch technology recently, the process itself is not well understood. They have many varied applications including anticorrosion deposition and welding [18].

### 2.3 Electrical characteristics of the ICP - The Transformer model.

One approach to studying the behaviour of the ICP is to look at its electrical characteristics. This can be done by viewing the system as a simple RF circuit, the discharge itself becoming part of the circuit. The transformer model is a useful method of analysing the ICP electrically. The model approximates the antenna and plasma to be a transformer [4,19]. The antenna is the primary and the plasma a one turn secondary (the antenna induces an electric field in the plasma which drives a closed current in the

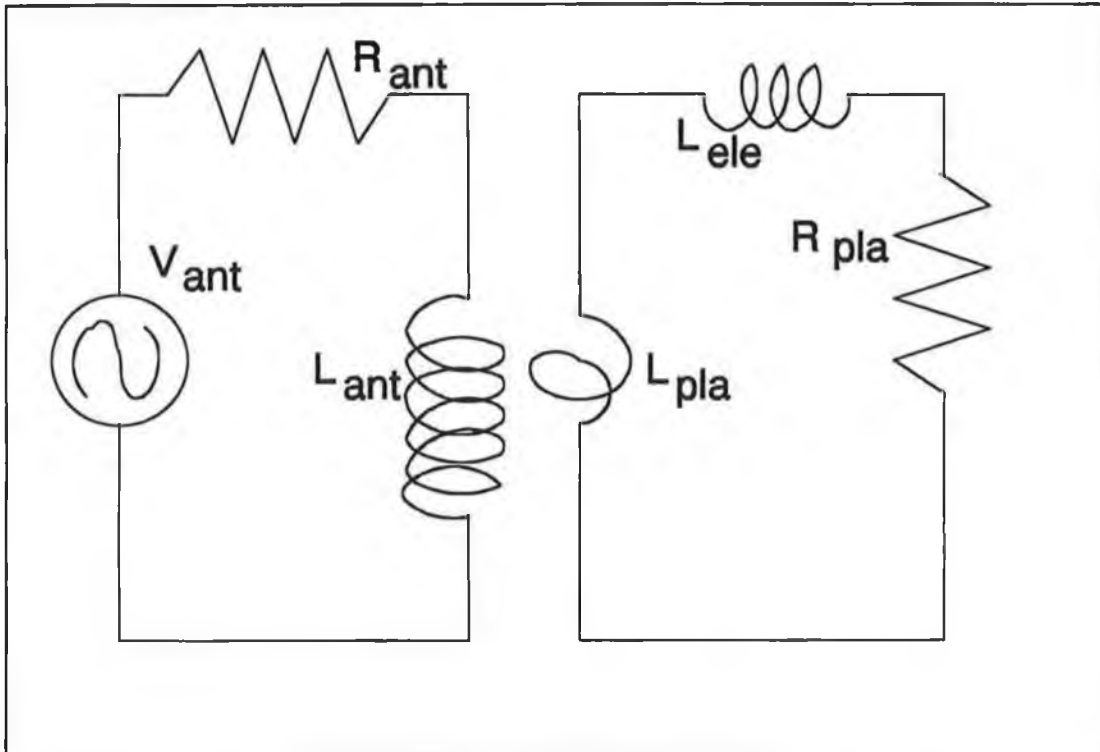


Figure 2.4(a): Equivalent circuit of the ICP antenna and plasma.

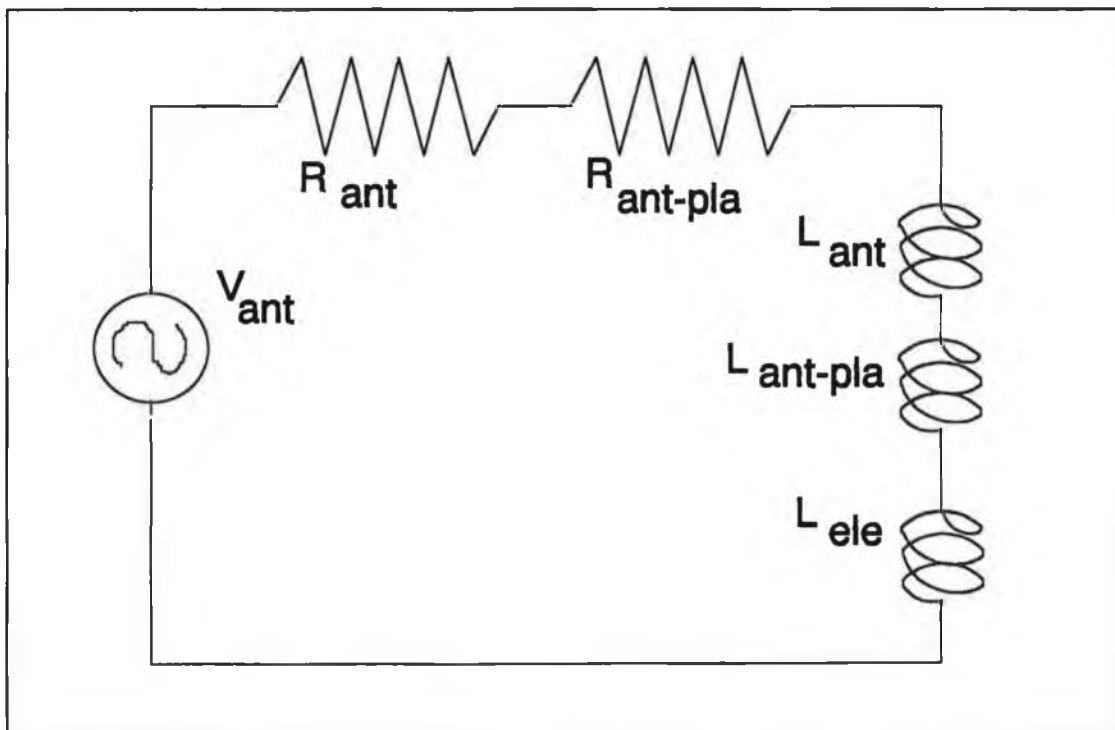


Figure 2.4(b): Transformed ICP circuit using circuit analysis.

the discharge and therefore the plasma is a one turn conductor). The model allows different ICP configurations, internal antenna, external antenna etc, to be analyzed by applying the same circuit analysis procedure. From circuit analysis one can predict the behaviour of the antenna-plasma impedance, a parameter which can be measured experimentally (section 4.3.2).

There are three components of the discharge impedance,  $L_{pla}$ ,  $R_{pla}$  and  $L_{ele}$  the latter two of which arise from the real and imaginary parts of the plasma conductivity. In the ICP a current of charged particles is driven by the electric field induced by an RF current flowing in the antenna,

$$\underline{J} = \sigma \underline{E} \quad 2.1$$

where the plasma conductivity  $\sigma$  is given by,

$$\sigma = \frac{n_e e^2}{m_e} \frac{1}{(\nu + i\omega)} \quad 2.2$$

where  $n_e$  is the electron density,  $m_e$  is the electron mass,  $\nu$  is the electron collision frequency and  $\omega$  is the frequency of the applied electric field. The real part of the plasma conductivity corresponds with a plasma current in phase with the induced RF electric field and the imaginary part is associated with a current ninety degrees out of phase. Power is deposited in the plasma if the discharge current and RF electric field are in phase, thus the real conductivity is inversely related to the plasma resistance  $R_{pla}$ . No power is deposited through the out of phase current and the imaginary conductivity corresponds to the inverse of the plasma inductance known as the electron inertia inductance. This inductance is related to the plasma resistance and is given by  $L_{ele} = R_{pla}/\nu$ .

The third component of the plasma impedance is the inductance of the plasma resulting from the path taken by the plasma current,  $L_{pla}$ . It is this inductance which is coupled with the antenna inductance,  $L_{ant}$ , through the mutual inductance  $M$ , where,

$$M^2 = k^2 L_{ant} L_{pla} \quad 2.3$$

k being the coupling coefficient between the two components [20]. For an ideal transformer  $k=1$  and one would be able to write  $L_{pla}=L_{ant}/n^2$ , where n is the number of turns in the antenna, but for the plasma one expects  $k < 1$ .

The complete circuit for the antenna and plasma is given in figure 2.4(a), where  $V_{ant}$  is the RF voltage at the antenna input and  $R_{ant}$  is the antenna resistance. This circuit can be transformed to an equivalent circuit, figure 2.4(b), using simple circuit theory. From this one can determine the resistance at the antenna input,  $R_{input}$ , to be,

$$R_{input} = R_{ant} + \omega^2 M^2 \frac{R_{pla}}{Z_{pla}^2} \quad 2.4$$

Here  $Z_{pla}$  is the plasma impedance  $R_{pla} + j\omega(L_{pla} + L_{ele})$ . Clearly from equation 2.4 one would expect to measure an increase in the input resistance when the plasma is fired.

The inductance at the antenna input is found similarly and is given by,

$$L_{input} = L_{ant} - \omega M^2 \frac{(\omega L_{pla} + \omega L_{ele})}{Z_{pla}^2} \quad 2.5$$

From equation 2.5 one can note that there is a decrease in measured inductance when a plasma is fired. The plasma current induces a magnetic field which opposes the magnetic field induced by the antenna, thereby reducing the total magnetic field present in the circuit,  $\underline{B}$ . This in turn reduces the inductance of the circuit.

$$\int_A \frac{\partial \underline{B}}{\partial t} \cdot d\underline{A} = j\omega L_{input} I(t) \quad 2.6$$

## 2.4 Plasma heating of the ICP.

To sustain an RF discharge the rate of plasma loss to the chamber walls must be balanced by ionisation in the plasma [21]. This requires a continuous energy input to the system. In the ICP the power source is the RF current flowing in the antenna. The

mechanism by which the discharge gains energy is pressure dependent. When the pressure is above a certain level ( $>20\text{mTorr}$  in Argon), the plasma is collisional and Ohmically heated. Below this pressure the plasma becomes collisionless and non-Ohmic heating is expected to occur. There is still much debate about plasma heating in the collisionless plasma and one proposed mechanism is described below.

#### 2.4.1 ICP initiation.

An important aspect of ICP operation is when the discharge is first fired and the input power is low ( $<20\text{W}$ ). The azimuthal electric field induced by the antenna current,  $E_\theta$ , is insufficient to maintain a balance between ionisation and diffusion losses. Instead the longitudinal electrostatic electric field between adjacent turns of the antenna,  $E_z$ , capacitively couples power into the discharge. A weak plasma is formed ( $n < 10^9\text{cm}^{-3}$ ) in a sheath next to the glass wall surrounding the antenna.

The ratio of  $E_z/E_\theta$  is constant in the absence of space charges, but when the electrostatic field between neighbouring antenna loops,  $E_z$ , becomes sufficient to support ionisation a space charge develops in a sheath next to the antenna and the situation changes. Due to the oscillatory motion of the electrons along the length of the antenna following the longitudinal electric field, the space charge develops at the ends of the antenna. As the antenna current is

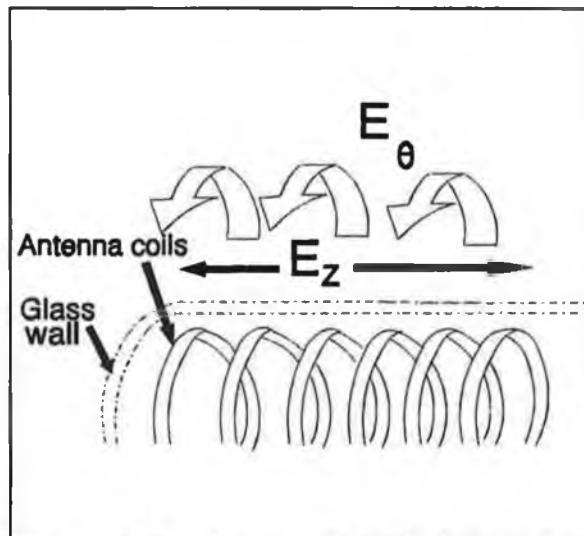


Figure 2.5. Azimuthal and longitudinal electric fields.

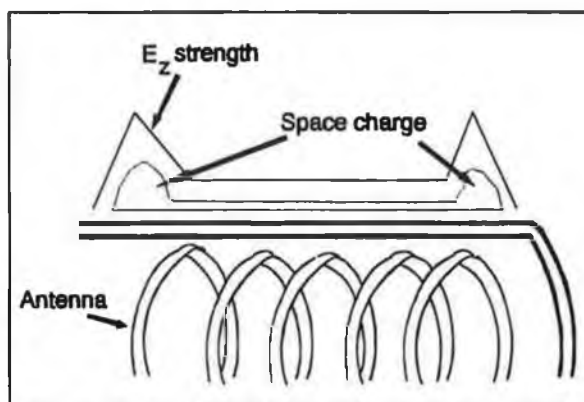


Figure 2.6. Development of space-charge and the electrostatic field at ends of antenna.

increased further the space charge density at the ends of the antenna increases which results in an increase in the longitudinal electric field there and a reduction of the longitudinal field in the centre of the discharge chamber. Thus as the input power is increased the azimuthal electric field becomes larger and the longitudinal electric becomes smaller in the centre of the discharge [22]. When the azimuthal electric field becomes large enough to support a discharge and the plasma switches from a capacitively coupled mode to an inductively coupled discharge.

Although the effect of capacitive coupling may be small when the ICP is fully established, it can be virtually eliminated if an electrostatic shield is put in place around the antenna. The shield is simply a slotted conductor which shorts out the electrostatic field lines, allowing only the azimuthal electric field to enter the plasma. The shield can take on various shapes depending on the ICP configuration used, here for example a copper tube can be used whereas flat topped ICP's usually employ a slotted copper disc.

#### 2.4.2 Ohmic heating.

When the electron collision frequency is greater than the RF driving frequency the discharge is said to be Ohmically heated [23,24]. The RF current in the antenna sets up an electric field in the plasma which in turn drives a current in the discharge. The current lies next to the antenna-plasma interface and penetrates approximately one skin depth into the bulk plasma. The size of this current is related to the applied electric field through the plasma conductivity,  $\sigma$ ,

$$\mathbf{J} = \sigma \mathbf{E} \quad 2.7$$

For an RF plasma the conductivity can be written as [25],

$$\sigma = \frac{n_e e^2}{m_e(\nu + i\omega)} \quad 2.8$$

The bulk plasma gains energy when the electrons in the current undergo elastic or inelastic collisions, Ohmic heating. The relation between the power absorbed by the load, the antenna and plasma, and antenna current is given by, where R is the load resistance.

$$P_{load} = \frac{1}{2}RI^2 \quad 2.9$$

In the investigation of the plasma impedance it is convenient to use the surface impedance [25],  $\zeta$ . It relates the power absorbed by the plasma to the antenna current and has a similar form to equation 2.9,

$$P_{plasma} = 1/2 \zeta_{re} |J_{ant}|^2 \quad 2.10$$

The surface impedance is derived by Turner [25] and is given by,

$$\zeta = \frac{i\omega\mu_0 \tanh kL}{k} \quad 2.11$$

where,

$$k = \frac{\omega_p}{c} \left[ \sqrt{\frac{\phi(1+\phi)}{2}} + i\sqrt{\frac{\phi(1+\phi)}{2}} \right] \quad 2.12$$

and

$$\phi = \frac{1}{\sqrt{1 + \frac{\nu^2}{\omega^2}}} \quad 2.13$$

This definition is valid for a cylindrical plasma such as the one used here when,

$$1 < kr_1 < kr_2 \quad 2.14$$

where  $r_1$  is the radius of the plasma-antenna interface and  $r_2$  the chamber radius. This inequality is valid here as  $k \gg 1$  under the conditions of interest. A plot of the collisional surface resistance for Argon is presented in figure 2.8. Obviously a different dependence is found for different gasses as collision frequencies,  $\nu$ , differ for different gasses.

The optimum condition for Ohmic heating occurs when the electron collision frequency becomes equal to the RF driving frequency, as electrons gain maximum energy from the RF electric field. As  $\nu$  becomes much greater than  $\omega$ , when the pressure is increased, Ohmic heating becomes less efficient. This is because the time between collisions becomes so small that electrons cannot gain maximum possible energy from the applied RF electric field between collisions, and consequently the bulk plasma is heated less efficiently (the load resistance drops). When the collision frequency is less than the driving frequency, at low pressures, the electrons fail to transfer their energy efficiently to the bulk plasma as collisions are rare [7]. Here the plasma is said to be collisionless and a non-Ohmic heating mechanism must dominate at low pressure ( $< 10\text{mTorr}$ ) if an ICP can still be sustained (chapter 5).

### 2.4.3 Collisionless heating.

At low pressures in capacitive discharges it is generally accepted that collisionless heating is the dominant process sustaining the plasma. It is claimed that electrons are heated by inelastic reflection from the oscillating RF sheaths at the electrodes. This form of collisionless heating is known as stochastic heating [26-28].

In the ICP however, the oscillating RF sheaths are not present. This is because, unlike in the capacitive discharge, the RF current is closed and the large electrostatic field does not exist here. Therefore in the purely inductively coupled plasma stochastic heating will not be significant. There can be a small fraction of capacitive coupling occurring in the real ICP however. An electrostatic electric field can occur between the neighbouring loops of the antenna and capacitive coupling can occur between the antenna and plasma through the dielectric wall between the two. This becomes insignificant however when the discharge is well established and when electrostatic shielding is in place as discussed in section 2.4.1.

The proposed collisionless heating mechanism for ICP's presented here is a warm plasma effect [25,29]. In order to gain energy, electrons must pass into and out of the region of RF field in a time less than one RF cycle. If the electrons are present in the skin depth for longer than one RF cycle, the energy they gain in the first half cycle will be lost in the second half cycle. Thus the electrons must have sufficient thermal velocity initially to gain energy from the RF field. This condition may be written as,

$$\omega \delta \leq \sqrt{\frac{k_B T_e}{m_e}} \quad 2.15$$

where  $\delta$  is the skin depth,  $k_B$  is Boltzmann's constant and  $T_e$  is the electron temperature.

The heated electrons on leaving the applied RF field will contribute to a current lying outside of the skin depth. Therefore the electric field at one point in the plasma can, at all later times, affect the current throughout the entire plasma. Thus one can no longer state,

$$\underline{J} = \sigma \underline{E} \quad 2.16$$

Now the conductivity must be replaced by some spatially dispersed conductivity and equation 2.16 is rewritten as,

$$\underline{J}(\underline{r}, t) = \int d\mathbf{r}'^3 \int_{-\infty}^t \sigma(\mathbf{r}, t) \underline{E}(\mathbf{r}', t') dt \quad 2.17$$

where the electric field  $\underline{E}$  is confined close to the antenna but the resulting current density  $\underline{J}$  can be found across the entire width of the plasma.

The classical collisional skin depth is given by,

$$\delta = \sqrt{\frac{2}{\mu \omega \sigma}} \quad 2.18$$

where  $\sigma$  is given in equation 2.8. In the collisionless plasma however, the form of the conductivity given in equation 2.8 is no longer valid and therefore the classical skin depth must be modified to account for the spatial dispersion of the conductivity (equation 2.17).

To determine the depth of penetration of the applied electric field in a collisionless plasma, or the collisionless skin depth, one can proceed as follows (the situation is analogous to the anomalous skin depth in low temperature metals which is discussed by Kittel [30] and Chambers [31]).

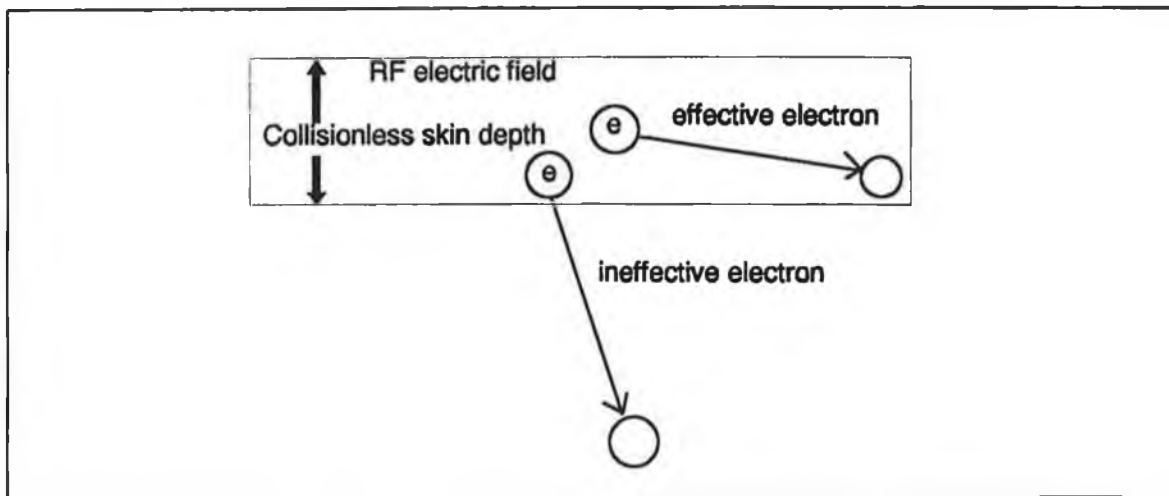


Figure 2.7. The RF electric field penetrates a finite distance into the plasma and electrons which remain within this region contribute to a current within the collisionless skin depth.

Even in the collisionless plasma there will still be a proportion of electrons which remain within the RF electric field region (figure 2.7), or collisionless skin depth,  $\delta_c$ , given by,

$$n_{E\text{-field}} = \frac{\delta_c}{\lambda} n_{\text{total}} \quad 2.19$$

where  $n_{E\text{-field}}$  is the electron concentration which remains within the RF electric field,  $n_{\text{total}}$  the total electron concentration contributing to the plasma current and  $\lambda$ , the electron mean free path. Equation 2.16 may be modified to just include the contribution of these electrons to a current within the skin depth,  $J_{\text{eff}}$ , using an effective plasma conductivity,  $\sigma_{\text{eff}}$ ,

$$J_{\text{eff}} = \sigma_{\text{eff}} E \quad 2.20$$

Using  $\sigma_{\text{eff}}$ , which is related to the RF electric field penetration depth, one can determine the collisionless skin depth. The effective conductivity of equation 2.20 is related to the classical conductivity,  $\sigma$ , of equation 2.16, by,

$$\sigma_{eff} \approx \frac{\delta_c}{\lambda} \sigma = \frac{\delta ne^2}{\lambda m v} = \frac{\delta ne^2}{v m} \quad 2.21$$

The collisionless skin depth now has the form,

$$\delta_c = \sqrt{\frac{2m v}{\mu \omega \delta ne^2}} \quad 2.22$$

which after some manipulation one finds the collisionless skin depth to be given by,

$$\delta_c = \left[ \frac{8 k_B T_e}{\pi m_e} \frac{2 c^2}{\omega_p^2 \omega} \right]^{\frac{1}{3}} \quad 2.23$$

A comparison between the classical and collisionless skin depths is shown in figure 2.9.

Obviously for collisionless heating to occur the skin depth must be smaller than the plasma diameter to allow the electrons to leave the field region. Therefore,

$$\delta_c > L \quad 2.24$$

where L is the plasma diameter.

The effect of collisionless heating will manifest itself in the form of a finite plasma resistance even at low pressures. The surface impedance in the collisionless regime is given by Turner[29],

$$\zeta_c = \frac{2\mu_o \omega \delta_c}{3} \left( \frac{1}{\sqrt{3}} + i \right) \quad 2.25$$

A plot of classical and collisionless surface impedances is given in figure 2.8.

To test for the presence of such a heating mechanism one would need to measure plasma resistance, skin depth and look for the presence of a current in the plasma. The plasma resistance should be higher than expected from collisional theory at low pressures. The measured skin depth should be smaller than that predicted by classical theory and one should observe a current of electrons extending beyond the skin depth. Such a survey was carried out and the results are given in chapter 5.

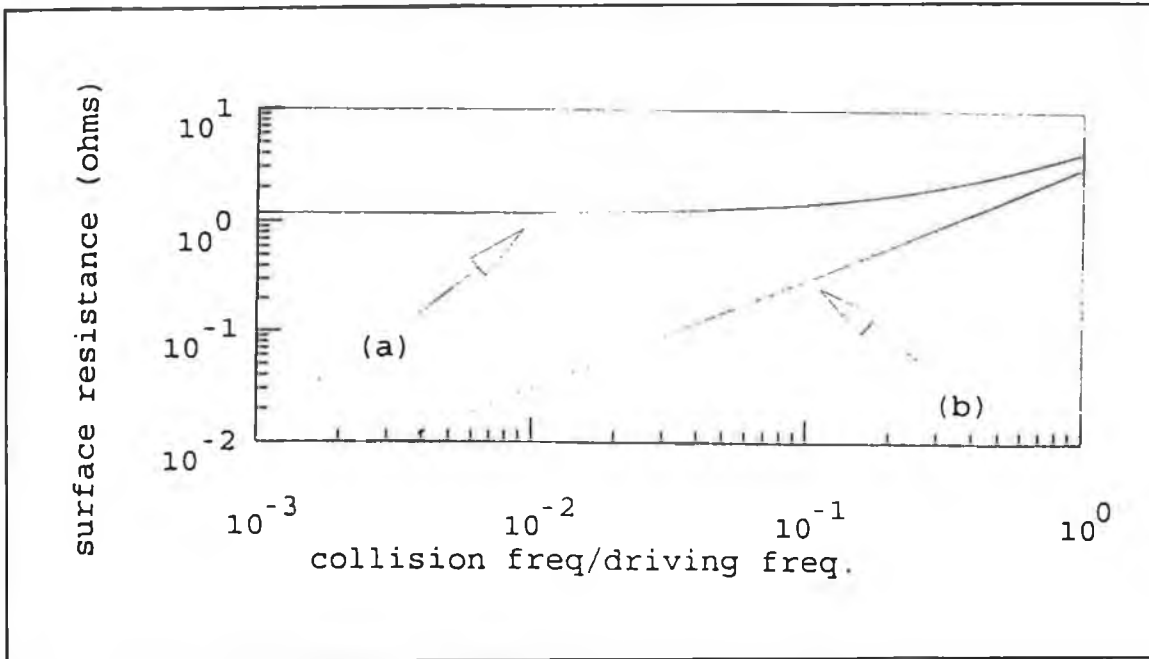


Figure 2.8. Comparison of (a)collisionless and (b)Ohmic surface resistances for a 4eV plasma,  $N_e=1 \times 10^{10} \text{cm}^{-3}$ .

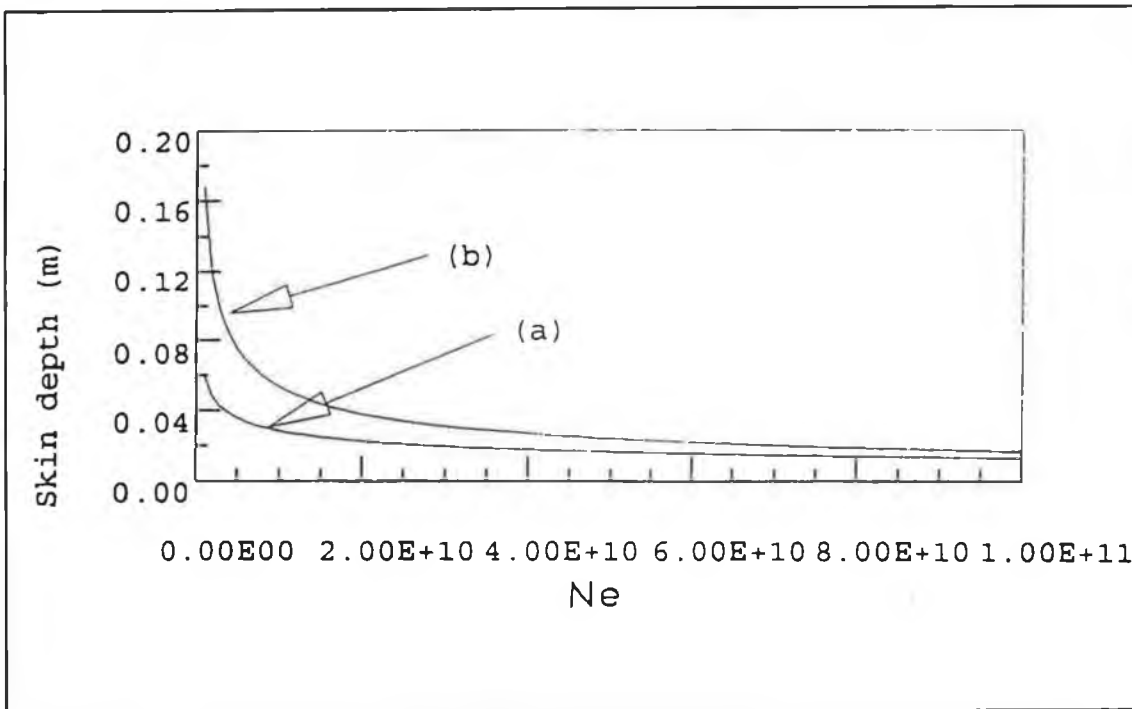


Figure 2.9. Comparison of (a)collisionless and (b)classical skin depths for a 4eV 10mTorr plasma.

## 2.5 Electron kinetics in the ICP.

### 2.5.1 The distribution function and Boltzmanns equation.

To obtain an exact description of a plasma, the position and velocity of each particle must be known, i.e. a complete description in six dimensional phase space with coordinates  $\underline{x}$ ,  $\underline{y}$ ,  $\underline{z}$ ,  $\underline{v}_x$ ,  $\underline{v}_y$ ,  $\underline{v}_z$ . Considering the number of particles in a typical plasma ( $> 3.5 \times 10^{13}$  per  $\text{cm}^3$  at 1mTorr ), the task may seem impossible. Fortunately a statistical approach can be taken to the problem where the average population of any volume in phase space,  $d\underline{r}^3 d\underline{v}^3$  at  $\underline{r}$ , can be determined from a distribution function  $f(\underline{r}, \underline{v}, t)$ .

$$dn = f(\underline{r}, \underline{v}, t) d^3\underline{r} d^3\underline{v} . \quad 2.26$$

The distribution function is normalised such that,

$$n(\underline{r}, t) = \int_{\underline{v}} f(\underline{r}, \underline{v}, t) d^3\underline{v} . \quad 2.27$$

A separate distribution function applies to each species of particle in the plasma, but since electrons are important in most plasma interactions it can be assumed from now on that one is dealing with the distribution function of electrons.

The plasma is obviously not a static system, charged particles gain energy from an applied electromagnetic field, lose energy due to collisions. Ionisation causes an increase in electron and ion densities whereas recombination and diffusion to the chamber walls reduce their populations.

The effects of these processes on the particle distribution functions must be included in any reasonable description of the plasma. The movement of particles will obviously have an effect on the distribution function as particles move

from one volume of phase space to another. Consider the particle flux into a volume of

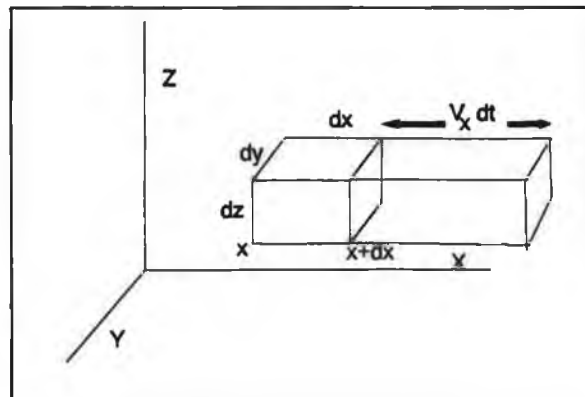


Figure 2.10. Volume in phase space,  $dx dy dz$ .

plasma at  $x$  given by  $dx dy dz$  (figure 2.10). The number of particles to enter from the positive  $x$ -direction in a time  $dt$  is given by,

$$(f v_x)_x dt d^3v dy dz \quad 2.28$$

The number of particles to leave this volume in the  $x$ -direction at  $x+dx$  in a time  $dt$  has a similar form and is given by,

$$(f v_x)_{x+dx} dt d^3v dy dz \quad 2.29$$

Therefore the net flux into this volume in the  $x$ -direction may be written as,

$$\left[ \frac{\partial n}{\partial t} \right]_x = \left[ \frac{\partial f}{\partial t} \right] dt d^3v dy dz = [(f v_x)_x - (f v_x)_{x+dx}] dt d^3v dy dz \quad 2.30$$

the right hand side of equation 2.30 may be rewritten as,

$$[(f v_x)_x - (f v_x)_{x+dx}] dt d^3v dy dz = - \left[ \frac{\partial f v_x}{\partial x} \right]_x dt d^3v dy dz \quad 2.31$$

Comparing equation 2.30 and equation 2.31 one finds,

$$\left[ \frac{\partial f}{\partial t} \right]_x = - \left[ \frac{\partial f v_x}{\partial x} \right]_x = - v_x \frac{\partial f}{\partial x} \quad 2.32$$

Similar expressions can be found for the change in the distribution function due to particle flux from the  $y$  and  $z$  directions. The total change in the distribution function due to the motion of particles can therefore be written as,

$$\left[ \frac{\partial f}{\partial t} \right]_r = - v_x \frac{\partial f}{\partial x} - v_y \frac{\partial f}{\partial y} - v_z \frac{\partial f}{\partial z} = \mathbf{v} \cdot \nabla_r (f) \quad 2.33$$

The distribution function may also be altered as a result of changes in the velocity of particles in the plasma i.e. particle acceleration. This may be a result of the force of internal or external electric and magnetic fields on plasma particles,

$$\mathbf{F} = m \mathbf{a} = m q (\mathbf{E} + \mathbf{v} \times \mathbf{B}) \quad 2.34$$

where  $\underline{a}$  is the particle acceleration,  $m$  the particle mass and  $q$  the particle charge. In this case the particle population in a volume of velocity space  $dv_x dv_y dv_z$ , changes and one may follow a similar argument to that given above. The change in particle the distribution function due to the flux of particles into and out of a volume of velocity space is,

$$\left[ \frac{\partial f}{\partial t} \right]_v = -a_x \frac{\partial f}{\partial v_x} - a_y \frac{\partial f}{\partial v_y} - a_z \frac{\partial f}{\partial v_z} = -\underline{a} \cdot \nabla_v(f) \quad 2.35$$

The effect of particle motion and forces on the plasma particles can therefore be described by,

$$\frac{\partial f}{\partial t} = -\underline{v} \cdot \nabla_r f - \underline{a} \cdot \nabla_v f \quad 2.36$$

Collisions must be included to get a complete description of the behaviour of the plasma, but the above arguments cannot be followed here as collisions sometimes cause particles to disappear from one element of phase space and appear in another e.g. electrons disappear from phase space as a result of recombination collisions with ions. A term must be included to account for collisions, called the collision integral, and added to equation 2.36,

$$\frac{\partial f}{\partial t} + \underline{v} \cdot \nabla_r f + \underline{a} \cdot \nabla_v f = \left[ \frac{\partial f}{\partial t} \right]_{colls} \quad 2.37$$

The collision integral can take various forms depending on the type of collision being considered. The change in the distribution function is related to the energy change of the particular collision. In an elastic collision for example the change in the distribution function is related to the energy transfer coefficient. Inelastic collisions alter the distribution function more strongly than elastic collisions as most of the electron energy, and therefore velocity, can be lost in an inelastic collision (see local and non-local models below).

Equation 2.37 is known as the kinetic or Boltzmann equation and describes the changes in the distribution function of a particular species in the plasma. A separate distribution function applies to each species of particle in the plasma, but since electrons are important in most plasma interactions it can be assumed from now on that one is

dealing with the distribution function of electrons or EDF.

The simplest situation to apply the Boltzmann equation is to a plasma in thermodynamic equilibrium with no external forces. In this case,

$$\frac{\partial f}{\partial t} = 0 = \left[ \frac{\partial f}{\partial t} \right]_{\text{colls}} \quad 2.38$$

A solution to this equation is the well known Maxwellian velocity distribution,

$$f(\mathbf{v}) = n \left( \frac{m}{2\pi kT} \right)^{3/2} \exp \left[ \frac{-m \mathbf{v}}{2kT} \right] \quad 2.39$$

An actual laboratory plasma is not in thermodynamic equilibrium since energy is gained by the discharge through one mechanism, from an applied electric field for example, and lost through another, plasma losses to walls. As a result the distribution function may be non-Maxwellian. The determination of the EDF of an actual plasma is highly complex and therefore a number of assumptions and approximations are made about the condition of the plasma.

In the ICP the discharge is powered by an induced electric field. To help determine the distribution function for this situation assume that this electric field points in the direction of the z axis (figure 2.11). To simplify the situation it can be assumed also that the distribution will be symmetric about the z axis (it will have no  $\phi$  dependence since the only force affecting the particles points in along the z axis). In this case it is convenient to use spherical coordinates and due to the assumed symmetry of the situation, expand the distribution function in terms of Legendre polynomials,

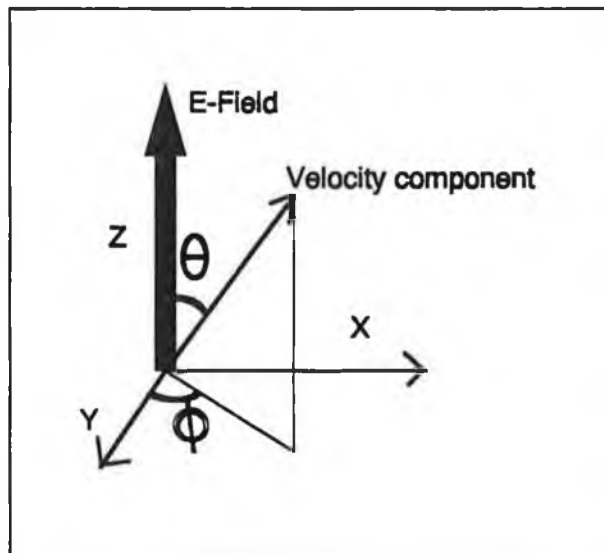


Figure 2.11. Diagram of electric field and velocity orientation.

$$f = \sum_k P_k(\cos\theta) f_k = f_0 + \cos\theta f_1 + \dots \quad 2.40$$

where  $\theta$  is the angle between the velocity component of  $f$  and the electric field (figure 2.11). The first component on the right hand side of equation is an isotropic component of the distribution function and the components of the expansion following this account for any anisotropies in the plasma. The smaller  $\theta$  is the greater will be the contribution of  $f_1$  to the overall distribution function  $f$ .

The electric field in the plasma will add an additional drift velocity to the electrons, but this velocity will be much less than the electron thermal velocity,

$$\left( \sqrt{\frac{8kT_e}{\pi m_e}} \right)_{thermal} \gg \left( \frac{-eE}{m_e(\nu + j\omega)} \right)_{drift} \quad 2.41$$

Therefore one can assume that the isotropic component of the EDF will be greater than the anisotropic components.

The expansion of the EDF into Legendre polynomials can be incorporated into the Boltzmann equation,

$$\frac{\partial \sum_k P_k f_k}{\partial t} + \nu \nabla_r \sum_k P_k f_k + \omega \nabla_v \sum_k P_k f_k = \left[ \frac{\partial \sum_k P_k f_k}{\partial t} \right]_{colls} \quad 2.42$$

From this form of the Boltzmann equation one can determine the electron kinetics in an actual plasma subject to an electric field.

## 2.6 Kinetic modelling of the ICP.

### 2.6.1 The local model.

In order to reduce the complexity of the Boltzmann equation a model of the plasma is usually employed i.e. assumptions are made about the characteristics of the plasma. This description is incorporated into the Boltzmann equation and the EDF is then calculated. One such model is known as the local model and may be applied to the inductively coupled plasma under certain conditions (electron mean free path less than plasma dimensions) [37].

There are several assumptions made about the plasma characteristics incorporated in the local model. Firstly the plasma is assumed to be homogeneous with no space charge field or diffusion of particles. Secondly the EDF is assumed to be in equilibrium with the local electric field. The version of the Boltzmann equation solved in this case is known as the homogeneous Boltzmann equation. It is found from an expansion of equation 2.42 using the assumptions stated here. It is convenient to use a distribution function of electron kinetic energy,  $f(u)$ , rather than speed,  $f(v)$ , as one is dealing with the energy gained from the applied RF field and the energy lost in collision processes. To change the electron distribution function from a speed to energy dependence consider,

$$n = \int_V f(v) dv = \int_V f(u) du \quad 2.43$$

where  $n$  is the total number of particles in volume  $v$ . But,

$$du = d\left(\frac{1}{2}m v^2\right) = m v dv \quad 2.44$$

Therefore from equation 2.43 one has,

$$f(v) = m v f(u) = \sqrt{2 m u} f(u) \quad 2.45$$

In terms of kinetic energy,  $u = mv^2/2e$  (kinetic energy in electronvolts), the kinetic equation for the local model becomes,

$$\frac{\partial}{\partial u} \left( \frac{2e}{3m} \frac{u^{3/2}}{v_m} E_{\text{eff}}^2(u) \frac{\partial F_0(u)}{\partial u} + \frac{2m_e}{M} u^{3/2} v_m F_0 \right) = \sum_k [v_k(u) \sqrt{u} F_0 - v_k(u + u_k) \sqrt{u + u_k} F_0(u + u_k)] + S_{ee} \quad 2.46$$

where,

$$E_{\text{eff}} = \frac{E_{\text{rf}}}{\sqrt{2}} \frac{v_m(u)}{(v_m^2(u) + \omega^2)^{1/2}} \quad 2.47$$

The first term of equation 2.46 represents electron heating due to the applied electric field,  $E_{\text{rf}}$ . The effective electric field strength,  $E_{\text{eff}}$  (equation 2.47), arises from the dependence of

heating efficiency on the momentum transfer collision frequency  $\nu_m(u)$  [37,38]. Electrons at a given energy with a low collision frequency will see the applied electric field  $E_{rf}$ , but will not transfer energy to the plasma as efficiently as electrons with a higher collision frequency at a different energy which also see  $E_{rf}$ . Thus  $E_{eff}$  will be larger for electrons with greater collision frequencies. The larger the effective electric field strength the greater will be the effect on the electron distribution function.

The second term in equation 2.46 is the change in the distribution function resulting from elastic collisions. This change is related to the energy transferred in an elastic collision which is the coefficient for elastic collisions,  $2m_e/M$ , times the energy of the electron undergoing the collision.

The first term on the right hand side of equation 2.46 represents the change in the electron distribution due to energy losses resulting from inelastic and electron-electron collisions respectively. Here  $u_k$  is the energy required for (and lost in) an inelastic collision of type  $k$ . The total change in the distribution function due to inelastic collisions is equal to the sum of the individual changes due to the various types of inelastic collision processes. Electron-electron collisions are denoted by the last term in equation 2.46. These collisions are important as they help to thermalise the EEDF as the transfer of energy between electrons due to these collisions can be very efficient.

For the inductively coupled plasma, where the electric field powering the plasma is inhomogeneous due to the skin effect, the EDF will be hotter (have a higher density of high energy electrons), nearest the antenna where the electric field is a maximum. Since ionisation

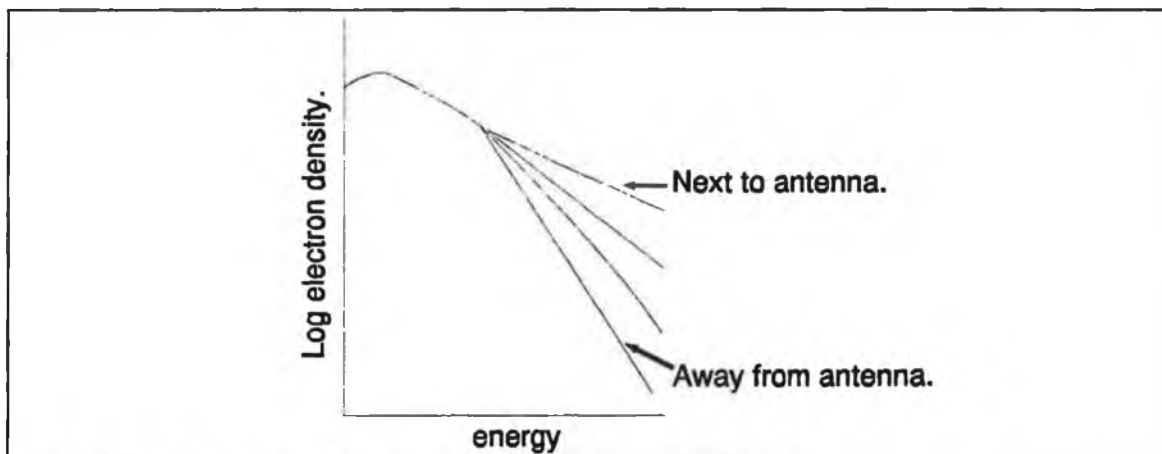


Figure 2.12. Sketch of EEDF under local kinetic conditions.

and excitation are sensitive to electron energy one would expect that most of these processes will occur within the skin depth according to the local model.

Moving away from the antenna the EDF will cool, there are fewer high energy electrons present since the heating field is not so strong. This assumes that the mean free path of the high energy electrons is of the order of a skin depth. The principle energy loss mechanism for the high energy electrons is inelastic collisions since most of the electrons' energy is lost in such a process [39,40]. The effect of the elastic collisions involving the bulk electrons may be ignored since the change in electron energy is small [40,41] (energy change per elastic collision  $\Delta u = u_i 2m_e/M$  where  $u_i$  is the initial electron energy). The short mean free path requirement for electrons undergoing inelastic collisions restricts the model to conditions of relatively high pressure. Figure 2.12 shows expected behaviour of the EEDF under local kinetic conditions.

### 2.6.2 Introduction to the non-local model.

An important aspect of the non-local model is the presence of a space-charge potential in the discharge. This effects the kinetic energy of all electrons in the discharge and restricts the motion of low energy electrons. The resulting behaviour of the EEDF is different to that predicted by the local model. It is sometimes convenient in this case to introduce the electron distribution function of total energy, kinetic plus potential energy. This can account for the effect of the space charge on the kinetic energies of electrons.

### 2.6.3 Non-local model.

The non-local model can be applied to plasma where the energy relaxation length of electrons is comparable to the plasma dimensions. Thus the non-local approach is particularly appropriate for the investigation of low pressure plasmas. The effect of diffusion and the space charge potential are included in the Boltzmann equation, and the EDF is not in equilibrium with the local electric field.

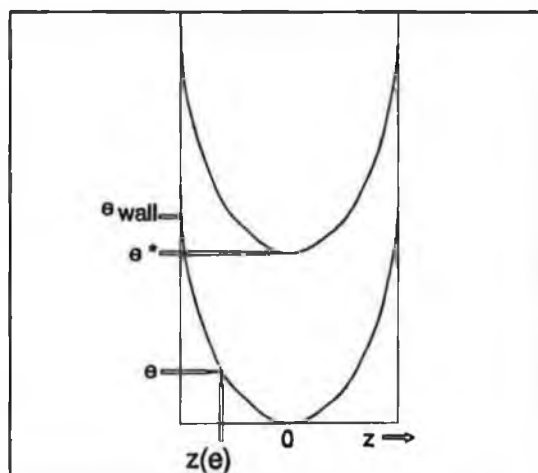


Figure 2.13. Schematic of space-charge potential energy profile,  $-\phi(z)$ .

A consequence of the long mean free path of electrons relative to the plasma size is that their spatial diffusion is much greater than their diffusion in energy space: electrons which gain energy within the driving RF electric field can migrate across the plasma without any loss in energy [3,42,43].

This fact must be coupled with the effect of the space charge potential which acts as a potential well for electrons. Electrons which traverse this potential gradient will lose kinetic energy but their total energy will remain constant. It is useful therefore to state the EDF in terms of total energy rather than kinetic energy.

It also follows from these arguments that there is one EDF of total energy,  $\epsilon$ ,  $F[\epsilon=u-\phi(z)]$ , applicable at any position in the plasma. In order to determine the EDF of kinetic energy,  $F_0[u,z]$ , at any position one simply back substitutes  $u=\epsilon+\phi(z)$  into the EDF of total energy.

The equations describing the non-local electron kinetics are those derived by Kortshagen et al [3,43]. In terms of the EDF of total energy  $F[\epsilon=u-F(z)]$ , the Boltzmann equation is written as,

$$\frac{\partial}{\partial \epsilon} \left( \overline{D}_\epsilon \frac{\partial F}{\partial \epsilon} + \overline{V}_\epsilon F \right) = \sum_k [\overline{v}_k(\epsilon) \sqrt{e} F - \overline{v}_k(\epsilon + u_k) \sqrt{e + u_k} F(\epsilon + u_k)] + \overline{S}_{ee} \quad 8 \quad 2.4$$

where

$$\overline{D}_\epsilon = \frac{2e}{3m} \int_0^{z(\epsilon)} u^{\frac{3}{2}}(z) \frac{E_T(z)^2}{2} \frac{v_m}{v_m^2 + \omega^2} dz \quad 2.49$$

and

$$\overline{v}_k(\epsilon) = \int_0^{z(\epsilon)} v_k(u) \sqrt{u(z)} dz . \quad 2.50$$

$$\overline{V}_\epsilon = \frac{2m}{M_a} \int_0^{z(\epsilon)} u^{3/2} v_m dz \quad 2.51$$

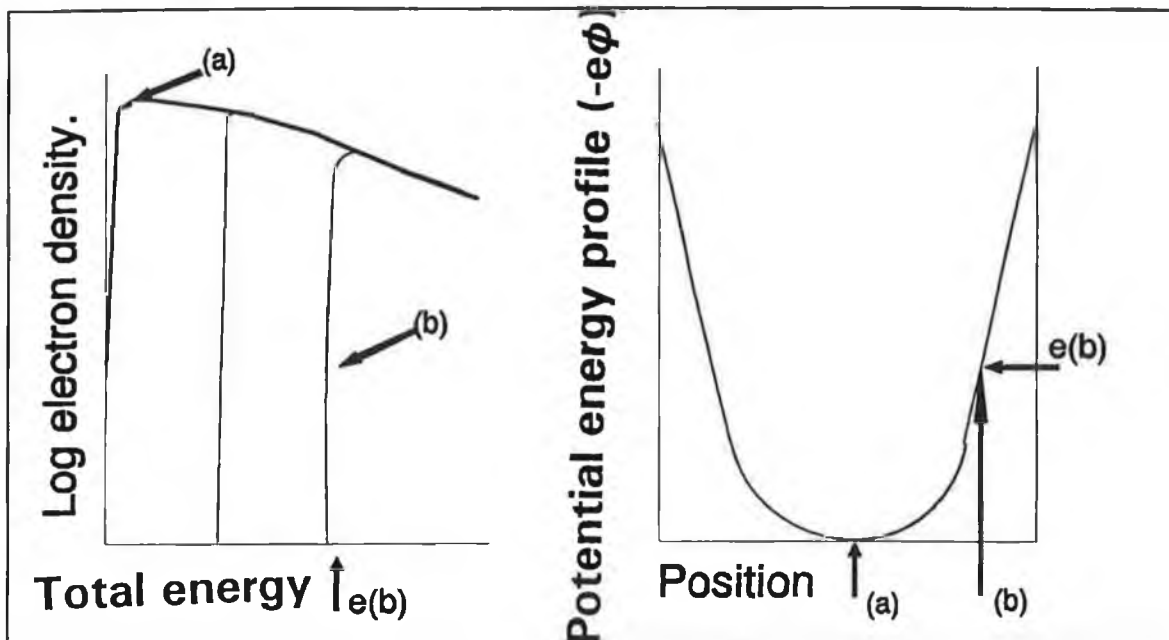


Figure 2.14. Sketch of EEDF of total energy under non-local kinetic conditions and potential energy profile.

The terms above account for the heating of electrons due to the applied RF electric field  $E_{rf}$  and energy losses due to elastic and inelastic collisions respectively. The parameters are spatially averaged over the discharge region from 0, the discharge centre, to  $z(\epsilon)$ , the extent to which an electron of total energy  $\epsilon$  can travel in the plasma. For the non-local model the heating terms dominates the equation.

A schematic of the potential energy gradient due to the presence of the space charge is given in figure 2.13. The electron potential energy minimum is found at the centre of the discharge and rises to a maximum at the chamber walls. Excitation and ionisation reactions are possible only for electrons with sufficient kinetic energy and so follow the same profile as the space charge potential energy. Unlike the local model where electron heating and ionisation occur in the same region of space, here much of the inelastic processes occur in the centre of the discharge, away from the antenna. In order for a plasma to be sustainable the minimum energy required for excitation must be less than the wall potential otherwise electrons would simply leave the plasma without any prospect of ionisation occurring.

Although the total energy of any electron may be constant, its kinetic energy may go to zero if it has insufficient energy to overcome the space charge potential energy

gradient and diffuse to the walls. In that case the electron will be trapped within a region of plasma by the space charge potential. Therefore if one were to determine the EDF of kinetic energy at a point greater than  $z(\epsilon)$ , electrons with total energies below  $\epsilon$  would not be included. Therefore the EDF of kinetic energy will differ across the plasma only by the absence of electrons which cannot reach that point in the plasma figure 2.14.

## 2.7. Conclusions.

In this chapter many aspects of ICP operation at low pressure were discussed. The electrical characteristics of the discharge, which can be derived from the straightforward transformer model, can give an insight into the electromagnetic interaction of the antenna and plasma. Low pressure heating is one area of ICP behaviour not fully understood, but one proposed mechanism from Turner [25] was presented here. The mechanism is a warm plasma effect and can explain the possibility of sustaining a low pressure ICP ( $< 10\text{mTorr}$ ) which could not be sustained solely by Ohmic heating. Electron kinetics in the ICP, particularly at low pressure, show interesting behaviour. At the low pressures at which the discharge is being operated, one would expect that the non-local model will dominate electron kinetics. Therefore one would expect to find an EEDF of total energy which is valid across the width of the discharge.

All of the aspects dealt with in this chapter are investigated experimentally in later chapters. A thorough characterisation of the principal plasma parameters of the ICP is presented in chapter 4. Low pressure heating of the ICP is experimentally investigated in chapter 5 with a survey of electron kinetics presented in chapter 6.

## References.

- [1] Hittorf. Wiedsmann Ann. d. Physik. **21** (1884) 90
- [2] G. I. Babat. J. Inst. Electron.Eng. **94** (1947) 27
- [3] U. Kortshagen, I. Pukropski and M. Zethoff. J. Appl. Phys. **76** (1994) 2048
- [4] J. L. Shohet IEEE Trans. Pla. Sci. **19** (1991) 725
- [5] J. M. Richardson, J. Mangano and A. Flusberg, *Electrodless Alkali Flashlamps for Pumping Nd:Yag Lasers*. 47<sup>th</sup> GEC, Gaithersburg, Maryland, USA 1994.
- [6] R. A. Stewart, P. Vitello and D. B. Graves. J. Vac. Sci. Technol. B. **12** (1994) 478
- [7] J. Hopwood, C. R. Guernieri, S. J. Whitehair and J. J. Cuomo. J. Vac. Sci. Technol. A. **11** (1993) 152
- [8] M. S. Barnes, J. C. Foster and J. H. Keller. Appl. Phys. Lett. **62** (1993) 2622
- [9] J. Assmussen. J. Vac. Sci. Technol. A. **7** (1989) 883
- [10] P. L. Ventzek, T. J. Sommerer, R. J. Hockstra and M. J. Kushner. Appl. Phys. Lett. **63** (1993) 605
- [11] Y. Ra, S. G. Bradley and C. H. Chen. J. Vac. Sci. Technol. A. **12** (1994) 1328.
- [12] J. H. Keller, J. C. Foster and M. S. Barnes. J. Vac. Sci. Technol. A. **11** (1993) 2487
- [13] H. Goede, W. F. DiVergilio, V. V. Fosnight, M. C. Vella, K. W. Ehlers, D. Kippenham, P. A. Pincosy and R. V. Pyle. Rev. Sci. Instrum. **57** (1986) 1261
- [14] K. N. Leung, G. J. DeVries, W. F. DiVergilio, R. W. Hamm, C. A. Hauck, W. B. Kunkel, D. S. McDonald and M. D. Williams. Rev. Sci. Instrum. **62** (1991) 100
- [15] M. C. Vella, K. W. Ehlers, D. Kippenham, P. A. Pincosy, R. V. Pyle, W. F. DiVergilio and V. V. Fosnight. J. Vac. Sci. Technol. A. **3** (1985) 1218
- [16] R. B. Piejak, V. A. Godyak and B. M. Alexandrovich. Plas. Sources Sci. Technol. **1** (1992) 179
- [17] J. M. Richardson, J. Mangano and A. Flusberg. 47<sup>th</sup> Gaseous Electronics Conference. October 1994.
- [18] G. L. Moore. *Introduction to inductively coupled plasma emission spectroscopy*. (Elsever, Amsterdam-New York, 1989).

- [19] J. W. Denneman. *J. Phys. D: Appl. Phys.* **293** (1990) 293
- [20] P. Lorrain, D. P. Corson and F. Lorrain. *Electromagnetic fields and waves*. (Freeman, 1988)
- [21] T. Artz. *J. Phys. D: Appl. Phys.* **21** (1988) 278
- [22] G. G. Lister and M. Cox. *Plas. Sources Sci. Technol.* **1** (1992) 67
- [23] C. C. Petty and D. K. Smith. *Rev. Sci. Instrum.* **57** (1986) 2409
- [24] U. Kortshagen and H. Schluter. *J. Phys. D: Appl. Phys.* **25** (1992) 644
- [25] M. M. Turner. *Phys. Rev. Lett.* **71** (1993) 1844
- [26] M. M. Turner and M. B. Hopkins. *Phys. Rev. Lett.* **69** (1992) 3511
- [27] D. Vender and R. W. Boswell. *J. Vac. Sci. Technol. A.* **10** (1992) 1331
- [28] H-M Katsch, K. G. Muller and E. Quandt. *J. Phys. D: Appl.* **26** (1993) 2168
- [29] V. A. Godyak, R. B. Piejak and B. M. Alexandrovich *Plasma Sources Sci. Technol.* **3** (1994) 169
- [30] C. Kittel, *Introduction to Solid State Physics*. (Wiley, New York, 1967), 3rd ed.
- [31] R. G. Chambers, *Electrons in Metals and Semiconductors*, (Chapman and Hall, London 1990)
- [32] B. E. Cherrington, *Gaseous Electronics and Gas lasers*. (Pergamon Press)
- [33] U. Kortshagen, H. Schluter and A. Shivarova. *J. Phys. D: Appl. Phys.* **24** (1991) 1571.
- [34] Golant, Zhilinsky, Sakharov and Brown. *Fundamentals of plasma physics*. (Wiley 1980).
- [35] N. A. Krall and A. W. Trivelpiece. *Principles of plasma physics* (McGraw-Hill 1973).
- [36] I. B. Bernstein and T. Holstein. *Phys. Rev.* **94** (1954) 1475.
- [37] U. Kortshagen. *J. Phys. D: Appl. Phys.* **26** (1993) 1691.
- [38] V. I. Kolobov, D. F. Beale, L. J. Mahoney and A. E. Wendt. *Appl. Phys. Lett.* **65** (1994) 537.
- [39] V. A. Godyak and R. B. Piejak. *Appl. Phys. Lett.* **63** (1993) 3137.

- [40] U. Kortshagen. J. Phys. D: Appl. Phys. 26 (1993) 1230.
- [41] W. P. Allis and S. C. Brown. Phys. Rev. 87 (1952) 419.
- [42] D. J. Rose and S. C. Brown. Phys. Rev. 98 (1953) 310.
- [43] U. Kortshagen and L. D. Tsendin. Appl. Phys. Lett. 65 (1994) 1355.
- [44] I. D. Kaganovich and L. D. Tsendin. IEEE Trans. Plasma. Sci. 20 (1992) 66.

## **Chapter 3: Plasma Diagnostic techniques.**

### **3.1 Introduction.**

In this chapter the diagnostic tools and diagnostic methods used in the project are discussed in detail. They include the RF circuit diagnostics, the RF probes, and the plasma diagnostics, the Langmuir and magnetic field probes. The methods used for parameter evaluation are also described, as well as the possible problems associated with each diagnostic.

### **3.2 RF electrical measurements.**

The measurement of the RF power, voltage and current are useful diagnostics in the investigation of the behaviour of the inductive plasma. For example, the switching from a capacitive to an inductive heating mode in the plasma at low power and pressure (20W at 5mTorr), can be seen clearly as a drop in the measured RF current and voltage to the antenna, although the measured power is unchanged. More power is actually being absorbed by the plasma in the inductive mode as the phase difference between the voltage and current is reduced. Knowing the electrical characteristics of the antenna circuit one can estimate the plasma resistance. This information can help investigate the heating process of the low pressure ICP (chapter 5). Most importantly the power input to the plasma can be determined, although this is not a straightforward procedure as will be discussed later. Since the matching of the overall system can be detrimentally affected by the addition of any electrical component to the overall circuit, the power, voltage and current probes are designed to have a minimal effect on the RF signal. To allow an accurate measurement of the voltage and current on the antenna, the probes are placed next to the antenna input, the power meter is placed next to the power supply as it has an input impedance of  $50\Omega$ . The power meter, RF voltage and current probes are described in detail below.

#### **3.2.1 The power meter.**

A directional power meter, Bird model 43, is used to measure the RF power. It has a power range of 1W to 1kW and a frequency range of .45MHz to 2300MHz. The meter contains a rotatable element to sense both forward and reverse powers. The

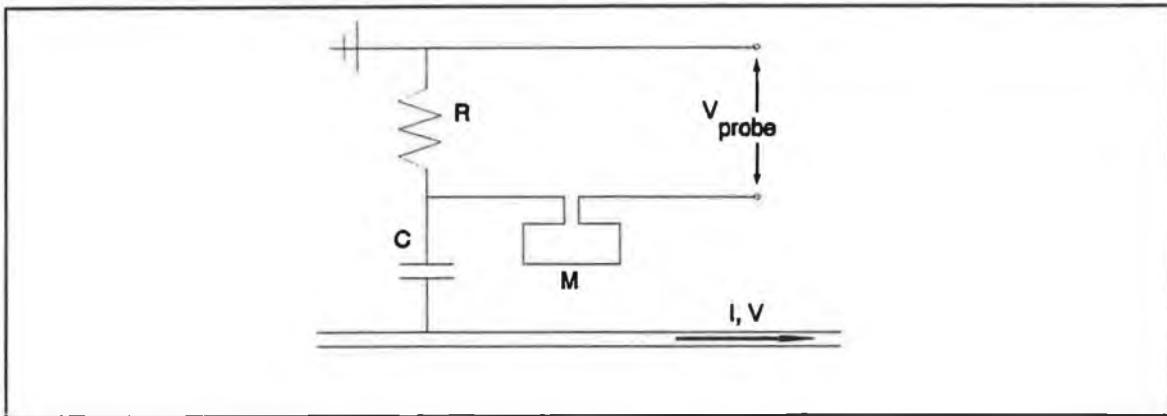


Figure 3.1: RF power meter circuit diagram.

element contains a loop which can detect the magnetic field in the nearby section of the RF current carrier. A voltage appears across the loop proportional to both the current in the current carrier and the mutual inductance between the loop and the current carrier.

The meter circuit is shown in figure 3.1. The voltage seen by the meter is the voltage drop across the resistor R plus the voltage drop across the loop with mutual inductance M with the RF line,

$$V_{probe} = j\omega CRV \pm j\omega MI \quad 3.1$$

The voltage across the loop can be either positive or negative depending on its orientation. The value of R is set very much smaller than the capacitor reactance and the components are also chosen such that,

$$CR = \frac{M}{Z_0} \quad 3.2$$

where  $Z_0$  is the characteristic impedance of the line carrying the RF current, which is  $50\Omega$ . The probe voltage is now,

$$V_{probe} = j\omega M \left( \frac{V}{Z_0} \pm I \right) \quad 3.3$$

The voltage at any point on the transmission line is equal to the sum of the forward and reflected voltages,  $V_f + V_r$ . The current is equal to the forward minus the reverse current,

$$I = \frac{V_f}{Z_0} - \frac{V_r}{Z_0} \quad 3.4$$

Thus when the probe element is turned to face the load, in the forward direction, the probe voltage becomes,

$$V_{probe} = \frac{j2 \omega M V_f}{Z_0} \quad 3.5$$

When the probe is rotated by 180° to face the source one finds,

$$V_{probe} = \frac{j2 \omega M V_r}{Z_0} \quad 3.6$$

The voltage on the probe is rectified to give a dc signal, and displayed on a meter calibrated in RF watts.

In practice not all of the forward power measured by the power meter will be deposited in the plasma. As much as 90% of the RF power can be lost in the RF circuit. As a result of the increase in component resistance at RF, due to the skin effect, much of the losses will occur at soldered joints in the line. Several methods for calculating power losses in the circuit are discussed in section 3.3.1.

### 3.2.2 The RF voltage probe.

The voltage probe circuit, shown in figure 3.2, is basically a voltage divider employing a capacitor and resistor. The presence of the capacitor means that the probe only samples the ac part of the RF signal. The voltage probe is placed between the matching unit and antenna to allow the voltage on the antenna to be determined as accurately as possible. A resistive divider network cannot be used as it would cause severe loading of the RF signal to the antenna. The voltage drop across the probe output is proportional to the voltage drop across the load. To ensure the current drawn by the probe is negligible compared with the current to the antenna, the impedance of the probe is kept high. The capacitance of the probe is 3-5pF, which at 13.56MHz has an

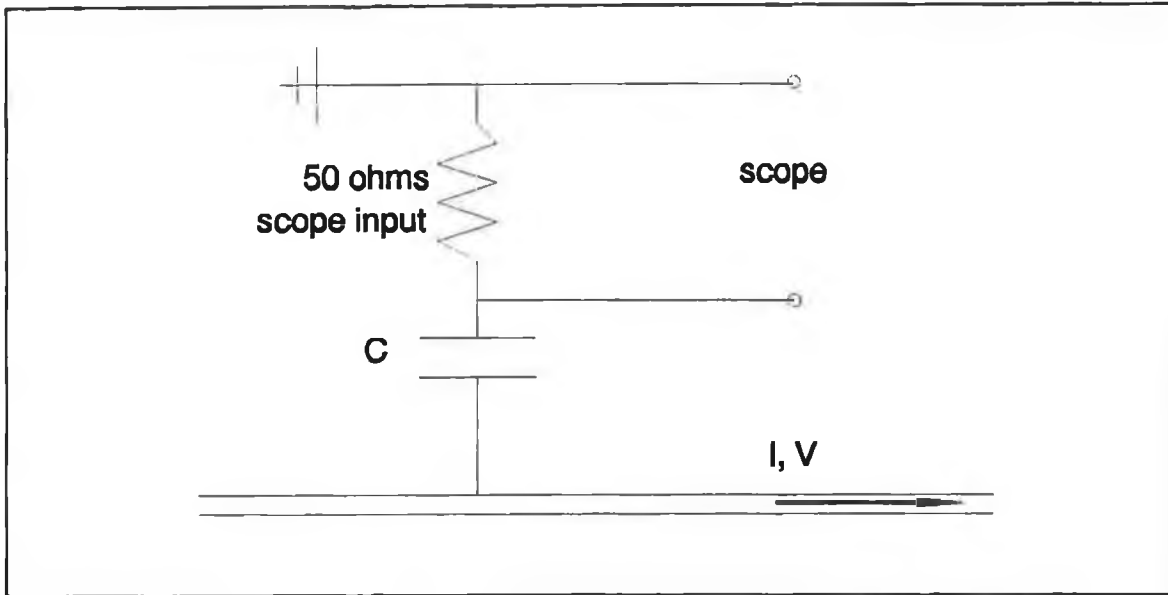


Figure 3.2: RF voltage probe circuit diagram.

impedance of 3.9-2.3k $\Omega$ . The probe can be read directly from a scope with a 50 $\Omega$  termination, and has a scaling factor of 213.7:1.

The circuit in figure 3.3 is used to calibrate the probe. The idea is to measure the actual voltage of the RF signal at the probe and compare it with the voltage output of the probe. A 50 $\Omega$  internal termination on the HP5402A scope allowed the line voltage to be determined accurately, the scope input being perfectly matched with the generator output of 50 $\Omega$ . A range of input powers, below 5W to prevent damaging the scope, were chosen to obtain an average ratio of input voltage to probe voltage.

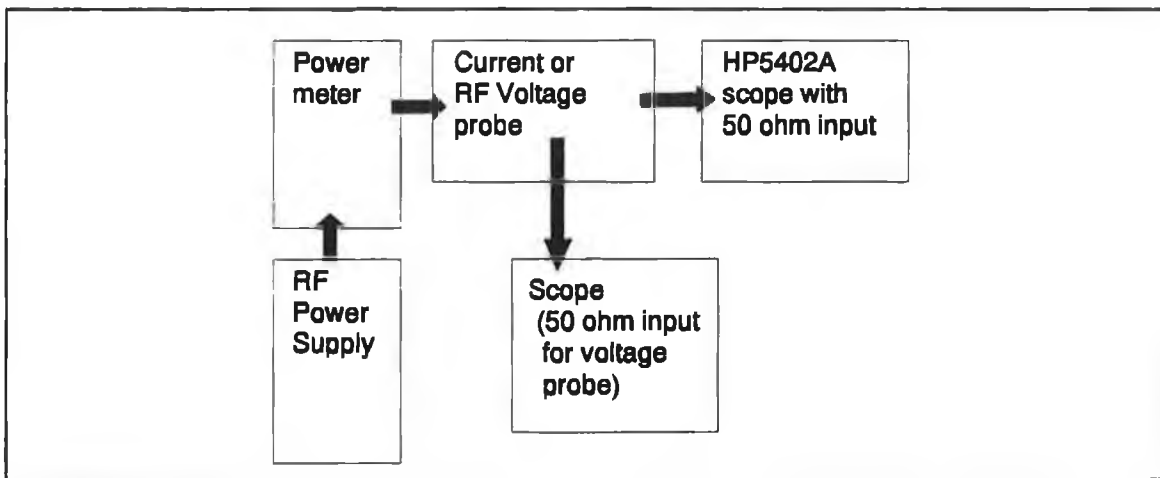


Figure 3.3: RF probe calibration setup.

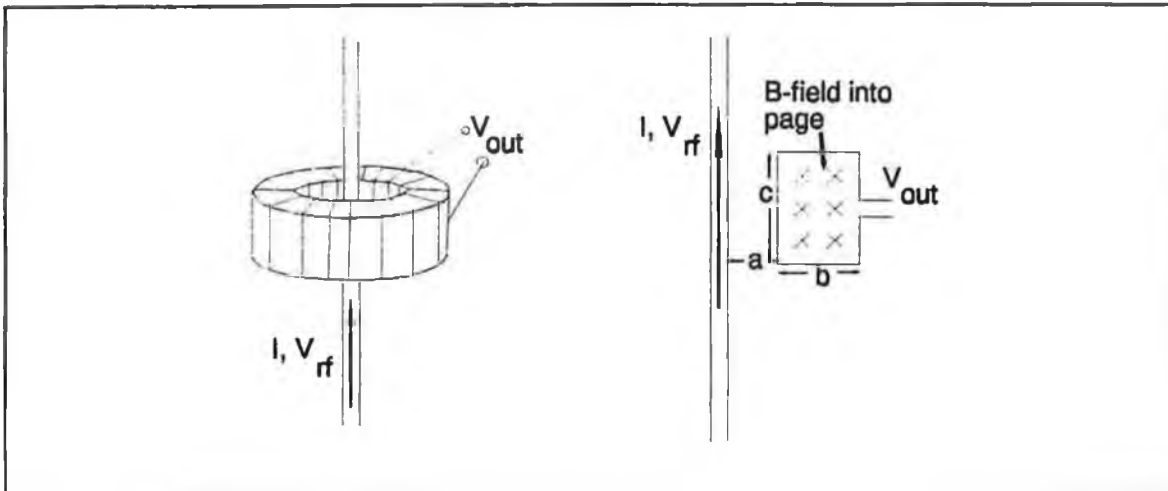


Figure 3.4: Rogowski coil and one loop of coil.

### 3.2.3 The RF current probe.

The RF current probe is used to measure the current at the antenna and is positioned between the voltage probe and the antenna. The probe itself is basically a Rogowski coil placed around the RF line as shown in figure 3.4. Rogowski coils are widely used high frequency current measuring devices [1,2]. The coil is made up of an insulating torus around which is wrapped a thin conducting wire. From Amperes law the magnetic flux from the RF current,  $I = I_0 \sin\omega t$ , flowing in the line is [3],

$$\underline{B} = \frac{\mu_0 I}{2\pi r} \quad 3.7$$

The magnetic flux  $\phi$  threading one loop is,

$$\phi = \int \underline{B} \cdot \underline{A} = \frac{\mu_0 I_0 \sin(\omega t) c}{2\pi} \int_a^{a+b} \frac{dr}{r} \quad 3.8$$

where a, b and c are the coil dimensions shown in figure 3.4. From Faradays induction law there will be a voltage induced on the loop as a result of the flux  $\phi$  threading the loop and also another contribution due to the loop inductance, L,

$$V = \frac{-d\phi}{dt} + L \frac{dI_c}{dt} \quad 3.9$$

where  $I_c$  is the current in the rogowski coil. One can also write this in terms of the coil resistance,  $R$ ,

$$I_c = -\frac{1}{R} \frac{d\phi}{dt} + \frac{L}{R} \frac{dI_c}{dt} \quad 3.10$$

By setting the value of  $L/R$  greater than the RF frequency one can relate the flux threading the rogowski loops and the current flow in the coil directly,

$$\frac{I_c}{L} \approx \phi \quad 3.11$$

One therefore can get a frequency independent response from the coil which is known as an integrating rogowski coil.

To prevent the rogowski coil itself acting as one large current sensing loop, the return wire is fed back along the torus through the centre of the individual loops. Another method to prevent a distorted signal is to reduce the magnetic flux linking the rogowski coil torus. This can be achieved by placing the coil inside a conducting shield. Any flux threading the torus will induce a current in the shield which in turn will

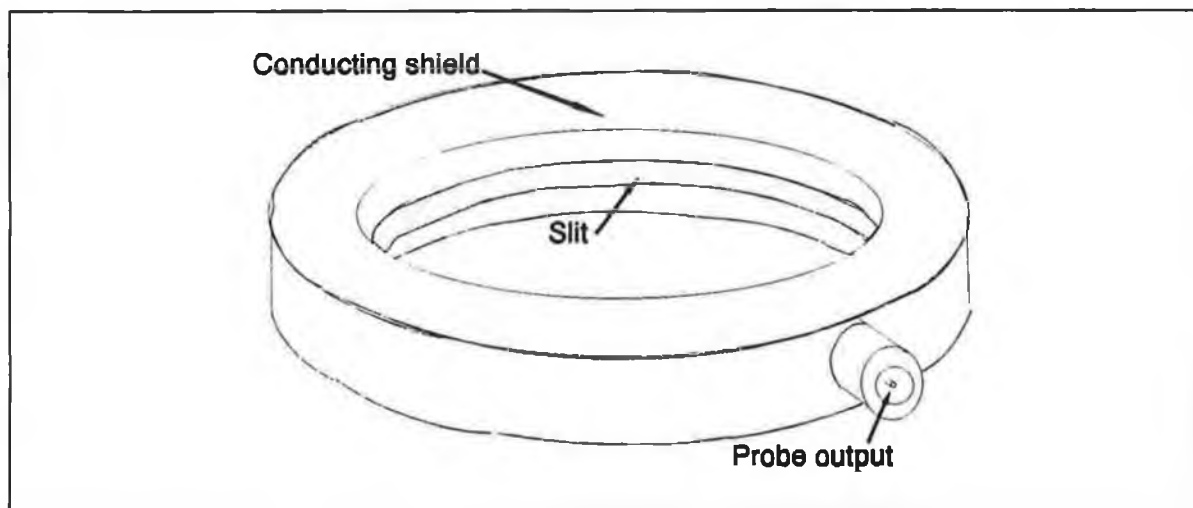


Figure 3.5: Rogowski coil shielding.

produce a magnetic field in the opposite direction, thus reducing the magnetic flux passing through the torus. There is a slit cut around the inside of the shield to allow measurement of the RF current in the line (figure 3.5) [1].

The probe is calibrated using a method similar to the voltage probe calibration, figure 3.3. An RF current is fed down the line to a 50Ω scope input. From a voltage reading on the scope the current in the line can be calculated and this is compared with the voltage output by the current probe itself. The RF power is reset at several values below 5W to allow a calibration curve to be determined without damaging the oscilloscope. The probe was found to have an output of 135mV per Amp.

### 3.3 RF parameter measurement.

#### 3.3.1 RF power measurement.

Obviously not all the power measured at the power meter, which is positioned at the power supply, will reach the antenna. There will be losses in the RF network at circuit connections and in the line itself. There are several methods used to determine the actual power which reaches the discharge [4]. One can obtain the discharge power using current and voltage probes positioned next to the antenna input if the phase difference between the two,  $\phi$ , is known,

$$P_d = V_{rms} I_{rms} \cos\Phi \quad 3.12$$

Another method is to multiply the voltage and current waveforms and integrate the result over one cycle,

$$P_d = \frac{1}{T} \int V(t)I(t)dt \quad 3.13$$

A third method used to determine the power dissipated in the discharge is to subtract the power dissipated in the circuit with a plasma present from that without a plasma. The plasma is switched on and the matcher is tuned until the power reflected is a minimum. The forward power is then determined using the power meter and the peak to peak voltage is measured on an oscilloscope using the RF voltage probe positioned at the

antenna. The power to the system is reduced until the plasma is extinguished. Without adjusting the matching unit, the power is increased again until the peak to peak voltage reaches the value measured with a plasma switched on. The forward power is then read off the power meter. The power to the discharge is simply the difference in the powers measured with and without a plasma. For the experiments carried out here the power is measured directly from the power meter as power losses are low when the discharge operates inductively (<15%).

### 3.3.2 Determination of the electrical characteristics of the antenna and plasma.

Investigating the behaviour of the load impedance, the impedance of the antenna and plasma, is a useful way of studying the characteristics of an ICP. It can give an insight into the interaction of the antenna electromagnetic fields and also provide evidence as to the heating mechanism prevailing in a low pressure discharge. These aspects are discussed in detail in sections 2.3 and 2.4.

The load impedance,  $Z_L = R_L + j\omega L_L$ , can be determined from RF power meter, RF current and RF voltage measurements where,

$$\frac{V_{rms}}{I_{rms}} = \sqrt{R_L^2 + \omega^2 L_L^2} \approx \omega L_L \quad 3.14$$

and,

$$R_L = \frac{Power}{I_{rms}^2} \quad 3.15$$

Equation 3.14 is a good approximation when the load resistance is very much less than the load reactance, which is usually the case.

Plasma resistance measurements taken for the investigation of the low pressure heating mechanism of the ICP require only relative values, the actual resistance is not required. Thus the resistance measurements taken here are sufficient even though the contribution of the antenna resistance is not subtracted. The contribution of the antenna

to the measured resistance is assumed to be constant for all measurements taken, so any changes in resistance are solely due to the plasma.

The same argument can be made for the inductance measurements. Any changes observed in the inductance of the load will be due to the plasma. The inductance measurements show the electromagnetic interaction of the antenna magnetic field and the magnetic field set up by the plasma current. The magnetic field produced by the plasma opposes the magnetic field of the antenna, thus reducing the overall magnetic flux of the system, which leads to a reduction in load inductance.

### 3.4 Plasma parameter diagnostics.

#### 3.4.1 The magnetic field probe.

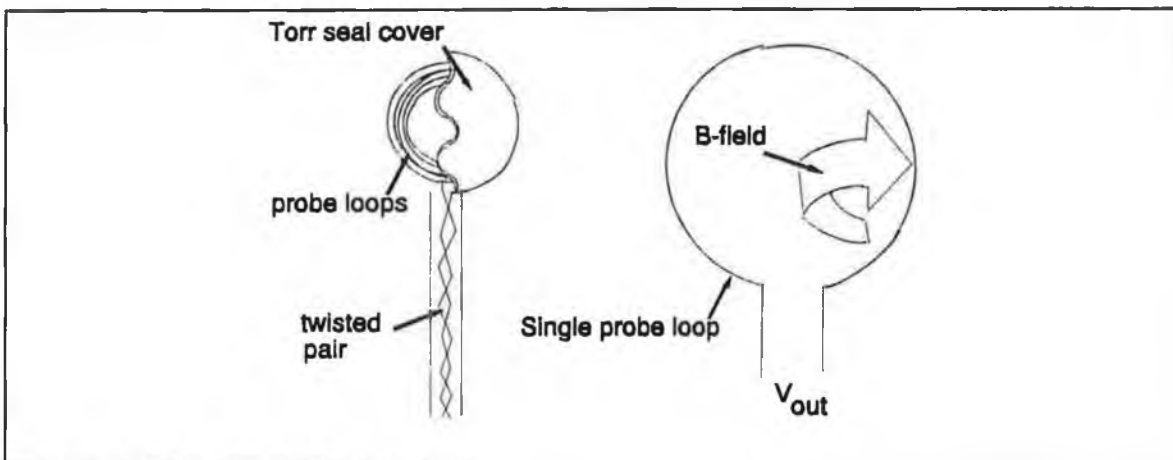


Figure 3.6: Magnetic field probe.

The magnetic field probe works on a similar principle to the Rogowski coil or RF current meter described above. It senses the magnetic field from the antenna in the plasma and a voltage can be measured at its output terminals which is proportional to the strength of the magnetic field. As before, from Faraday's induction law, voltage is induced on a conducting coil when magnetic flux passes through it [5,6],

$$V_p = -\frac{d\phi}{dt} = -\int \frac{dB}{dt} \cdot dA \quad 3.16$$

The probe output is therefore proportional to the time rate of change of the magnetic

field (which is proportional to the magnetic field strength), and the probe is also referred to as a "B dot" probe. The probe usually has several loops of wire are wrapped around a central holder to magnify the induced voltage on the probe Figure 3.6.

The probe constructed for this experiment was made from .4mm diameter wire looped 15 times around a 1cm circular holder. The probe tip was covered with Torr Seal resin and the probe terminals were extracted as a twisted pair through a 4mm diameter pyrex tube through a Wilson seal. By wrapping the output terminals of the probe as a twisted pair distortion of the signal is reduced as the only induced voltage measured would be that due to the magnetic field threading the probe tip. The Wilson seal allowed radial movement of the probe from next to the antenna to near the chamber wall. Care was made that measurements were taken when the probe output was a maximum i.e. when probe loops faced parallel to the antenna axis and perpendicular to the antenna magnetic field. With the probe inserted into the plasma there was no appreciable change in the reflected power measured by the power meter indicating that the effect of the probe on the discharge was negligible.

### **3.5 The Langmuir probe.**

#### **3.5.1 Introduction.**

The Langmuir probe is a widely used plasma diagnostic technique for the determination of discharge parameters such as electron and ion density, electron temperature, plasma potential, floating potential and electron energy distribution function (EEDF). By careful design the probe may be made to take measurements of local discharge conditions at any required position within the plasma. Interpretation of probe measurements is not straightforward, but there are well established theories for low pressure plasmas such as those of Laframboise and Druyvestyn, for analysing probe data. Using the Langmuir probe in RF plasmas can cause complications as the probe output can be distorted. This problem will be discussed in this section as well as a brief explanation of the probe theories used.

#### **3.5.2 Theory of probe operation.**

The Langmuir probe is a biasable conductor placed in the plasma. As the voltage

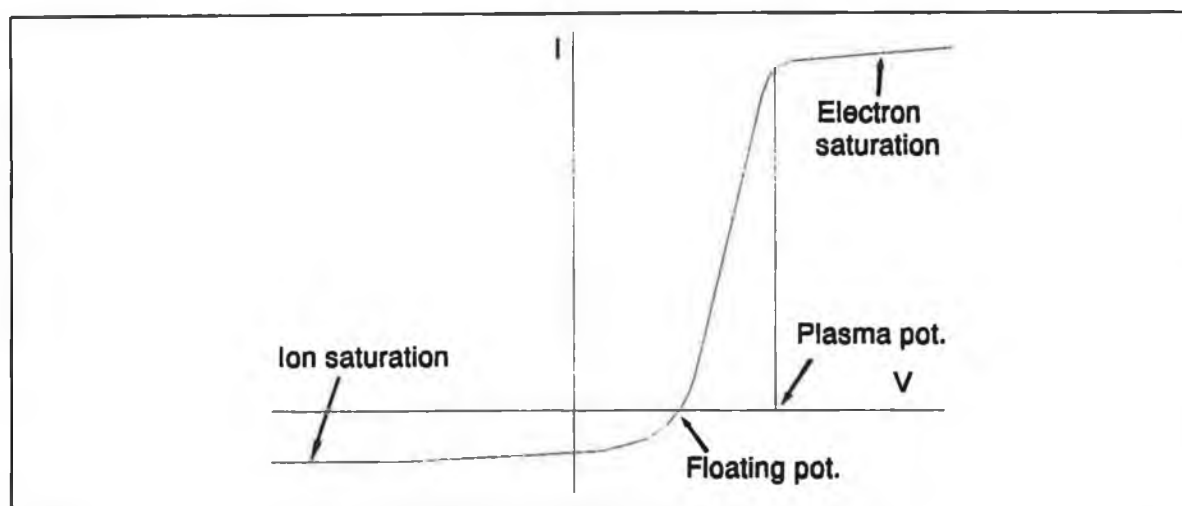


Figure 3.7: Ideal probe characteristic.

put on the probe with respect to the discharge chamber is changed, the current drawn by the probe also changes. It is the relation between the probe current and voltage, which is the key to the Langmuir probe diagnostic. The probe conductor is usually small so that it does not perturb the plasma. It can be cylindrical, plane or spherical in shape depending on the application. A plane disc probe with one exposed face was used specifically for directional measurements in this project, section 5.2, while a cylindrical probe was used for measurement of general plasma characteristics.

The theory which one applies to analyze this data depends on the gas pressure in the plasma being examined. The low pressure theory of Laframboise and Druyvestyn [7-9] can be applied when,

$$r_p < \lambda ; \lambda_D < \lambda \quad 3.17$$

where  $r_p$  is the probe radius,  $\lambda_D$  is the debye length and  $\lambda$  is the electron mean free path. Thus the plasma is collisionless around the probe and the possibility of electrons being accelerated to the probe and causing ionisation of neutral particles there is discounted. If this ionisation were to occur it would add a component to the probe current not present in the bulk plasma. One must also make some further assumptions: the bulk plasma is made up of a quasi-neutral collection of neutrals, electrons and single charge positive ions, the plasma is sufficiently collisional for these particles to be described by a Maxwellian energy distributions, there are no magnetic fields present and all charged particles which

reach the probe are collected [9]. The final assumption prevents the occurrence of secondary electron emission from the probe surface. If highly energetic electrons strike the probe surface with energies above the work function of the probe they may dislodge charged particles from its surface [7]. These electrons would then contribute a current to the probe which is not present in the background plasma. Obviously the real plasma may not conform to these assumptions, so one must appreciate this fact when interpreting the probe results.

When a voltage is placed on the probe it attracts charge of the opposite sign and repels charges of the same sign. Thus around the probe a sheath of oppositely charged particles forms which tends to shield the probe electric field from the surrounding plasma. There is a quasi-neutral presheath region between the probe sheath and bulk plasma into which the probe potential penetrates, according to the Bohm criterion for sheath formation [10]. In the presheath, the probe potential accelerates the ions to energies of half the electron temperature at the sheath edge,  $E_+ = kT_e/2$ , which is required for stable sheath formation. The sheath is effectively a potential well for charged particles of opposite sign to the probe potential and a potential gradient for like charged particles. Therefore the majority of oppositely charged particles which enter the sheath will be collected; some charged particles can form orbits around the probe and not be collected (orbit limited current [7]) Those particles of like charge have to have sufficient energy to overcome the sheath potential in order to be collected by the probe.

This behaviour can be noted from the shape of the I-V characteristic, figure 3.7. When the probe potential is sufficiently negative only ions which enter the probe sheath are collected as there are no electrons with sufficient energy to overcome the potential barrier around the probe. The current collected by the probe is known as the ion saturation current and is given by,

$$I_{+sat} = n_+ e v_+ S \quad 3.18$$

where  $v_+$  is the average ion or acoustic ion velocity, and  $S$  the probe collecting area or in this case the sheath area around the probe (a function of probe voltage).

When the probe voltage is increased the probe begins to pick up energetic

electrons. This region of the probe characteristic is known as the electron retardation region. The probe current now becomes,

$$I_{probe} = n_+ e v_+ S - \frac{n_e e v_e S}{4} \exp\left(\frac{e(V_{pro} - V_{pla})}{kT_e}\right) \quad 3.19$$

where  $V_{pro}$  is the probe voltage and  $V_{pla}$  is the plasma potential.

A point is reached, the floating potential, when the net current collected by the probe is zero i.e. the electron and ion fluxes to the probe are equal,

$$n_+ e v_+ S = \frac{n_e e v_e S}{4} \exp\left(\frac{e(V_{pro} - V_{pla})}{kT_e}\right) \quad 3.20$$

As the probe voltage is raised still further, more and more electrons are collected as the sheath potential is reduced. When the probe sits at the plasma potential, the sheath disappears and the probe current is due only to the thermal flux of electrons and ions. The current collected now is,

$$I_{probe} = \frac{n_+ e v_+ S}{4} - \frac{n_e e v_e S}{4} \quad 3.21$$

Since the electron velocity is very much greater than the ion velocity the probe current is electron dominated. As the ion energies are very much less than the electron energies, the fall off of the ion current to the probe occurs quickly as the probe voltage is raised a few volts above the plasma potential. When the probe voltage is sufficiently positive so that only electrons are collected by the probe, the probe current is known as the electron saturation current,

$$I_{esat} = \frac{n_e e v_e S}{4} \quad 3.22$$

### 3.5.3 Langmuir probe plasma parameter measurement.

From the I-V characteristic one can determine some of the characteristics of the plasma [11]. Considering the electron current to the probe in the electron retardation region to be given by,

$$I_e = \frac{n_e e v_e S}{4} \exp\left(\frac{e(V_{pro} - V_{pla})}{kT_e}\right) \quad 3.23$$

Taking the log of this equation and differentiating both sides with respect to the probe voltage one finds,

$$\frac{d \ln I_e}{dV} = \frac{e}{kT_e} \quad 3.24$$

Thus from the inverse of the slope of a plot of  $\ln I_e$  versus probe voltage one can determine the electron temperature. One problem in determining this parameter is knowing the electron current to the probe. To do this one must first know the ion current to the probe and take it away from the total probe current. An estimate of the ion current present can be found from the ion saturation current taken from the I-V characteristic.

The plasma potential can be estimated from the maximum of the first derivative of the I-V characteristic,

$$\left. \frac{dI}{dV} \right|_{\max} = V_p \quad 3.25$$

This is not quite accurate as the maximum in the derivative can occur below the voltage where electron saturation is reached. This can be corrected using the current and voltage found at the maximum derivative,

$$I_{\maxderiv} = I_0 \exp\left(\frac{V_{\maxderiv} - V_p}{kT_e}\right) \quad 3.26$$

where  $I_0$  is the electron saturation current. From this one finds the plasma potential to be,

$$V_p = V_{maxderiv} + kT_e \ln\left(\frac{I_0}{I_{maxderiv}}\right) \quad 3.27$$

The floating potential can be found where the I-V characteristic crosses the voltage axis when the probe draws no net current. When the electron saturation current and electron temperature are known, equation 3.22, one may determine the electron density,

$$n_e = \frac{4I_0}{e v_e S} = \frac{4I_0}{e S} \left(\frac{\pi m_e}{8kT_e}\right)^{1/2} \quad 3.28$$

This analysis is derived from the theory of Laframboise where the assumptions mentioned above are made.

#### 3.5.4 EEDF measurement.

One of the most important characteristics of a plasma is the electron energy distribution function or EEDF. From it one can determine average characteristics of the plasma,

$$\int f(\epsilon) X(\epsilon) d\epsilon = \langle X \rangle \quad 3.29$$

where  $X(\epsilon)$  is the quantity of interest [12]. It is important for the calculation of process rates involving electrons, such as ionisation,

$$\int f(\epsilon) \sigma(\epsilon) v(\epsilon) d\epsilon = \langle \sigma v \rangle \quad 3.30$$

The Druyvestyn formula may be used to determine the EEDF of an isotropic plasma from the second derivative of the electron retardation region of the I-V characteristic, and is given by,

$$\frac{d^2 I}{dV^2} = \frac{en_e S}{2} \left(\frac{e}{2m_e}\right)^{1/2} f(\epsilon)(\epsilon)^{-1/2} \quad 3.31$$

The assumptions made about the condition of the plasma which were made in the Laframboise analysis also apply here.

To determine the EEDF for a given plasma, the plasma potential is firstly ascertained, often using the analysis above or the voltage at which the second derivative of the I-V characteristic goes to zero. The plasma potential is then the zero energy reference for the energy distribution. In this project the second derivative of the I-V characteristic was taken at energy steps of .5eV at low electron energies, up to 5eV, and 1eV steps at higher electron energies up to 50eV. Having determined the EEDF one can integrate it to give the electron density at probe position.

### 3.5.5 Langmuir probes in RF plasmas.

The use of Langmuir probes in RF plasmas is not straightforward as RF distortion of the probe characteristic can occur. Unlike dc plasmas where the plasma potential is time invariant, the plasma potential of an RF plasma is time dependent. A fixed bias probe will therefore draw a time dependent current as the voltage drop across the plasma-probe sheath changes. It can be assumed that the plasma density and electron temperature are time independent if the inequalities,

$$\omega > \nu_{ion} \quad ; \quad \omega > \kappa \nu_{en} \quad 3.32$$

hold, where  $\kappa$  is the proportion of energy transferred per electron neutral collision ( $2m_e/M$ ). For the low pressure Argon plasmas in this study these conditions are satisfied [13].

The current drawn by a probe placed in an RF plasma can be written as [14],

$$I_{probe} = I_+ - I_e(t) \quad 3.33$$

The positive ion current collected by the probe is not modulated by the RF as the ion frequency is less than the driving frequency, and ions cannot follow the changes in the RF field,

$$\omega > \left( \frac{ne^2}{m_+ \epsilon_0} \right)^{1/2} \quad 3.34$$

Assuming that the plasma potential in an RF plasma has a sinusoidal variation it can be given by,

$$V_p(t) = V_{pdc} + V_{prf}(t) = V_{pdc} + V_{prf} \sin \omega t \quad 3.35$$

where  $V_{pdc}$  is the dc component of the plasma potential and  $V_{prf}$  is the RF component. Therefore equation 3.33 becomes,

$$I_{probe}(t) = -I_0 \exp(e(V - V_{pdc} - V_{prf})) + I_+ \quad 3.36$$

An instantaneous measurement of the probe current will include the RF distortion and a subsequent measurement at the same probe bias at a later time may produce a different result. Taking instead the time averaged probe current one finds,

$$\bar{I}_{probe} = -\frac{I_0}{T} \exp(e(V - V_{pdc})) \int_0^T \exp(e(-V_{prf} \sin \omega t)) dt + \bar{I}_+ \quad 3.37$$

or,

$$I_{probe} = -AI_{dc} + I_+ \quad A > 0 \quad 3.38$$

Thus the electron current to the probe in the electron retardation region is increased due to the RF distortion.

At the floating potential the electron and positive ion currents drawn by the probe are equal. In an RF plasma the floating potential occurs at a lower probe voltage than in a dc plasma, because the probe will draw enough electrons at a lower bias to cancel the positive ion current. The electron temperature, which can be found using equation 3.24, will be overestimated as the slope of the electron retardation part of the I-V characteristic is reduced. From equation 3.28, one can also see that the electron density calculated will be underestimated. Typical dc and RF I-V characteristics are compared in figure 3.8 and

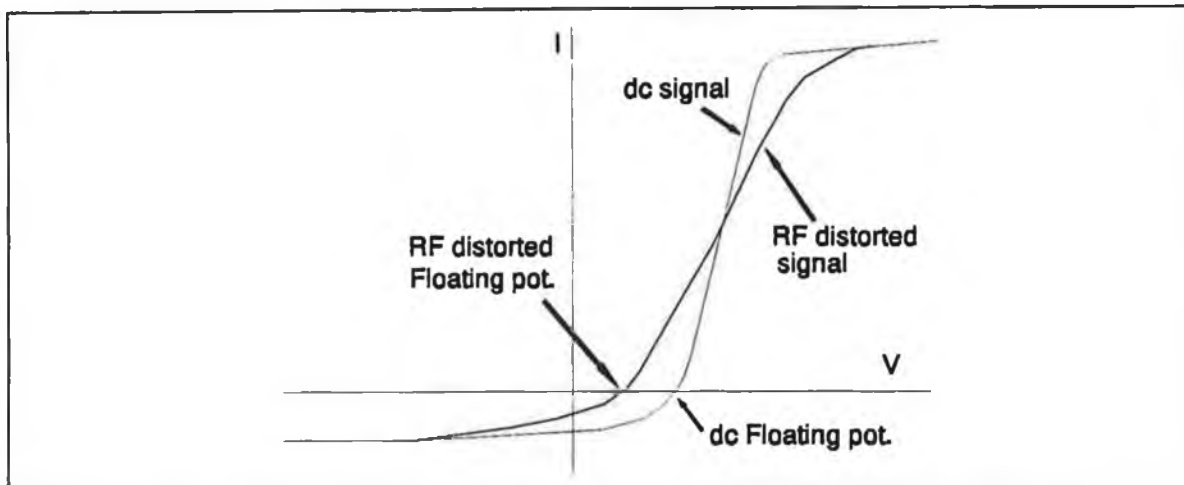


Figure 3.8: Comparison of dc and RF distorted I-V characteristic.

show the probe distortion resulting from the RF fluctuation of the plasma potential. This distortion will obviously effect the first and second derivative of the I-V curve and therefore effect EEDF measurements [8,15,16].

The problem with Langmuir probe operation in RF plasmas is to remove the RF voltage from the applied RF probe voltage.

### 3.5.6 The tuned probe.

There are several possible approaches used to acquire an undistorted probe characteristic from an RF plasma. Time-resolving the probe output from an ordinary Langmuir probe is one possibility, but it requires fast measurement times, much less than one RF cycle [17]. This is difficult at high RF frequencies ( $> 1\text{MHz}$ ) as a sheath, as demanded by the probe theory, cannot fully form in less than one RF cycle as ions cannot follow the instantaneous RF field,  $\omega > \omega_i$ . Another method is to superimpose an RF signal of the same frequency, amplitude and phase on the probe and thus eliminate the RF voltage across the probe plasma sheath [18]. This is difficult in practice as the plasma RF signal is likely to include harmonics which would be difficult to match using external circuitry. A capacitive probe can be used to measure the actual time varying plasma potential and then the distorted I-V characteristic can be 'undistorted' using complex numerical techniques [19].

The method used here is to employ a tuned probe which filters out the RF signal

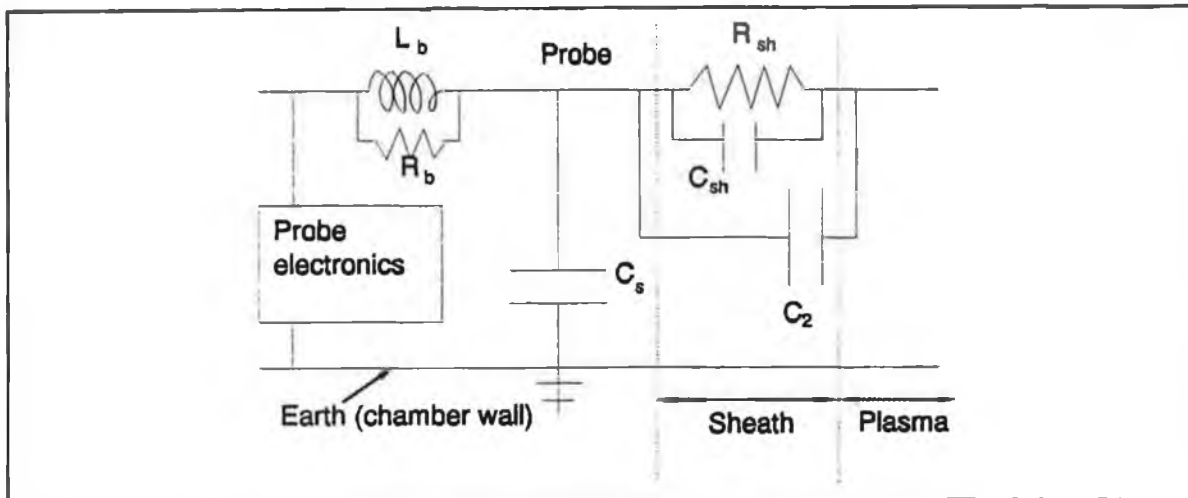


Figure 3.9: Probe circuit diagram including plasma.

before it reaches the probe diagnostic hardware [20,21]. To reduce the distortion of the probe signal the probe sheath potential must be low, less than the electron temperature. Thus only a small fraction of the RF fluctuation occurring in the plasma can be allowed fall across the probe-plasma boundary.

A circuit diagram of the tuned probe is shown in figure 3.9.  $C_{sh}$  and  $R_{sh}$  represent the probe sheath impedance and  $C_s$  the stray impedance between the probe and chamber wall. From simple component analysis one can approximate the probe sheath impedance to be that of a cylindrical capacitor,

$$C_{sh} = 2\pi\epsilon_0 \frac{1}{\ln[(r_{sh} + r_p)/r_p]} \quad 3.39$$

where  $r_p$  is the probe radius and  $r_{sh}$  is the sheath radius. The probe sheath thickness may be estimated from the Langmuir equation,

$$r_s \approx (1 + V/kT_e)^{1/2} \cdot \lambda_D \quad 3.40$$

where  $V$  is the probe voltage with respect to the plasma potential and  $\lambda_D$  the Debye length. This is approximately .59pF for a plasma density of  $1 \times 10^{10} \text{cm}^{-3}$  electron temperature of 2eV and letting  $r_s \approx 2\lambda_D$ . Compared with a stray capacitance of approximately 2-5pF, one can see that most of the RF voltage will fall across the probe sheath. By inserting a capacitor in parallel with  $C_2$  one can immediately reduce the probe

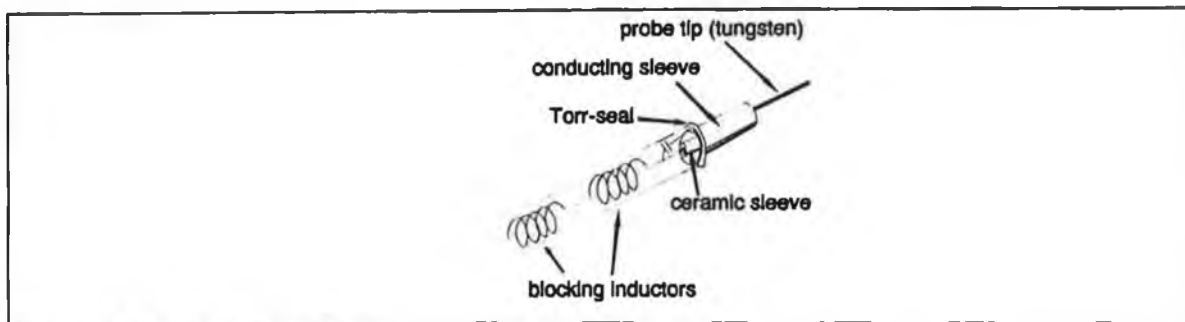


Figure 3.10: Tuned probe.

impedance. This new capacitor takes the form of a thin 1.5mm radius, conducting cylinder linked capacitively to the probe tip. The cylinder is unbiased but in contact with the plasma and therefore a sheath of approximately one Debye lengths thickness forms around it. Using equation 3.40 above one can again estimate this sheath resistance to be approximately 18pF. As the probe capacitance is now dominated by an unbiased capacitance  $C_2$ , the probe capacitance is now independent of probe bias. The voltage drop across the probe sheath is reduced as more of the RF voltage will now appear across the stray impedance.

To reduce the RF voltage drop across the probe sheath still further the impedance of the probe to ground can be increased with the introduction of a blocking self-resonant inductor,  $L_b$ . The inductor ( $100\mu\text{H}$ ) has a self resonant frequency of approximately 13.56MHz i.e. at that frequency it presents a large impedance to the RF signal. This results in a very large probe to ground impedance meaning that less of the RF signal will be dropped across the probe sheath, resulting in an undistorted probe signal.

Figure 3.10 shows a diagram of the tuned probe. The ceramic cylinder is used to separate the probe tip from the metallic sleeve. The probe tip is usually short, 5mm to 10mm, of .2mm to .5mm radius and made from tungsten. The inductors are placed as close as possible to the probe tip to reduce the loading of the probe output due to parasitic capacitances.

Another version of the tuned probe is a tuned disc probe, figure 5.1, which was used to take directional measurements in the plasma. It could be rotated to face in the direction of interest, principally in the azimuthal direction where an electron current was detected and then in the longitudinal direction to sample the background plasma. As the probe has only one open face it detected the electron current, which followed the induced

electric field, during every alternate half cycle and thus acted as a diode. The probe output is therefore given by,

$$I_{probe} = I_{dc} + \int_0^{\pi} I_{0ele} \sin(\omega t) d\omega = I_{dc} + A \quad A > 0 \quad 3.41$$

where  $I_{dc}$  is the probe current due to the background plasma and the electron current is assumed to be sinusoidal with the probe sampling it for half a cycle, 0 to  $\pi$ . Thus there is an extra component on the probe output, regardless of the probe tuning, due to the electron current. EEDF measurements were taken using the probe and did show a directional dependence (section 5.1).

The probe is still of course open to measurement errors, the principal reason for measurement errors being probe contamination. The probe tip may become covered in spluttered material, glass from the test tube covering the antenna for example, which can contribute to additional resistance in the probe circuit. The collecting characteristics of the probe may also change when the probe gets hot due to high probe currents as the probe voltage is raised. This leads to a change in the probe work function meaning that the electron collecting properties of the probe tip can change. This effect can be seen as a hysteresis in the probe characteristic. Contamination can be reduced by bombarding the probe tip with ions by placing a high negative voltage on the probe (-1kV) or by heating the probe to white hot for a few seconds by placing a positive voltage on the probe tip (+100V) [8].

### 3.5.7 Probe diagnostic hardware.

In order to get fast and reliable plasma parameter measurements from the tuned probe output the probe system was fully automated [22]. Probe diagnostics hardware includes two digital to analogue convertors to read probe current and voltage measurements and to connect with a computer. The computer runs a QuickBasic program which sets the voltage on the probe and reads the probe current. Plasma parameters are calculated and then recorded by the computer.

### **3.6 Conclusion.**

Using the diagnostic techniques above, RF probes and plasma probes, one can make a detailed survey of the ICP. Although the probe techniques are quite versatile one must keep in mind the possibility of measurement errors occurring due to incorrect data interpretation or faults in diagnostic technique. To this end particular measurements were retaken several times to ensure the results had general agreement.

## References

- [1] D. G. Pellinen, M. S. Di Capua, S. E. Sampayan, H. Gerbracht and M. Wang. *Rev. Sci. Instrum.* **51**, 1535, (1980)
- [2] P. N. Murgatroyd, A. K. Y. Chu, G. K. Richardson, D. West, G. A. Yearly and A. J. Spencer. *Meas. Sci. Technol.* **2**, 1218, (1991)
- [3] P. Lorrain, D. P. Corson and F. Lorrain, *Electromagnetic Fields and Waves*, Freeman 1988.
- [4] V. A. Godyak and R. B. Piejak. *J. Vac. Sci. Technol. A*, **8**, 3833, (1990)
- [5] N. A. Krall and A. W. Trivelpiece. *Principles of Plasma Physics*. McGraw-Hill, (1973)
- [6] J. Hopwood, C. R. Guarnieri, S. J. Whitehair and J. J. Cuomo. *J. Vac. Sci. Technol. A*. **11**, 147, (1993)
- [7] J. G. Laframboise, Univ. of Toronto, Institute for Aerospace Studies, *Report no. 100*, (1966)
- [8] V. A. Godyak, R. B. Piejak and B. M. Alexandrovich. *Plasma Sources Sci. Technol.* **1**, 36, (1992)
- [9] L. Schott, *Plasma Diagnostics*, North Holland Publishing, Amsterdam, (1968)
- [10] B. N. Chapman, *Glow Discharge Processes*, Wiley, (1980)
- [11] M. B. Hopkins and G. W. Graham. *Rev. Sci. Instrum.* **57**, 2210, (1986)
- [12] B. E. Cherrington, *Gaseous Electronics and Gas Lasers*. Pergamon press, (1979)
- [13] J. V. Scanlan, Ph.D. thesis, Dublin City University, (1991)
- [14] A. P. Paranjpe, J. P. McVittie and S. A. Self. *J. Appl. Phys.* **67**, 6718, (1990)
- [15] N. St.J. Braithwaite, *Plasma parameters and the use of Langmuir probes*, internal report.
- [16] V. A. Godyak and R. B. Piejak, *Phys. Rev. Lett.* **65**, 996, (1990)
- [17] M. B. Hopkins, C. A. Anderson and W. G. Graham, *Europhys Lett.* **8**, 141, (1989)
- [18] N. St.J. Braithwaite and N. M. P. Benjamin and J. E. Allen, *J. Phys. E.* **20**, 1046, (1987)
- [19] N. Hershkowitz, M. H. Cho, C. H. Nam and T. Intrator, *Plasma Chem. Plasma*

Process. **8**, 35, (1988)

[20] R. R. J. Gagne and A. Cantin, *J. Appl. Phys.* **43**, 2639, (1972)

[21] J. V. Scanlan and M. B. Hopkins, *J. Vac. Sci. Technol. A.* **10**, 1207, (1992)

## **Chapter 4: ICP parameter measurement.**

### **4.1 Introduction.**

In this chapter results of an experimental investigation of the ICP system are presented. Measurements were taken in an Argon and also in a Hydrogen discharge using the diagnostic techniques described in chapter 3. The parameter measurements can be divided into two broad areas. Firstly external electrical measurements taken at the RF circuit powering the plasma. They give an insight into the mechanism by which power is coupled into to the discharge and allow the RF power absorbed by the plasma to be determined. The second category covers the measurements taken in the plasma using the Langmuir and magnetic field probes (the Hydrogen measurements were taken at a fixed probe position only whereas Argon measurements were taken radially as well as at a fixed position inside the discharge). Some of these measurements are examined in greater detail in chapters 5 and 6 in relation to specific aspects of low pressure ICP operation.

### **4.2 The experimental system.**

The experimental system is an ICP with an internal antenna positioned along the axis of the cylindrical discharge chamber as shown in figure 4.1. The system consists of four main component groups: the chamber and vacuum hardware, the RF circuit providing power to the antenna, the antenna and finally the diagnostic probes. The diagnostic probes are described in detail in chapter 3.

#### **4.2.1 The discharge chamber.**

The discharge chamber is a stainless steel cylinder, 30cm long and 20cm inside diameter (figure 4.1). At one end there is a 5cm diameter entry port for the introduction of the antenna piece. There are a total of eight NW25 ports available on the discharge chamber, allowing the connection of plasma probes and pressure gauges. Baratron, penning and pirani gauges are used for gas pressure measurement, the first two being used for the low pressure work. The base pressure of the system was  $10^{-6}$ Torr.

Behind the discharge chamber lies a second cylindrical chamber which formerly held an accelerator and faraday cup array for use as an accelerator in a negative ion experiment. Negative ions were produced in a pulsed filament driven multicusp Hydrogen

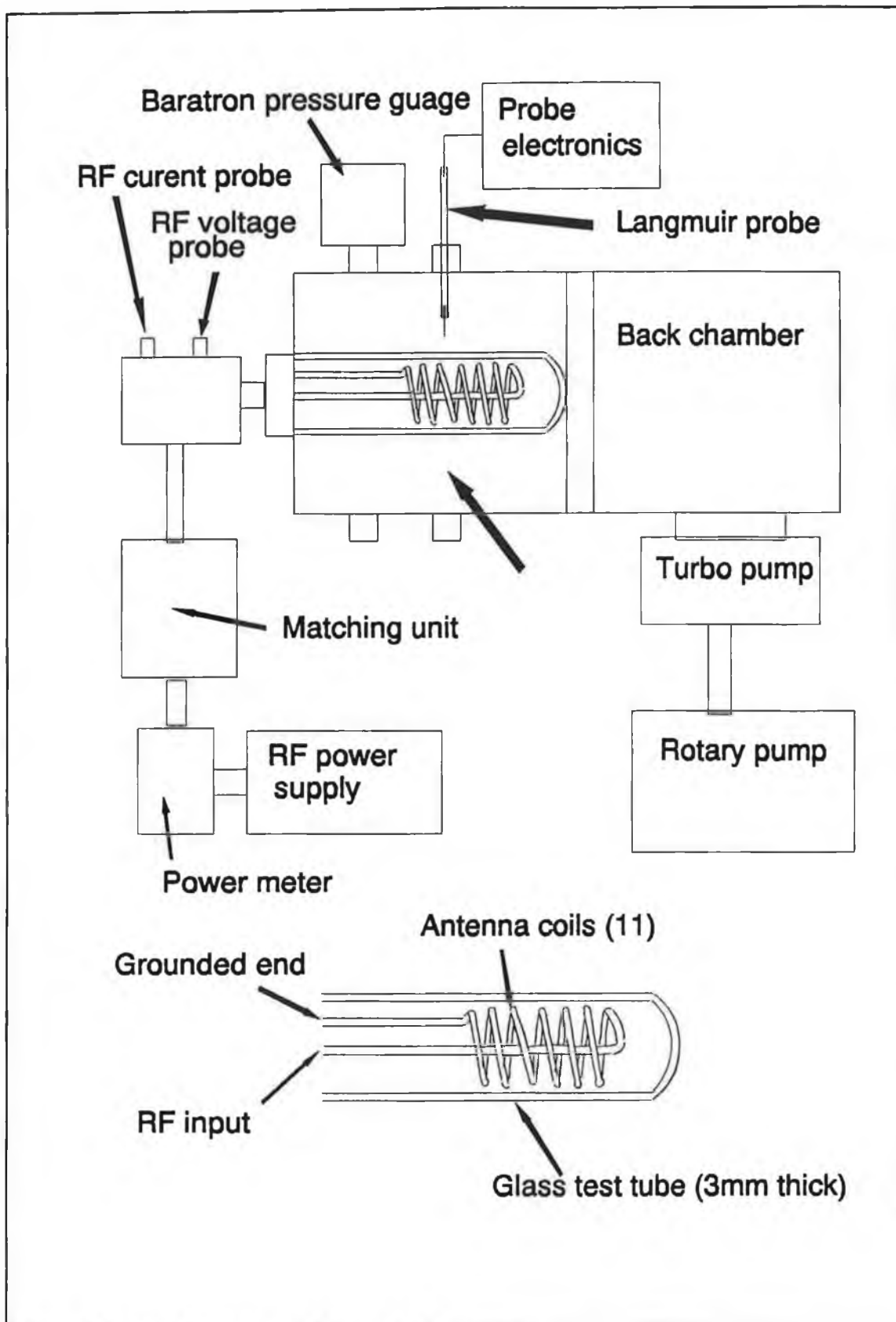


Figure 4.1. ICP experimental setup with antenna.

discharge and extracted by a positively biased accelerator placed close to one end of the discharge chamber. Extracted electrons were removed by placing magnets in the entry to the accelerator. The negative ions were then detected by a faraday cup placed behind the accelerator. Results seem to show an increase in extracted negative ion current shortly after discharge shutdown ( $100\mu\text{s}$ ) [1,2].

Connected to this second chamber is a 230l/s turbo pump coupled with a backing pump. The gas was introduced via a mass flow controller which allowed very sensitive adjustment of the chamber pressure.

#### **4.2.2 RF design considerations and the RF Circuit.**

Attention to safety must remain a priority when using RF. Contact with live high voltage RF equipment can cause severe burns, but the likelihood of such accidents can be reduced by properly shielding circuit elements and correctly earthing exposed equipment. The radiation emanating from the system at 13.56MHz is not close to the  $\text{H}_2\text{O}$  resonance frequency of 2.45GHz, used in microwave cooking, to be of great danger. However exposure to high radiation levels is inadvisable.

Radiated power at radio frequencies can cause problems with sensitive equipment. The power radiated from an oscillating voltage source is proportional to the fourth power of the frequency of oscillation [3]. Thus at RF, radiation losses can be significant. To prevent radiation leakage aluminium foil and aluminium shielding is used to cover any potential radiation sources, such as at lead connections etc. Equipment liable to be affected by the RF radiation, such as the langmuir probe diagnostic electronics, are housed in faraday cages.

Before work can begin on examining the inductively coupled plasma using the available diagnostic tools the problem of feeding RF power from the generator to the discharge must be overcome. A circuit must be designed to transfer maximum power to the plasma, but to do this the subtleties of circuit design at RF must be appreciated. At RF complications arise since circuit components can acquire properties unseen at dc or low frequencies. A component with a high impedance at low frequency can have a low impedance at RF. Even a piece of wire can have a non-negligible inductance and a significant resistance at RF. The effect of RF on probe measurements taken in the plasma should also be considered (section 3.3.8).

At low frequencies the entire cross-sectional area of a conductor is used as a transport medium for charge carriers, but as the frequency increases to RF levels the situation changes [4]. At RF a magnetic field is set up at the centre of the conductor as a result of the moving charges. This magnetic field impedes the flow of current down the centre of the conductor, so that more of the current flows around the perimeter. This phenomena is known as the skin depth effect, where the skin depth of the conductor is defined as the depth at which the current flowing in a conductor falls to 1/e of its value at the surface. Classically the skin depth of a particular material is related to its conductivity,  $\sigma$ , its permeability,  $\mu$ , and the applied frequency,  $\omega$ , as,

$$\delta = \left( \frac{2}{\omega \mu \sigma} \right)^{1/2} \quad 4.1$$

The resistance of conductors is increased at RF due to the skin depth effect as the current carrying cross-section is reduced (figure 4.2),

$$R_{RF} = R_{dc} \frac{r^2}{2\delta r - \delta^2} \quad 4.2$$

where  $r$  is the conductor radius [5].

Operating at RF can also effect the impedance properties of components. At low frequencies the impedance of a wire is insignificant, but the situation changes at RF. A magnetic field is setup outside a current carrier at RF and this alternating field induces a voltage on the wire which opposes the current flow. This property is known as self inductance. Also the resistance of the wire will increase due to the reduction of the cross-

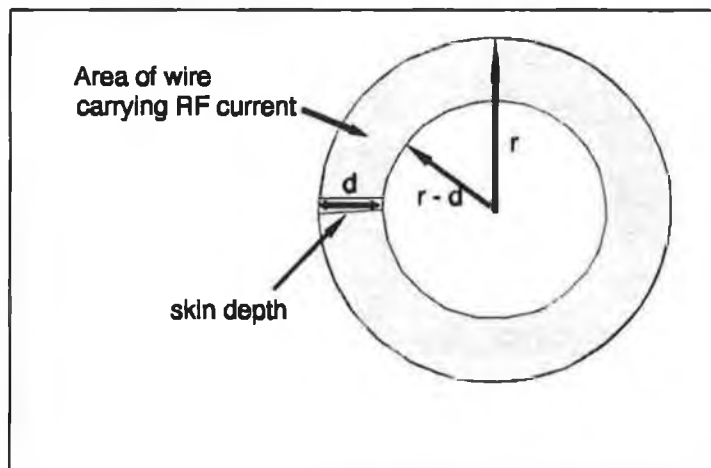


Figure 4.2. Effect of RF on current carrying conductor cross-section.

section of the wire due to the skin depth effect. A straight 1m piece of copper wire, 1mm in diameter has a dc resistance of  $.02\Omega$  but at 13.56MHz the same wire has a resistance of almost  $1\Omega$ .

In the case of inductors at RF, such as the antenna, a capacitance forms between adjacent loops of the coil. This capacitance is called a distributed capacitance. The distributed capacitance is due to the voltage drop occurring between neighbouring loops, as a result of increased conductor impedance at RF.

The effect of increased conductor impedance at RF means that care should be taken in the design of earth leads. Ideally grounding wires should have as large a surface area as possible as most of the RF current flows near the conductor surface. Usually braided wire or straps of copper or aluminium are used.

The RF circuit up to the antenna is critical in ICP operation, as power transfer at RF frequencies is dependent on the relation between the output impedance of the source and input impedance of the load. The maximum power theorem states that for maximum power transfer to occur in an RF circuit the impedance of the load must be equal to the complex conjugate of the source impedance [4],

$$R_s + jX_s = R_l - jX_l \tag{4.3}$$

Consider circuit 4.3(a) where the output voltage  $V_l$ , is given by,

$$V_l = \frac{R_l}{R_s + R_l} (V_s) \tag{4.4}$$

where  $V_s$  is the source voltage. The power transferred to the load, across  $R_l$  is given by,

$$Power = \frac{V_l^2}{R_l} = \frac{R_l}{(R_l + R_s)^2} \tag{4.5}$$

which is a maximum when  $R_l=R_s$ . In the case of the RF circuit one also has the requirement that the overall reactance of the circuit is zero so that all the power is dropped across a purely resistive load.

For the power supplies used in this system, a variable frequency 1.5kW power supply and a 350W fixed frequency power supply, the source impedance is  $50\Omega$ . Thus

the antenna which has a resistive and inductive component to its impedance, must be made to look like a purely resistive 50Ω load from the point of view of the source for maximum efficiency. This task is possible with the introduction of additional circuit components, collectively known as a matching unit.

To calculate the components needed the following procedure was carried out. Consider the circuit shown in figure 4.3(b) where  $jX_L = j\omega L$  is the antenna reactance,  $R_L$  is the antenna resistance and  $R_s$  is the source resistance, 50Ω. The first step is to make the load resistance equal 50Ω. This is achieved by introducing a capacitor,  $C_1$  in parallel with the antenna. The load impedance then becomes,

$$Z_L = \frac{-jX_{C_1}(R_L + jX_L)}{-jX_{C_1} + (R_L + jX_L)} \quad 4.6$$

where  $-jX_{C_2} = 1/j\omega C_2$ , the reactance of the capacitor. Extracting the real components from this equation one can calculate the value of the capacitance required to make the

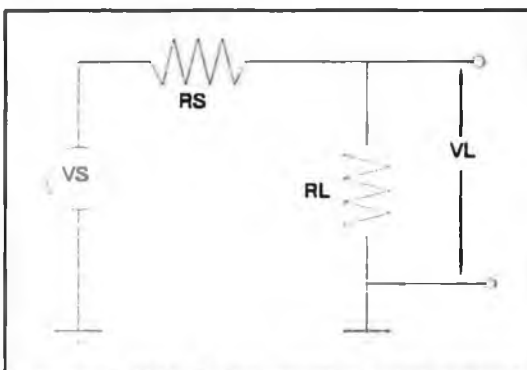


Figure 4.3(a). Maximum power circuit.

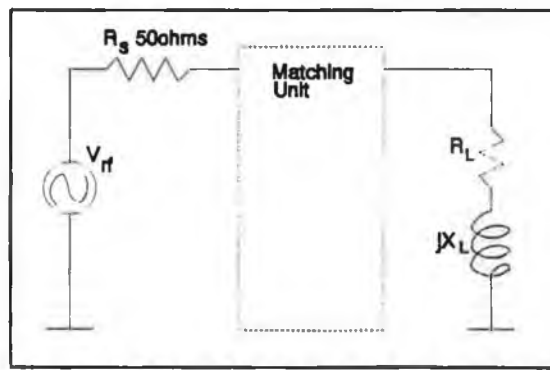


Figure 4.3(b). RF circuit to be matched.

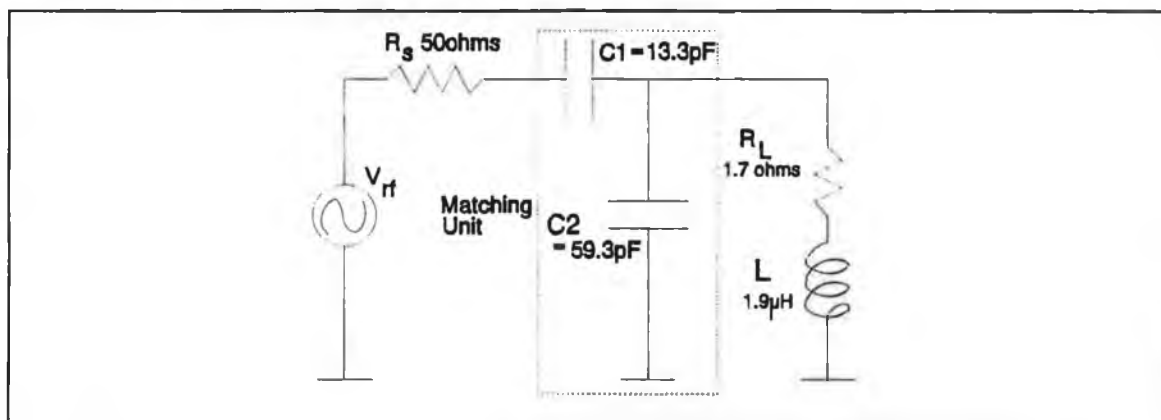


Figure 4.3(c). RF circuit with matching circuit.

load resistance equal to  $50\Omega$ .

$$\frac{X_{C_1}^2 R_L}{R_L^2 + (X_L - X_{C_1})^2} = 50\Omega \quad 4.7$$

Once this capacitance is calculated one must now remove the reactive component from the load. This time a capacitor is introduced in series with the antenna. Considering the imaginary components of the load one now needs the capacitor  $C_2$  to have a value such that,

$$\frac{R_L^2 + X_L^2 - X_{C_1} X_L}{R_L^2 + (X_L - X_{C_1})^2} - X_{C_2} = 0 \quad 4.8$$

A QuickBasic computer program was written to help calculate the required component values,  $C_1 = 59.3\text{pF}$  and  $C_2 = 13.3\text{pF}$ , and the resulting circuit is shown in figure 4.3(c). This is not the only possible matching network in this case, but it is the simplest as only two components are required. By adding more components one change the component values required which may be convenient if the capacitors calculated here are not available.

Variable capacitors are used as the presence of a plasma will affect the impedance of the load, the resistance is increased and the inductance is reduced (section 2.3), and adjustments to the matching values can be made. Variable air gap capacitors were used but this put a restriction on the maximum power available to the plasma (300W). Above this power level the matching unit tended to breakdown, with arcing occurring between the capacitor vanes. The capacitor plates were coated in a thin layer of insulator to prevent dust accumulating on the plates and this reduced the problem.

#### 4.2.3 The Antenna.

The antenna is constructed from 2mm diameter copper tubing and the coil was formed by wrapping the copper around a section of cylinder of appropriate size. The coil is 6cm long with 11 turns and a diameter of 3.4cm. The antenna has a resistance of  $1.7\Omega$  and an inductance of  $1.9\mu\text{H}$ . The antenna rests down the centre of the discharge chamber inside a glass test tube of thickness 3-5mm, figure 4.1. The test tube prevents

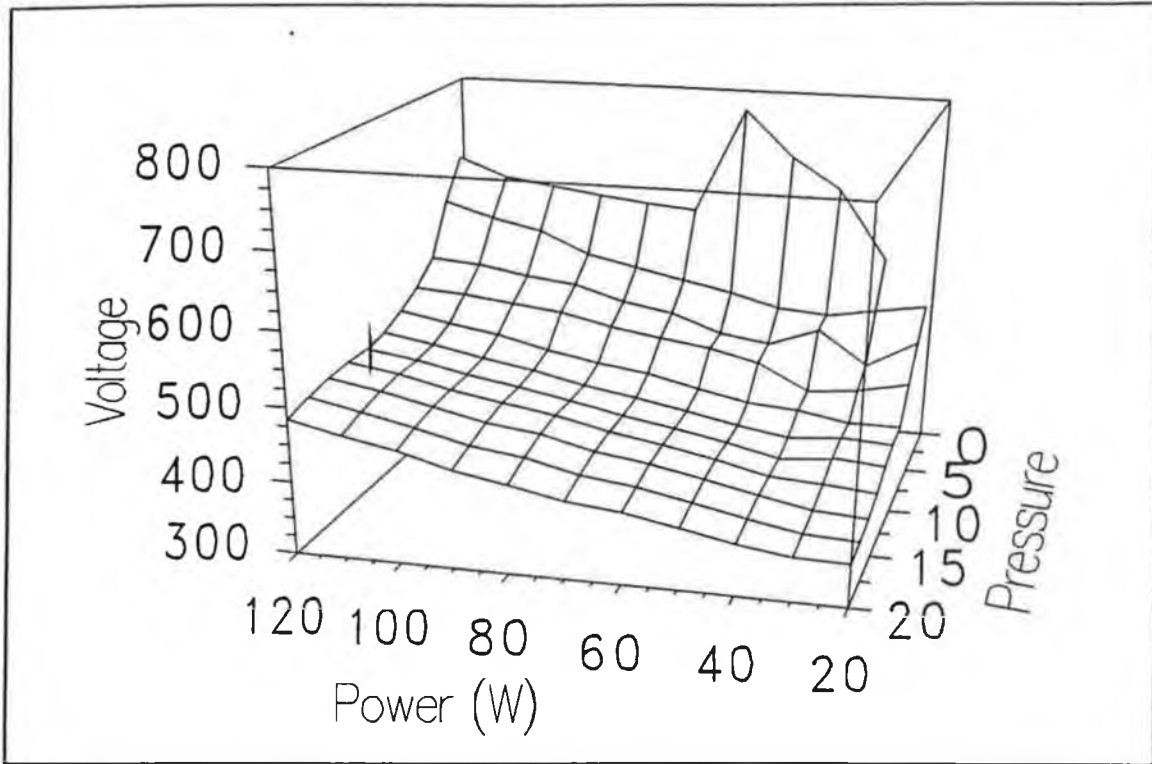


Figure 4.4(a). RF Voltage (rms) measured at antenna at pressures from 1mTorr to 20mTorr.

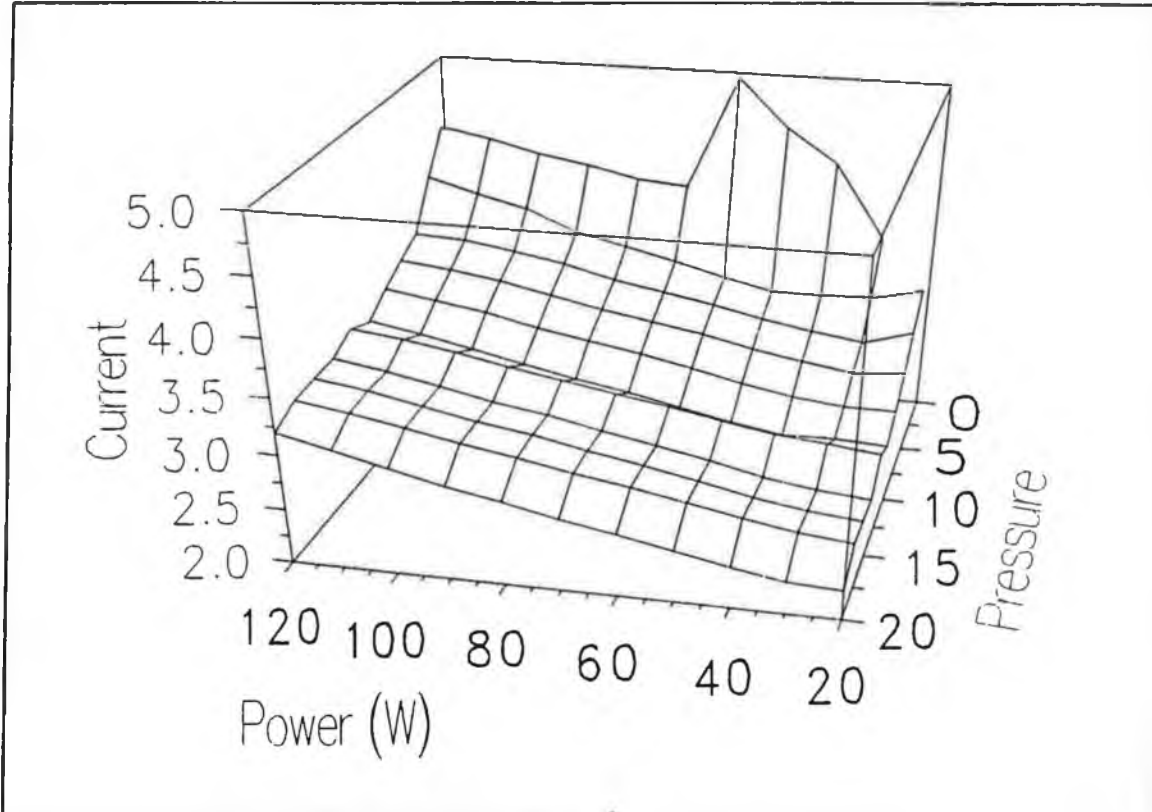


Figure 4.4(b). RF Current (rms) measured at antenna under same conditions as figure 4.5(a).

the antenna from coming in direct contact with the plasma and keeps the antenna at atmospheric pressure, reducing the possibility of arcing. If the antenna were to come in contact with the plasma, the coil would deplete the electron population by attracting electrons during the positive half of the RF cycle. This can lead to weak plasmas and damage, due to overheating, of the antenna. The type of glass used was Boro Silicate which is 80% silicon dioxide but includes some  $\text{Al}_2\text{O}_3$  (2%). This causes problems when working at high RF powers as the glass was liable to crack, probably due to arcing through the glass. Quartz glass is ideal as it is a very good insulator and would not be heated by the induced electric field from the antenna. The antenna resistance can also change as it gets heated during prolonged operation, this can affect the efficiency of the power transfer to the plasma. This effect was reduced by air cooling the antenna.

### 4.3 External electrical measurements.

#### 4.3.1 RF voltage and current measurements.

The RF voltage and current measurements are taken over a range of pressures, .75mTorr to 20mTorr, and powers, from 20W to 120W (figures 4.4(a) and 4.4(b)). Measurements taken at .75mTorr show an interesting feature. As the power to the antenna is raised to 60W the voltage and current both rise steeply. The plasma is weak and barely visible at this stage. Above 60W the voltage and current to the antenna both drop and the visible discharge intensity suddenly increases. This marks the change from a capacitive heating mode to an inductive heating mode [6]. The plasma in the capacitive heating mode is powered by an electrostatic field between adjacent antenna loops and between the antenna and chamber wall, while in the inductive heating mode the plasma is powered by an induced electric field in the discharge [7] (section 2.41). Even though the power to the antenna is increased the voltage and current both drop meaning that the power is more efficiently coupled to the plasma in the inductive mode. The voltage and current drop is related to an increase in the power factor,  $\cos\theta$ ,

$$Power = I_{rms} V_{rms} \cos\theta \quad \cos\theta = \frac{R}{|Z|} \quad 4.9$$

where R is the load resistance and Z the load impedance [5].

The voltage and current to the antenna both show similar trends, with both quantities increasing with power to the antenna. At the higher pressures, up to 20mTorr, less current and voltage are measured as power is more efficiently coupled into the denser plasmas which occur at these pressures.

#### 4.3.2 Load impedance measurements.

The antenna and plasma impedance measurements are shown in figures 4.5(a) and 4.5(b). These values were calculated using equations 3.14 and 3.15. The measurements show a gradual decrease in load reactance, which is purely inductive, as the power and pressure are raised. This is a result of the electron current set up in the plasma which produces a magnetic field opposing the antenna magnetic field, thus reducing the reactance seen at the antenna (section 2.3). The antenna reactance with no plasma is  $162\Omega$ .

The resistance measurements show an opposite trend, the load resistance increases with increasing power and pressure up to 20mTorr. This occurs since the plasma density and electron collision frequency increase at higher pressure leading to an increase in load resistance (see section 5.4 for a detailed explanation),

$$R_{load} \propto n_e \frac{\nu}{\nu^2 + \omega^2} \quad 4.10$$

(Above approximately 20mTorr one would expect the load resistance would begin to drop as the collision frequency becomes greater than the RF driving frequency). One may also note the jump in plasma resistance at .5mtorr from  $2.4\Omega$  at 60W to  $4.4\Omega$  at 70W. This coincides with a change from a capacitive to an inductive heating mode. The antenna resistance without a plasma is  $1.7\Omega$ .

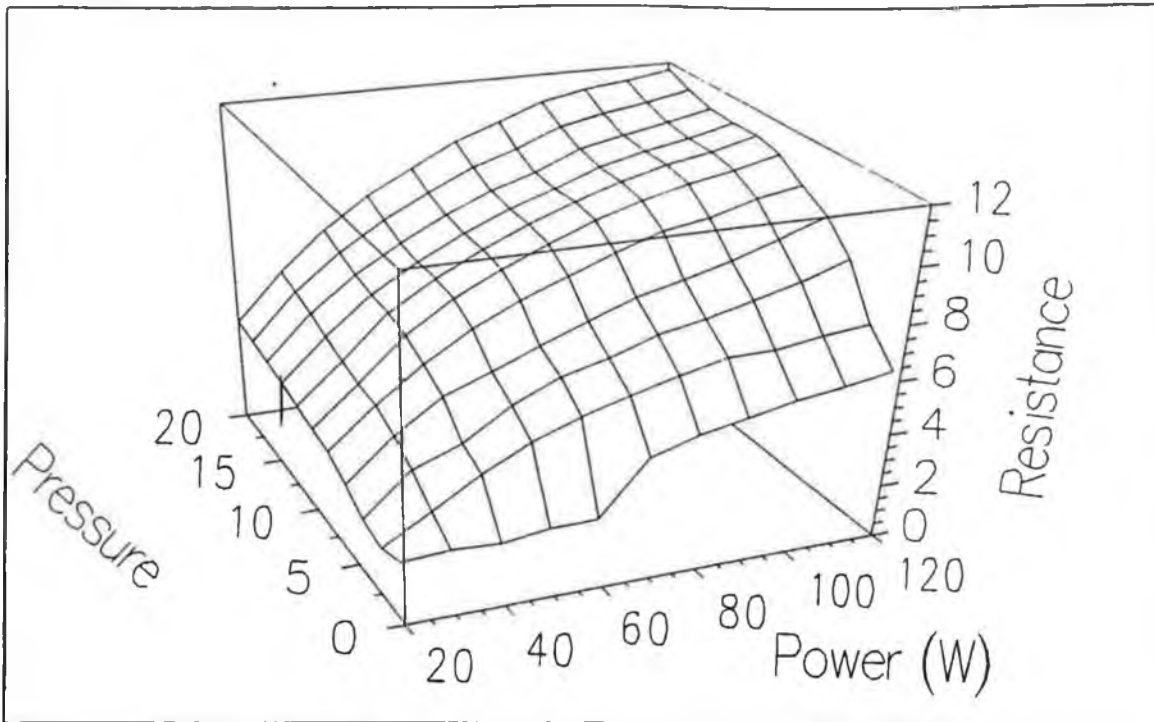


Figure 4.5(a). Load resistance measurements (ohms). Antenna resistance is 1.7ohms.

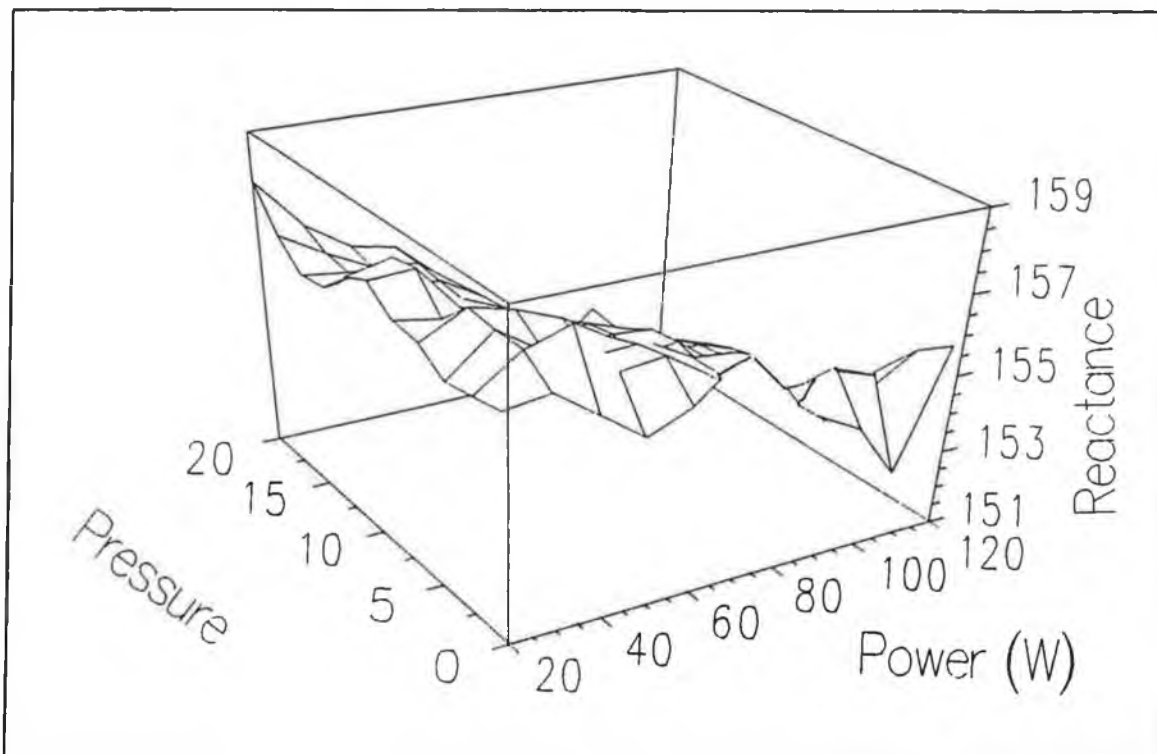


Figure 4.5(b). Load reactance (ohms). Antenna reactance is 162ohms.

#### 4.4 Plasma parameter measurements in Argon at a fixed position.

##### 4.4.1 Electron and ion density.

A plot of electron density in an Argon ICP over a range of pressures and powers is given in figure 4.7. The measurements were taken using a tuned Langmuir probe positioned 1.8cm from the antenna-plasma boundary. This position was chosen as it was the approximate maximum of radial electron density measurements. The results show a linear dependence of electron density on both pressure and power. The rate of electron density increase with power being greatest at the highest pressure, reaching a density of  $6 \times 10^{10} \text{cm}^{-3}$  at 20mTorr and at 120W. At 5mTorr the increase is minimal as the power is not being coupled into the plasma as efficiently due to the lower electron collision frequency and consequently a lower load resistance.

Ion density measurements, figure 4.8, show ion populations to be generally twice to three times that of the electron population at all plasma conditions measured. One expects, in a quasineutral plasma, that electron and ion densities would be similar. The large difference in these measurements is probably due to an overestimation of the ion density by the probe. This occurs because of the greater probe collecting area in the ion saturation region where ion density measurements are taken than in the electron saturation region where electron density measurements are taken. The ion and electron saturation currents, equations 3.18 and 3.23, are related to the probe collecting area  $S$ . The probe collecting area for the cylindrical probe

is related to the sheath radius,

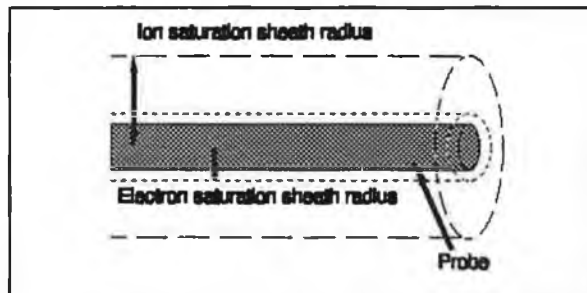


Figure 4.6. Sheath radii at ion and electron saturation.

$$S = 2 \pi r_s L \tag{4.11}$$

where  $r_s$  is the sheath radius and  $L$  the probe length (figure 4.6). The probe sheath radius is given by [8],

$$r_s = r_p \left( 1 - \frac{(V - V_p)}{kT_e} \right)^{\frac{1}{2}} \tag{4.12}$$

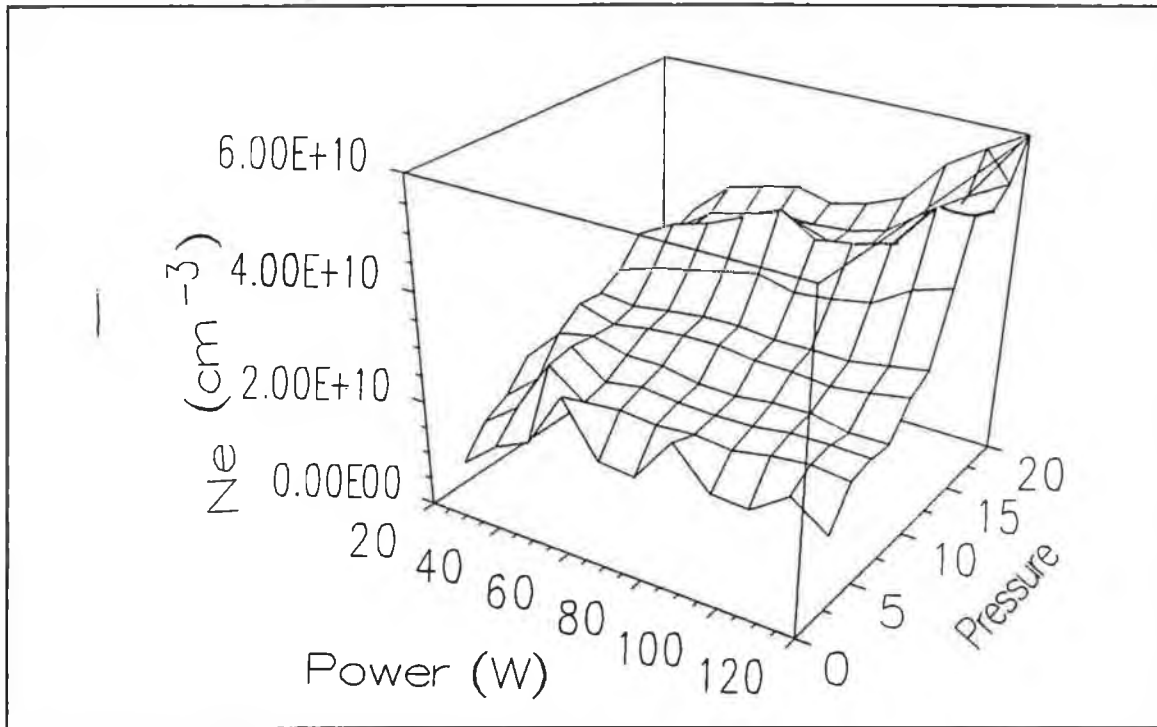


Figure 4.7. Argon electron density measurements.

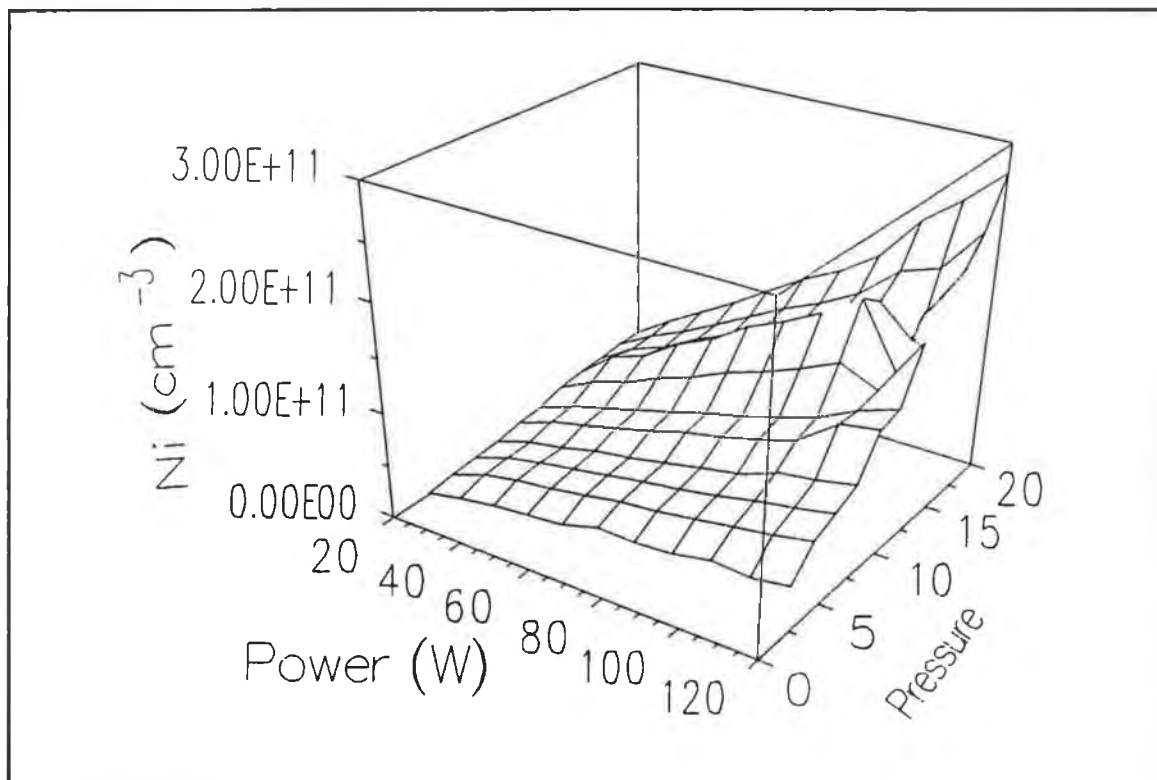


Figure 4.8. Argon ion density measurements.

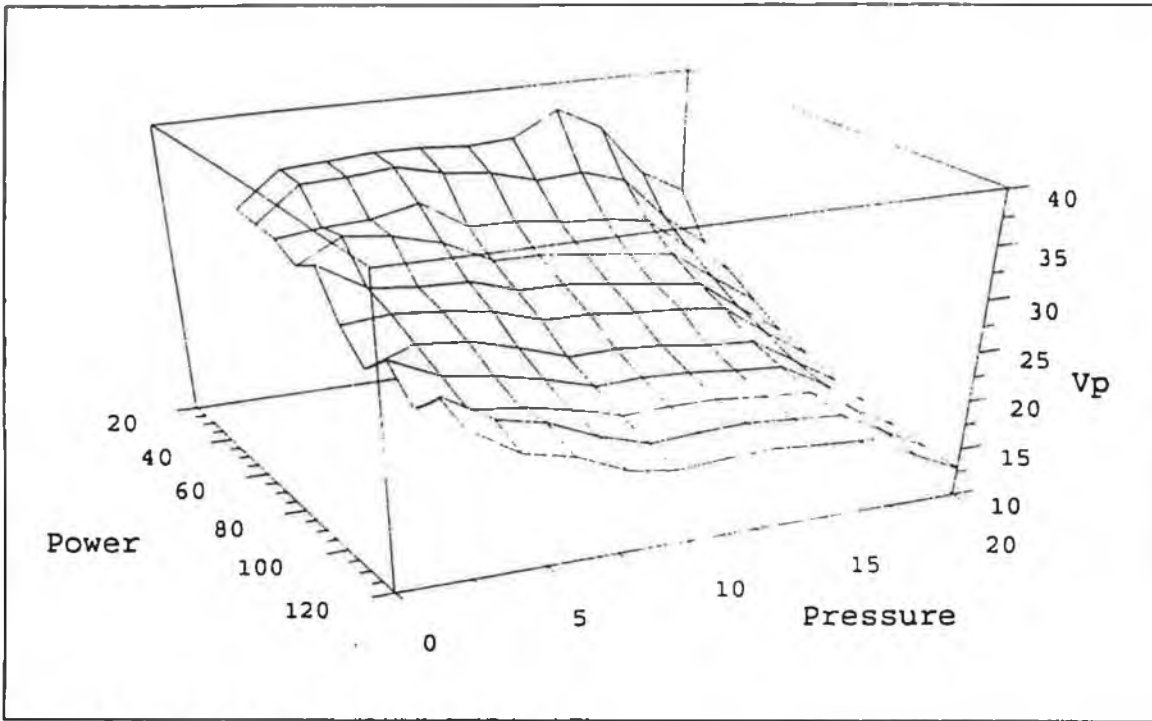


Figure 4.8. Argon plasma potential (V).

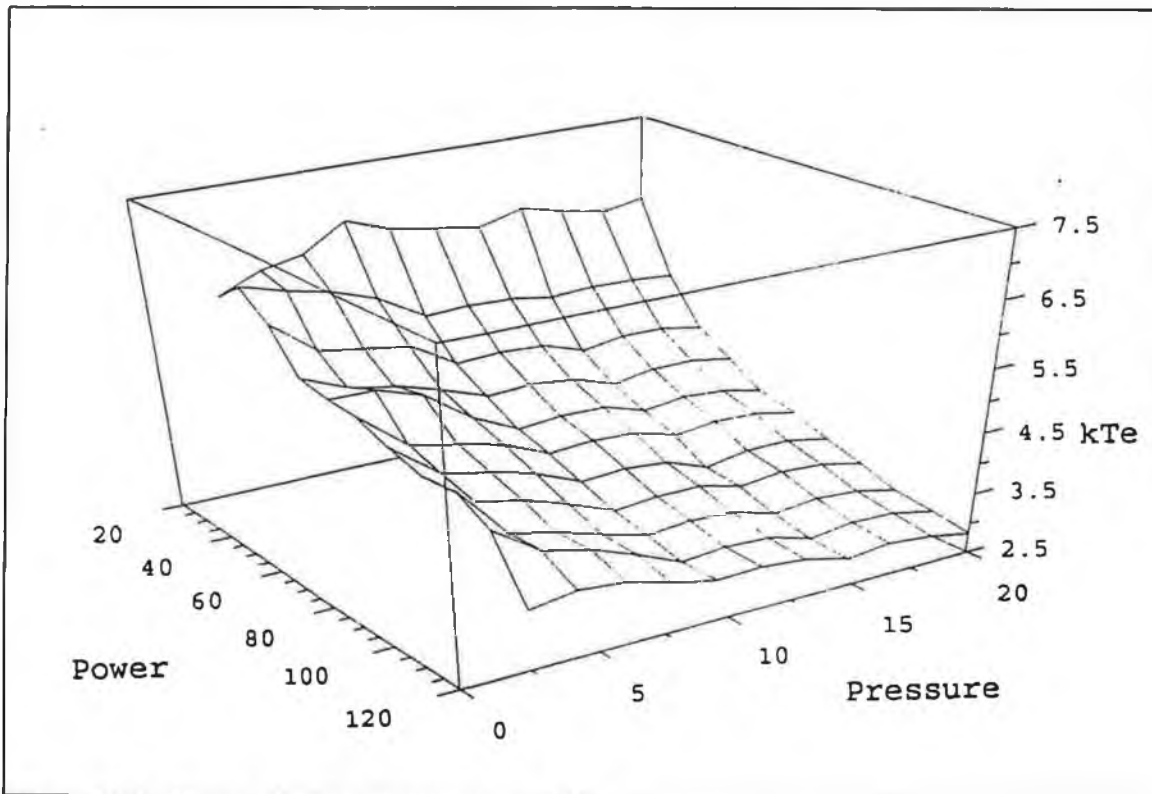


Figure 4.9. Argon electron temperature (eV).

where  $V$  is the probe bias and  $V_p$  is the plasma potential. In the probe saturation region the probe bias can be typically 50-60Volts less than the plasma potential. At an electron temperature of 4eV the sheath radius is approximately 3 times the probe radius in the ion saturation region. In the electron saturation region, where the probe voltage is a few volts above the plasma potential, the sheath radius is approximately equal to the probe radius (the sheath thickness is approximately equal to the Debye length which is small compared to the probe radius at the electron densities and temperatures of interest here).

#### 4.4.2 Plasma potential and electron temperature.

From figure 4.9 one can see a decrease in plasma potential at high powers and pressures in an Argon discharge, down to 12.8V at an input power of 120W at 20mTorr. The plot of electron temperature, figure 4.10, shows similar trends and it seems that both quantities are related in this ICP. At these pressures the correlation exists because there must be a sufficient plasma potential present to balance ionisation and charged particle losses from the plasma. The higher the electron temperature the greater the electron drift velocity and therefore the higher the plasma potential must be reduce electron diffusion to the discharge chamber walls and so sustain a discharge. The number of electrons which can reach the chamber walls,  $n_{wall}$ , is related to the electron temperature and to the difference between the plasma potential and wall potentials,

$$n_{wall} \propto \exp\left(\frac{V_{wall} - V_p}{k T_e}\right) \quad 4.13$$

The factor on the right hand side of equation 4.13 is known as the Boltzmann factor [9] and to sustain a discharge this must be kept constant.

The trends of electron temperature and plasma potential with power and pressure reflect the nature of the ICP. At low powers and pressures the discharge is dominated by a capacitive heating mode and at higher powers and pressures the inductive mode dominates. One would expect higher electron temperatures in the capacitive heating mode due to the high electrostatic fields sustaining the discharge (section 2.4.1). As the pressure increases the rate of electron collisions also increases leading to a downward trend in electron temperatures.

#### 4.5 Plasma parameter measurements in Hydrogen at a fixed position.

Measurements were taken in a Hydrogen plasma to make a comparison with the Argon measurements. The two gasses are quite different, the Argon atom being almost 40amu while the Hydrogen molecule being almost 2amu. Argon is also inert while in the Hydrogen plasma complex reactions can occur, it can combine with electronegative species such as Oxygen if they are present, and the gas can be found in atomic and molecular form in the plasma. These differences and also the characteristics of the ICP discharge can be seen in the results presented.

It was difficult, if not impossible, to fire a Hydrogen plasma inductively under the low pressure conditions where the Argon plasma were readily sustainable (<20mTorr). Magnets of alternate polarity were placed around the discharge chamber to improve electron confinement in the plasma and so increase the likelihood of energy transfer collisions occurring [8]. This improved the situation, but high pressures (<50mTorr) were still required to sustain a Hydrogen ICP.

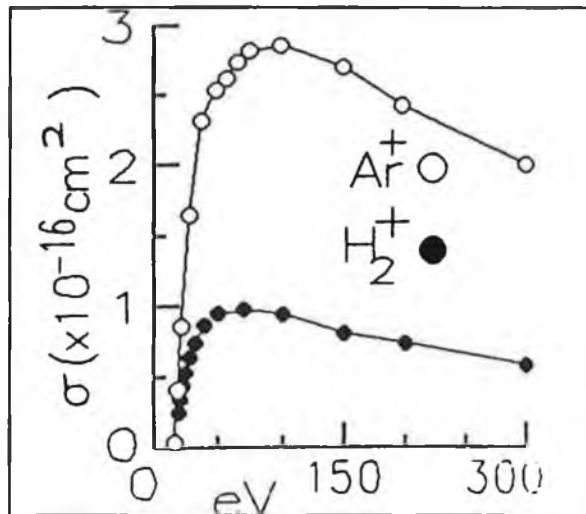


Figure 4.11. Ionisation cross-section of Argon and Hydrogen.

##### 4.5.1 Electron and ion density measurements.

The electron density measurements show a gradual increase in electron populations with pressure and power up to approximately 500mTorr, reaching  $1.8 \times 10^{10} \text{cm}^{-3}$  at 200W (figure 4.12). At higher pressures the electron density begins to level off and at the lowest power, 100W, it drops slightly from  $1.9 \times 10^{10} \text{cm}^{-3}$  at 600mTorr to  $1.8 \times 10^{10} \text{cm}^{-3}$  at 1Torr. At pressures of 1Torr the sheath around the Langmuir probe is no longer collisionless and particle collisions can cause a reduction in the charged particle current collected by the probe [8]. These densities are lower than electron densities found in the Argon plasma. This reflects the lower ionisation cross-section of Hydrogen in comparison with Argon (figure 4.11) and the increased plasma losses due to

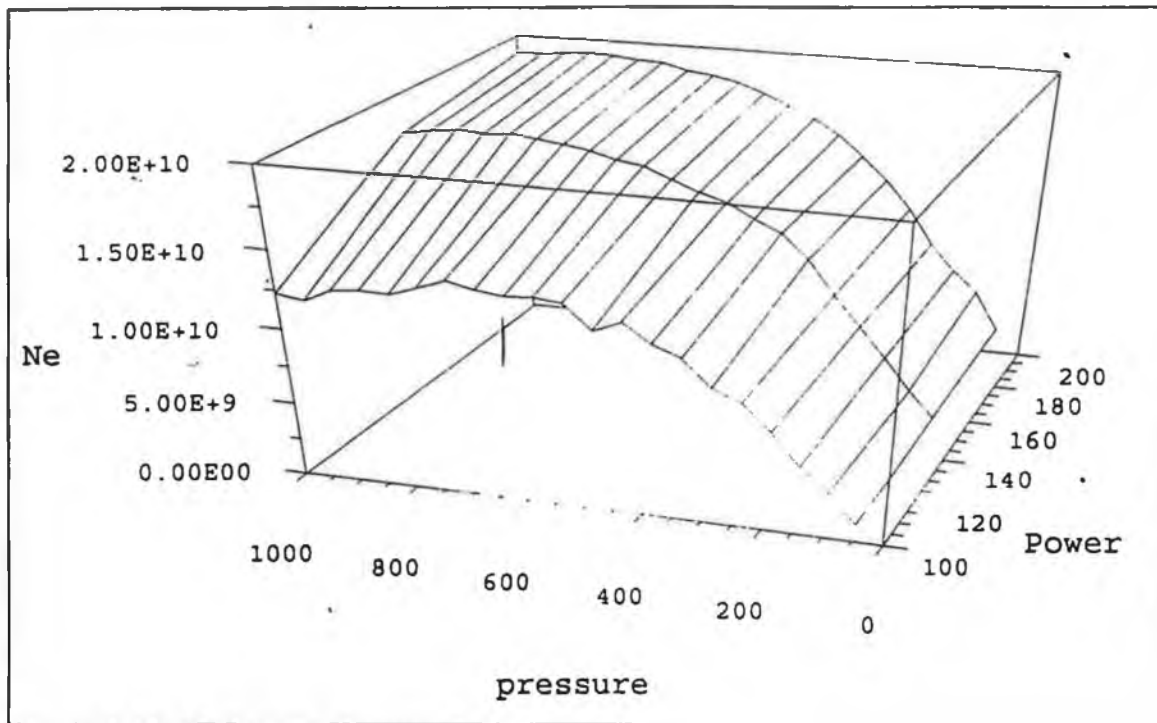


Figure 4.11. Hydrogen electron density.

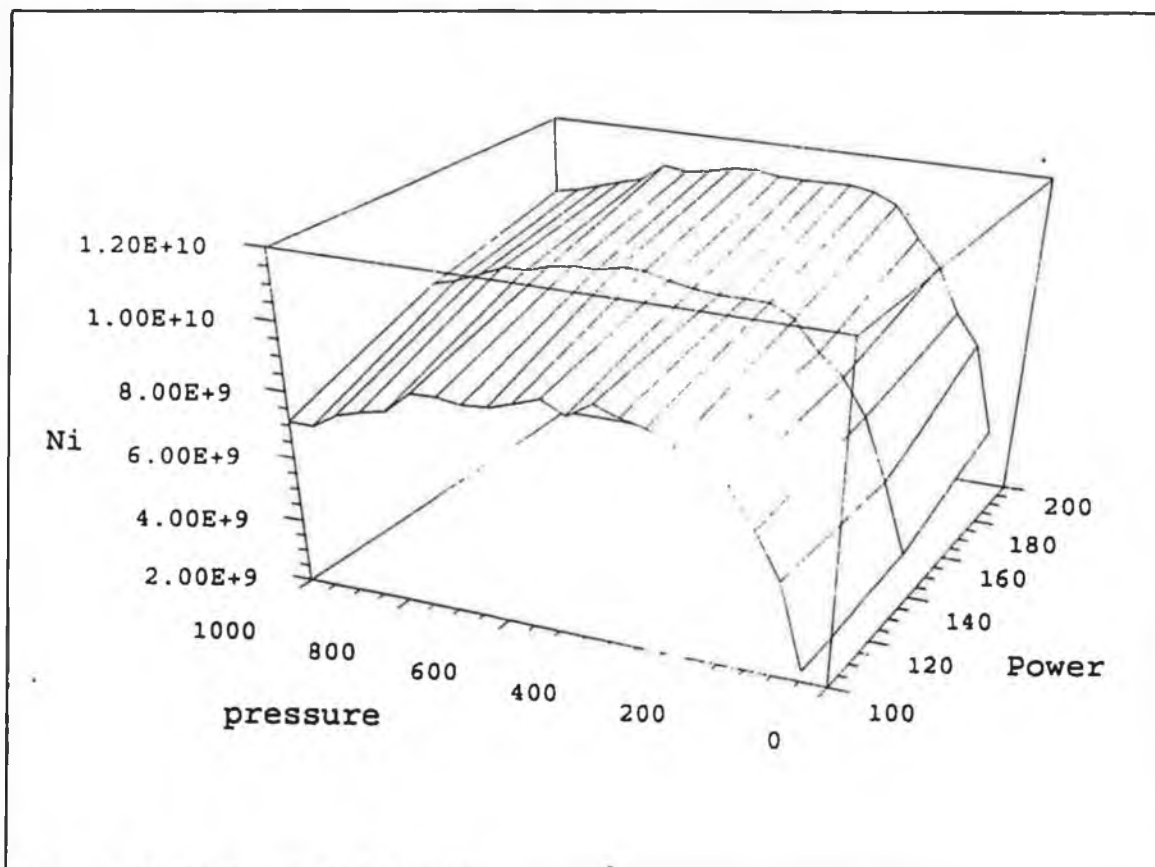


Figure 4.12. Hydrogen ion density.

the lower mass of the Hydrogen ions. The ion density profile, shown in figure 4.13, shows similar characteristics to the electron density measurements; it seems to decrease at higher pressures. Again this is probably due to collisions occurring in the probe sheath.

#### **4.5.2 Plasma potential and electron temperature.**

Plasma potential measurements in Hydrogen show interesting features (figure 4.13). It is high at low pressures, 33V at 50mTorr and 200W, but drops and reaches a minimum at approximately 250mTorr, 22V at 250mTorr and 200W. It then rises again to over 37V at 1Torr over all powers of interest. The reason for the high plasma potential at the low pressures may be the dominance of capacitive coupling where the plasma is heated by high electrostatic fields.

This view is also supported by the results of electron temperature measurements taken in the Hydrogen discharge (figure 4.14). At low powers the electron temperature is high, which may be due to capacitive coupling of the discharge. The electron collision frequency increases at higher pressures and therefore electrons will lose energy more easily resulting in lower electron temperatures. The measurements are also subject to error at high pressures (up to 1Torr) as the probe sheath is no longer collisionless.

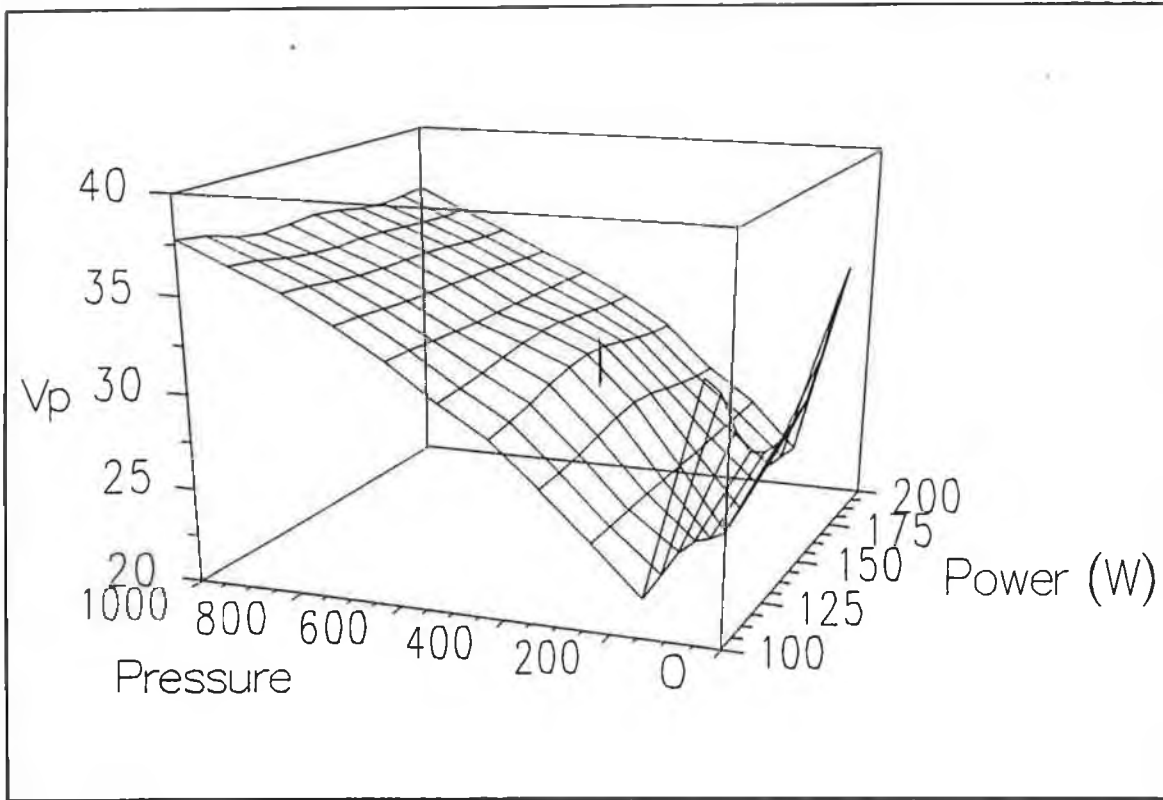


Figure 4.13. Hydrogen plasma potential (V).

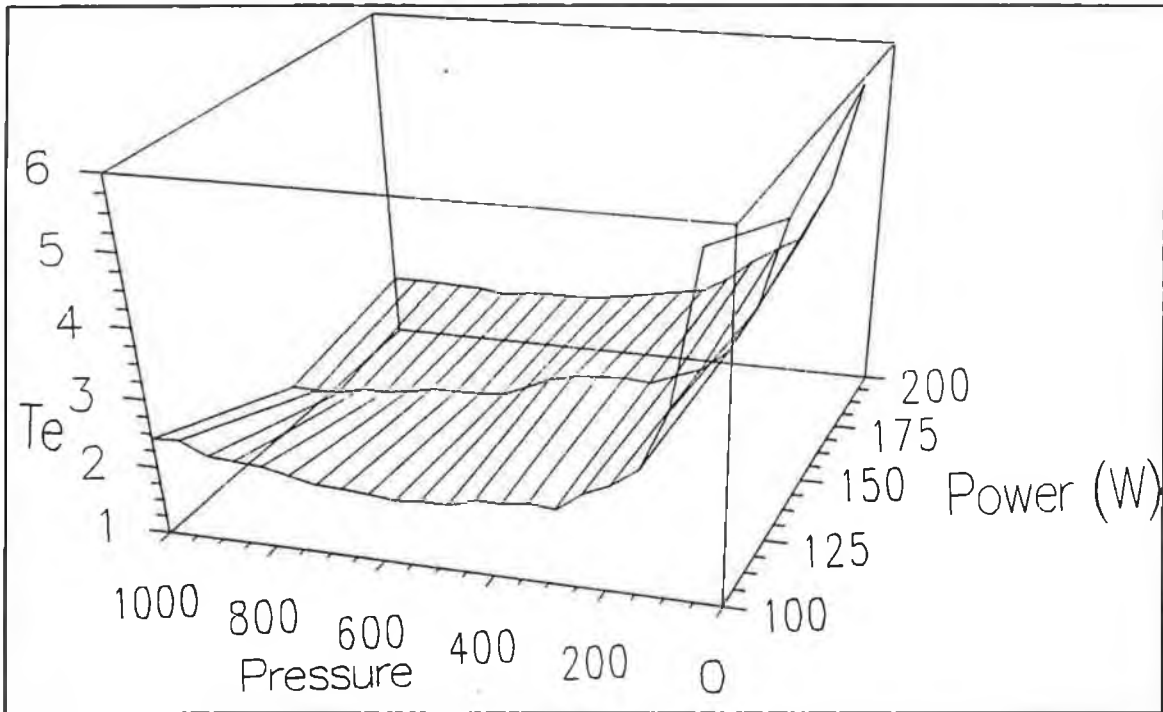


Figure 4.14. Hydrogen electron temperature (eV).

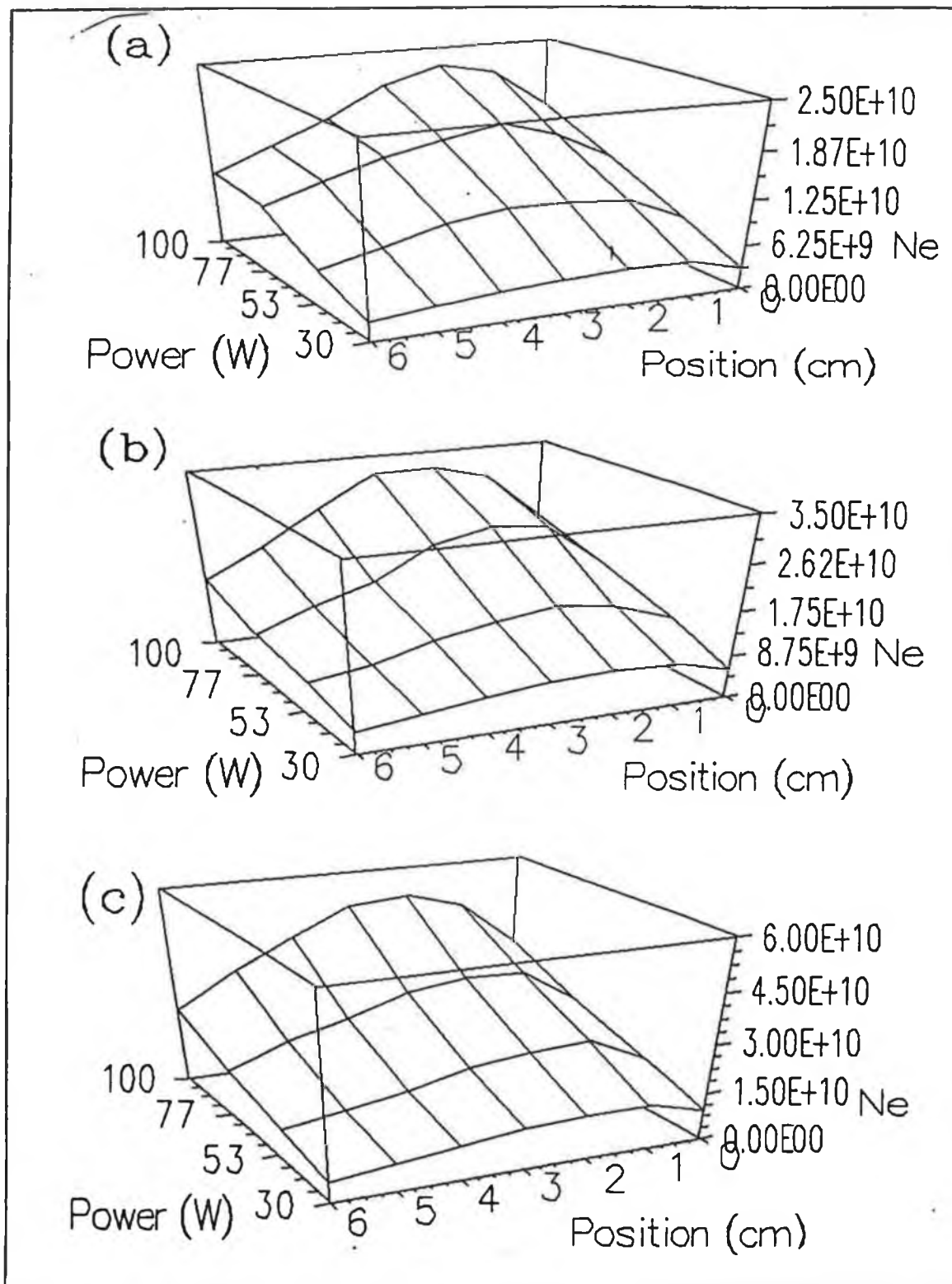


Figure 4.15. Radial electron density measurements in Argon at (a) 5mTorr, (b) 10mTorr and (c) 20mTorr.

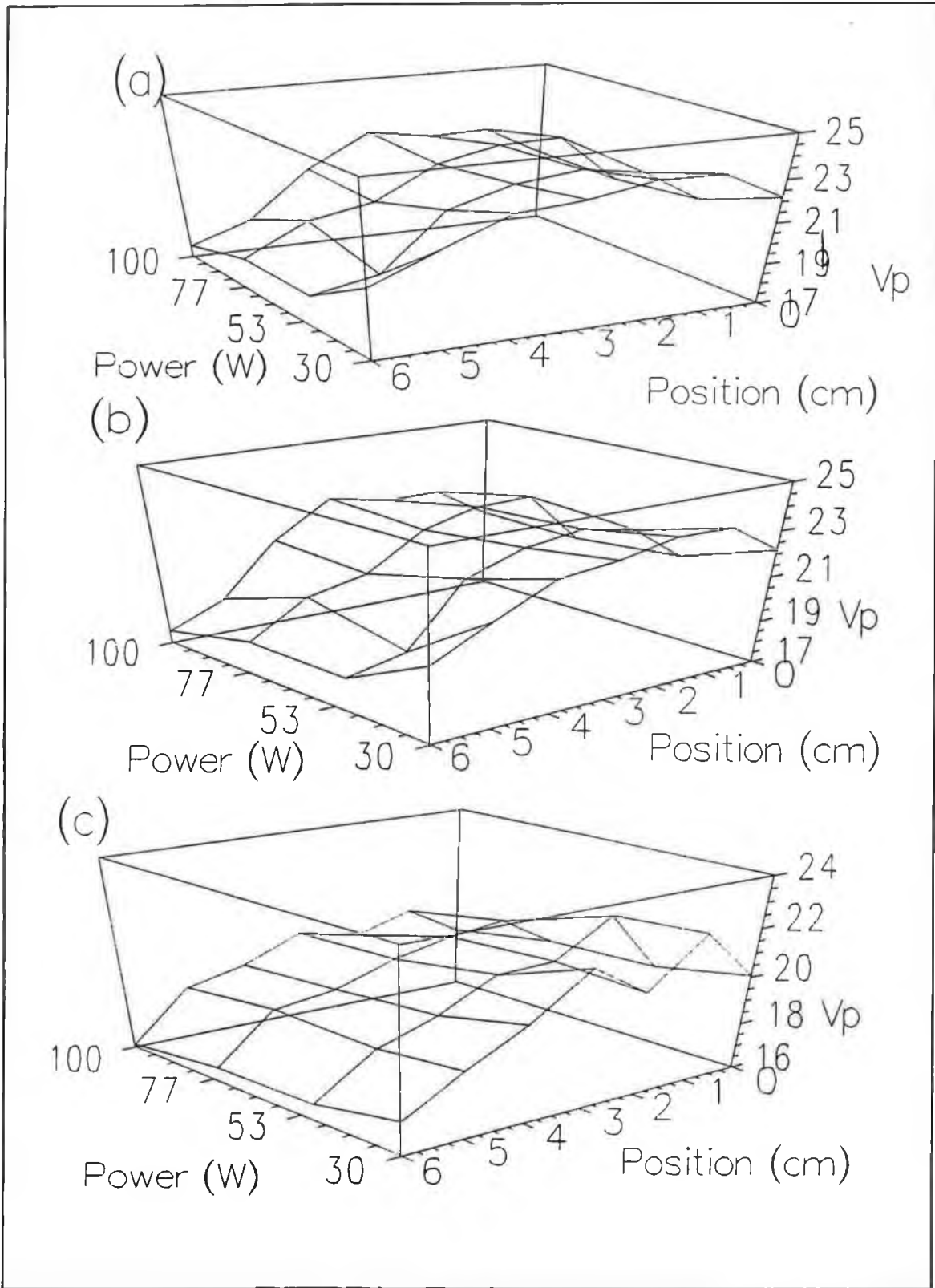


Figure 4.16. Radial plasma potential measurements in Argon at (a) 5mTorr, (b) 10mTorr and (c) 20mTorr.

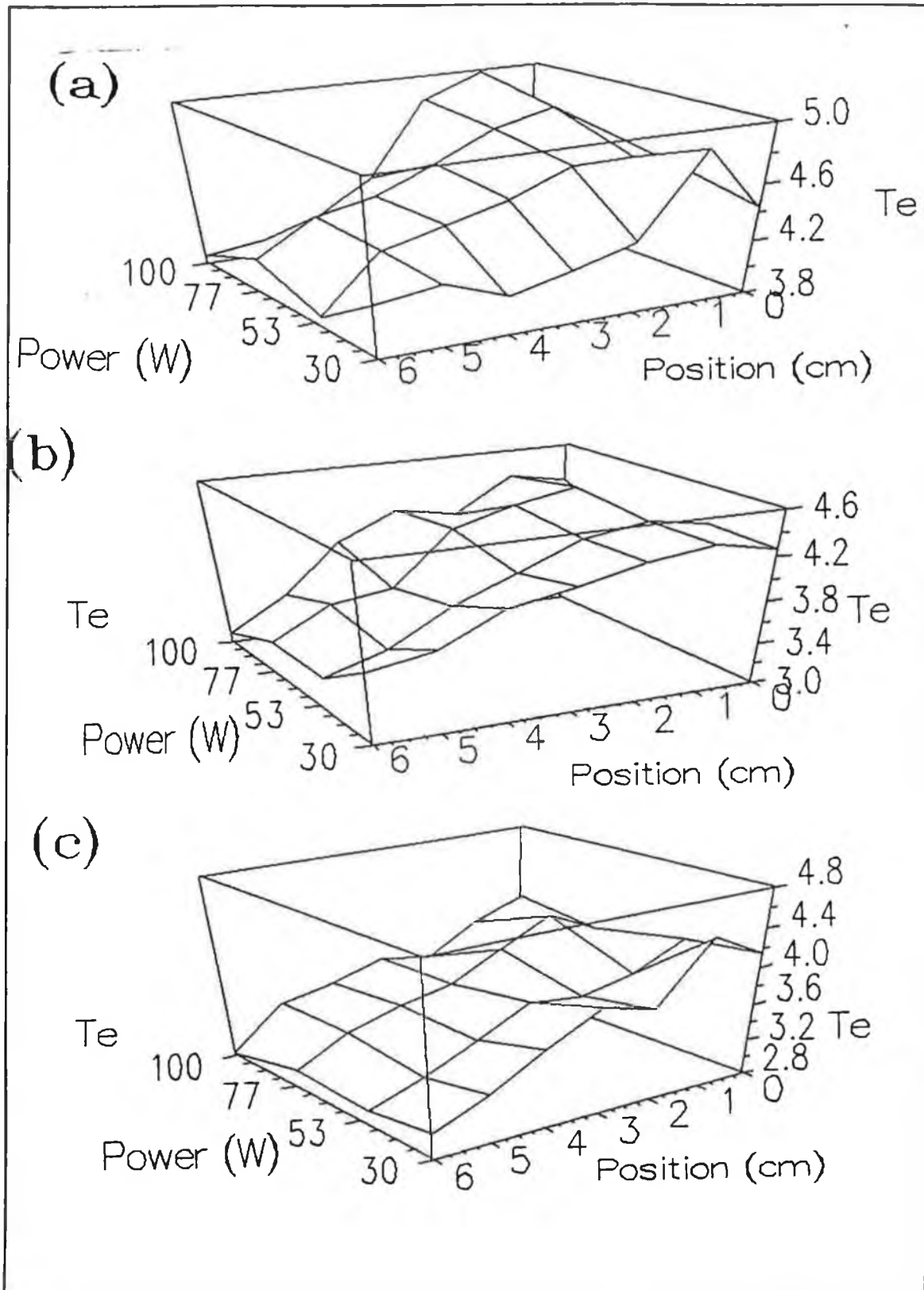


Figure 4.17. Radial electron temperature measurements in Argon at (a) 5mTorr, (b) 10mTorr and (c) 20mTorr.

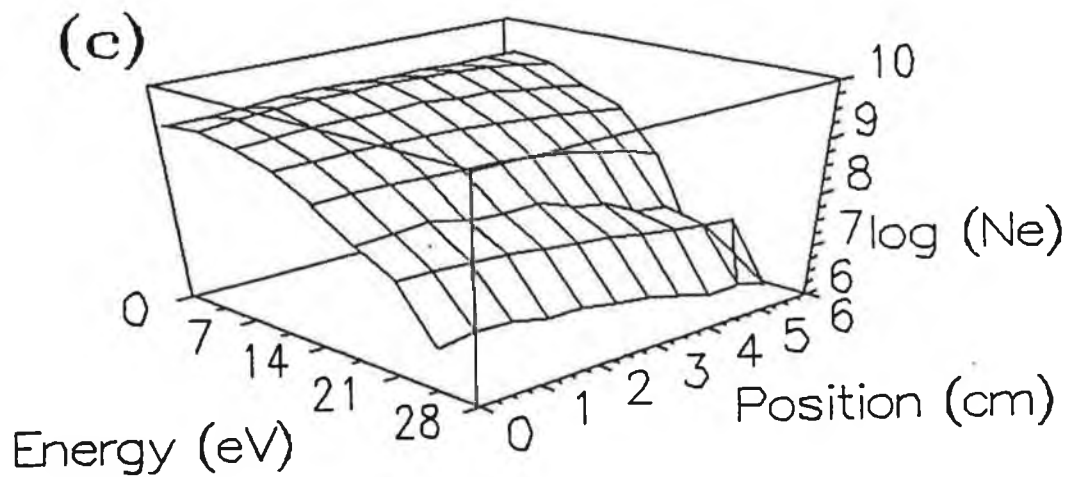
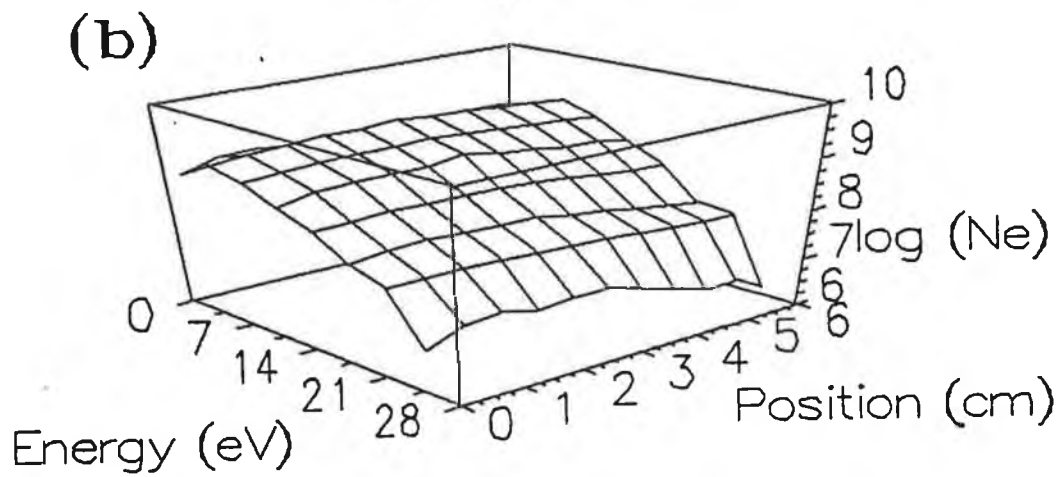
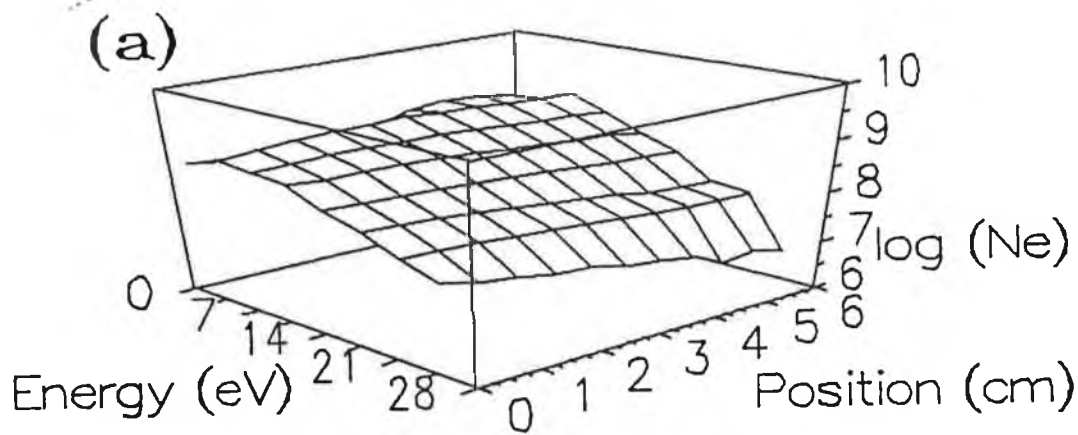


Figure 4.18. Radial EEDF measurements in Argon at (a) 5mTorr, (b) 10mTorr and (c) 20mTorr.

## 4.6 Radial measurements.

Plasma parameter measurements were taken radially in Argon using a cylindrical tuned Langmuir probe which could be moved from the glass wall around the antenna to close to the chamber wall. A Wilson seal allowed probe movement without breaking the vacuum. The measurements were taken at three power settings; 30W, 50W, 75W and 100W, and at pressures of 5mTorr, 10mTorr and 20mTorr.

### 4.6.1 Electron density measurements.

Radial electron density measurements are shown in figure 4.16. They show that the electron density increases with power at each pressure. This is consistent with an increased ionisation rate as more energy is being fed into the plasma. The spatial peak in electron density seems to occur within 2-3cm from the antenna-plasma boundary. This suggests that much of the ionisation occurs at this position which is close to the electron current driven by the induced antenna electric field. The electron density drops significantly approaching the chamber wall. At 10mTorr and 100W for example the electron density is  $3.2 \times 10^{10} \text{cm}^{-3}$  at 2cm from the glass wall surrounding the antenna and drops to  $1.4 \times 10^{10} \text{cm}^{-3}$  at the chamber wall.

### 4.6.2 Plasma potential and electron temperature.

Plasma potential measurements have a similar spatial dependence to electron density measurements (figure 4.16). The plasma potential has peak values between 1cm and 3cm from the glass wall surrounding the antenna, 20V at 100W and 20mTorr and drop as the chamber wall is approached, 16.1V at 100W and 20mTorr. There is also a decrease in relative plasma potential values as the pressure and power are increased; the plasma potential is 23.5V at 10mTorr and 30W, but only 19.5V at 20mTorr and 100W.

Electron temperature measurements, figure 4.17, again show similar trends to plasma potential measurements. The electron temperature is a maximum close to the antenna and then drops as the chamber wall is approached: the electron temperature is 4.95eV at 1cm from the glass wall surrounding the antenna at 5mTorr and 100W, but is 3.85eV at 6cm. Like the plasma potential, the electron temperature drops with increasing power and pressure.

### 4.6.3 Radial EEDF measurements.

EEDF measurements were taken radially at pressures of 5, 10 and 20mTorr in a 100W Argon plasma using a cylindrical Langmuir probe (figure 4.18). The plots show an increase in the size of the EEDF towards the centre of the discharge in agreement with the electron density measurements which show an increase in density near the discharge centre. The plots show a non-negligible hot electron population at each position although the hot electron population does seem to decrease as one moves towards the chamber wall.

The EEDF's are approximately Maxwellian in shape but there is evidence of a decrease in the high energy electron populations above 20eV. This may be due to the high collision cross-section for high energy electrons in an Argon plasma. The EEDF's also show directional character when measurements taken in the azimuthal and longitudinal direction are compared (section 5.2).

### 4.7 Conclusions.

In this chapter results of an indepth investigation of the characteristics of the ICP were presented. The RF electrical measurements help in the understanding of ICP initiation. The azimuthal induced electric field from the antenna must be sufficient to balance the ionisation and energy losses in the discharge, but when the RF power is insufficient a weak capacitively coupled plasma is sustained by the longitudinal electrostatic field between neighbour loops of the antenna. This behaviour could be seen in the RF voltage measurements where a drop in antenna voltage was recorded at ICP switch on at low pressures and powers (5mTorr and 60W). Load impedance measurements demonstrated the interaction of the antenna and plasma magnetic fields. The plasma magnetic field arises from an electron current set up by the induced electric field from the antenna. This plasma magnetic field opposes the antenna magnetic field and thus reduces the inductance of the antenna [5]. Load resistance measurements give an insight into power absorption by the plasma; the plasma is powered through electron collisions, although at low pressures, <10mTorr, a collisionless mechanism may contribute to plasma heating (Chapter 5) [10,11]. As the plasma density increases so does the load resistance, since the number of electrons and the number of electron collisions in the plasma increases (section 5.4).

Plasma parameter measurements were taken at a fixed position at various powers and pressures, and also radially in an Argon plasma. Results reveal the nature of the inductive discharge which is characterised by relatively high electron densities and low plasma potentials; the ICP does not have a significant electrostatic field present as in the case of the capacitive discharge. One can also notice that the inductive properties of the discharge 'improve' at higher powers and pressures. This is because a greater proportion of the input power is being channelled into heating via the induced electric field than through the longitudinal electrostatic field mentioned earlier. EEDF measurements show a relatively hot distribution with a noticeable proportion of hot electrons present. These EEDF measurements are discussed in chapter 5 with relevance to the induced electron current in the discharge, and in chapter 6 the EEDF are discussed in relation to local and non-local electron kinetics.

Measurements were also carried out in Hydrogen. The discharge proved difficult to initiate even when magnets were placed around the discharge chamber. This may be due to the low electron collision cross-section in a Hydrogen plasma and the high ion losses due to the low mass of the Hydrogen ions. The discharge was fired at high pressures and powers ( $> 50\text{mTorr}$  and  $100\text{W}$ ). There were difficulties with the Langmuir probe diagnostic at high pressures in Hydrogen as the Laframboise theory assumes a collisionless sheath around the probe. The problem manifested itself in a decrease in measured electron and ion populations at pressures approaching  $1\text{Torr}$ .

## References.

- [1] K. N. Mellon, B. P. Coonan and M. B. Hopkins. *J. Phys. D: Appl. Phys.* **28** (1995) 473
- [2] K. N. Mellon, B. P. Coonan and M. B. Hopkins. *J. Phys. D: Appl. Phys.* **27** (1994) 2480
- [3] E. R. Dobbs. "*Electromagnetic Waves*". (Routledge and Kegan Paul. London 1985)
- [4] C. Bowick. "*RF Circuit Design*". (Howard Sams and Co. Indiana, USA. 1982)
- [5] P. Lorrain, D. P. Corson and F. Lorrain. "*Electromagnetic Fields and Waves*". (Freeman. New York. 1988)
- [6] R. B. Piejak, V. A. Godyak and B. M. Alexandrovich. *Plasma Sources Sci. Technol.* **1** (1992) 179.
- [7] G. G. Lister and M. Cox. *Plasma Sources Sci. Technol.* **1** (1992) 67.
- [8] L. Schott. "*Plasma Diagnostics*". North Holland Publishing. Amsterdam. (1968)
- [9] S. C. Brown *Introduction to Electrical Discharges in Gases*". John Wiley and Sons. New York.
- [10] Y. Ohara, M. Akiba, H. Horiike, H. Inami, Y. Okumura and S. Tanaka. *J. Appl. Phys.* **61** (1987) 1323.
- [11] M. M. Turner. *Phys. Rev. Lett.* **71** (1993) 1844
- [12] V. A. Godyak, R. B. Piejak and B. M. Alexandrovich. *Plasma Sources Sci. Technol.* **3** (1994) 169

## 5.2 Detection of the electron current in the plasma.

Using the disc probe, figure 5.1, EEDF measurements were taken facing into the current driven by the induced RF electric field, the azimuthal direction, and perpendicular to this current, the longitudinal direction. Measurements taken in the longitudinal direction were assumed to coincide with the background plasma. In the background plasma one expects the EEDF to be isotropic. The electron velocities are independent of direction and therefore EEDF's taken in different directions in the background plasma would be similar. Here it is expected that the two sets of EEDF measurements taken in the azimuthal and longitudinal directions would differ only by the presence of the current of electrons driven by the RF electric field.

The EEDF's shown in figures 5.2 and 5.3 were taken at 2mTorr and 10mTorr at 100W. The graphs show the EEDF's taken in the two directions superimposed on each other at each position. The EEDF's were taken at 1cm intervals from 0cm, the position of the antenna-plasma interface, to 6cm, a position 1.5cm from the plasma chamber wall.

The 2mTorr measurements show a clear difference in the EEDF's taken in both directions close to the antenna. There is a greater hot electron population, ( $> 18\text{eV}$ ), measured in the azimuthal direction near the antenna. Moving out to 3cm from the glass wall surrounding the antenna the difference is slight but can still be recognised. Beyond 3cm however, the EEDF's taken in both directions are practically identical. The situation is similar at 10mTorr, although the difference in the EEDF's taken in and out of the current falls off more rapidly moving away from the antenna. At 2cm from the antenna-plasma interface the difference between the EEDF's is slight.

Beyond 3cm at 2mTorr and 2cm at 10mTorr, the discharge shows characteristics consistent with an isotropic plasma. The electron velocities, and energies, are independent of direction. Also the consistent agreement of the EEDF's taken in the isotropic plasma shows the repeatability and reliability of the probe measurement system.

One must be careful in interpreting the log plots as a difference in electron population at the hot end of the EEDF's where the density is low ( $10^5\text{cm}^{-3}$ ), will be more apparent than the same difference appearing at the low energy end where the densities are higher ( $10^9\text{cm}^{-3}$ ). Thus there may actually be a contribution of electrons with energies less than 18eV, to the electron current although it may not be obvious from the EEDF's.

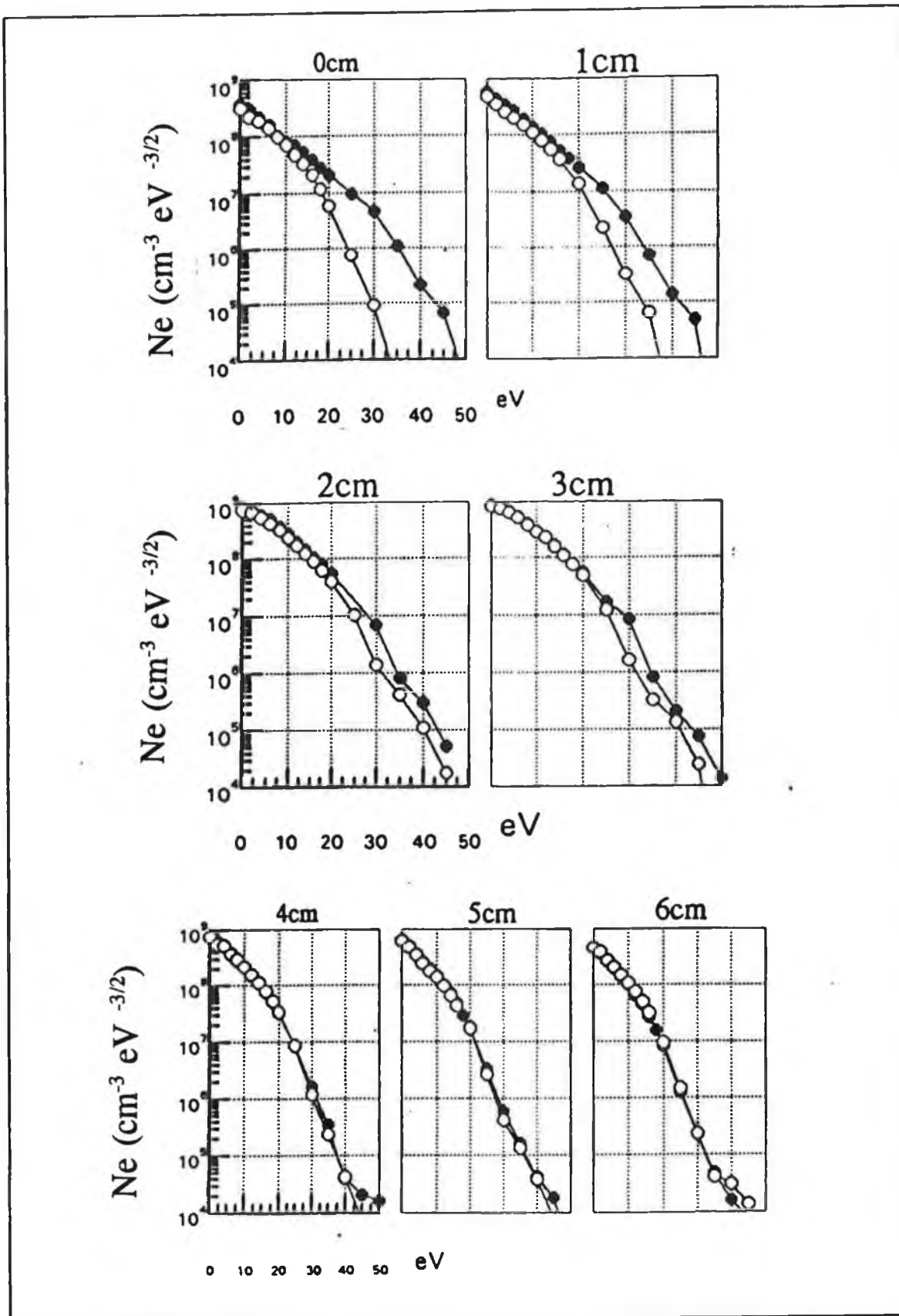


Figure 5.2. 2mTorr 100W directional EEDF scan (white data points taken in azimuthal direction, black points taken in longitudinal direction. 0cm corresponds with to position next to the antenna)

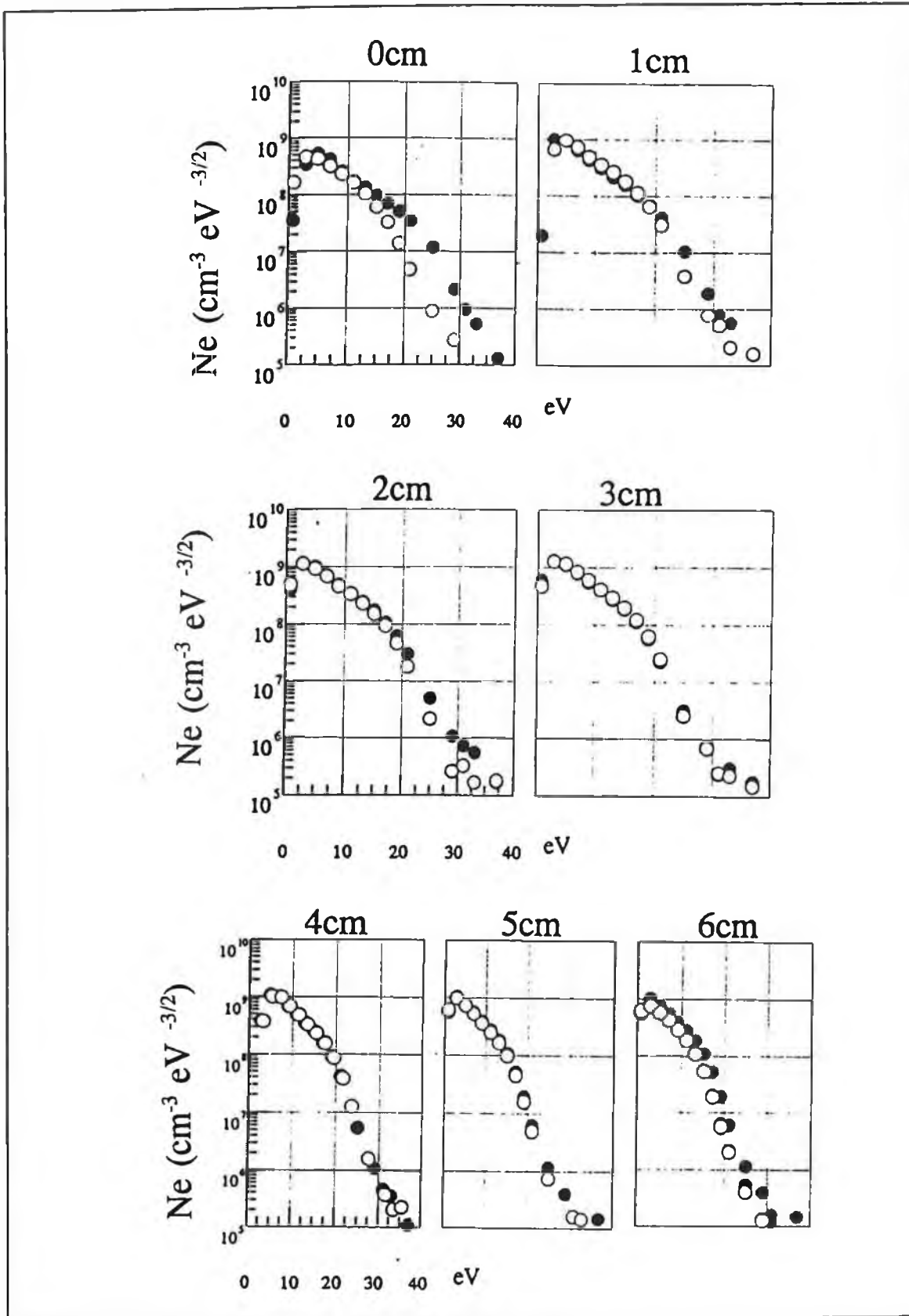


Figure 5.3. 10mTorr 100W directional EEDF scan (white data points taken in azimuthal direction, black data points taken in longitudinal direction. 0cm corresponds with a position next to the antenna).

### 5.3 Skin depth measurements.

The skin depth measurements were taken using the magnetic field probe described in section 3.4.1. The probe could be moved across the width of the discharge, allowing a profile of the magnetic field strength to be determined. The probe was uncalibrated as only the relative field strength is required for this analysis. The skin depth itself is a measure of the penetration of an electromagnetic field in a conductor [3]. Classically the skin depth is given by equation 2.18, but for the collisionless plasma it is expected to be described by equation 2.23.

To investigate the behaviour of the electromagnetic fields in the ICP one can apply Maxwells equations, following Lister and Cox [4]. Specifically,

$$\nabla \times \underline{H} = \underline{J} + \epsilon_o \frac{d\underline{E}}{dt} \quad 5.1$$

and,

$$\nabla \times \underline{E} = -\mu_o \frac{d\underline{H}}{dt} \quad 5.2$$

where  $\epsilon_r$  is the relative permittivity of the plasma and  $\underline{J} = \sigma \underline{E}$ . The first term on the right hand side of equation 5.1 corresponds with the plasma conduction current, while the second term accounts for the plasma displacement current. For an electromagnetic wave where the electric and magnetic fields are given by  $\underline{E} = \underline{E}_o e^{j\omega t}$  and  $\underline{B} = \underline{B}_o e^{j\omega t}$  equations 5.1 and 5.2 can be written as,

$$\nabla \times \underline{H} = \sigma \underline{E} + j\epsilon_o \omega \underline{E} = \frac{n_e e^2}{m_e(\nu + j\omega)} \underline{E} + j\epsilon_o \omega \underline{E} \quad 5.3$$

and

$$\nabla \times \underline{E} = -j\omega \mu_o \underline{H} \quad 5.4$$

One can also write equation 5.3 in terms of the dielectric constant of the plasma,  $\epsilon = \epsilon_o \epsilon_r$ ,

$$\nabla \times \underline{H} = j \epsilon \omega \underline{E} \quad 5.5$$

Therefore comparing equations 5.3 and 5.5 one finds that the relative permittivity of the plasma is given by,

$$\epsilon_r = 1 + \frac{n_e e^2}{j \omega \epsilon_0 m_e (\nu + j \omega)} = 1 - \frac{j \omega_p^2}{\omega (\nu + j \omega)} \quad 5.6$$

When the plasma frequency,  $\omega_p$  is much greater than the driving frequency  $\omega$  (as in this case), the relative permittivity becomes dominated by second term on the right hand side of equation 5.1, corresponding with the plasma conduction current. The contribution of the displacement may therefore be ignored and equation 5.1 rewritten as,

$$\nabla \times \underline{H} = \sigma \underline{E} \quad 5.7$$

Taking account of the cylindrical geometry of the system equations 5.7 and 5.2 become,

$$\frac{d \underline{H}_z}{d t} = -\sigma \underline{E}_\theta \quad 5.8$$

and

$$\frac{1}{r} \frac{d}{d r} r \underline{E}_\theta = -j \omega \mu_0 \underline{H}_z \quad 5.9$$

where the electric field points in the azimuthal direction and the magnetic field in the longitudinal direction. Combining equations 5.8 and 5.9 one obtains,

$$\frac{1}{r} \frac{d}{d r} r \frac{d \underline{E}_\theta}{d r} - \left( j \mu_0 \omega \sigma(r) R^2 + \frac{1}{r^2} \right) \underline{E}_\theta = 0 \quad 5.10$$

$r$  is the normalised position in the discharge given by  $r = r/R$ , where  $R$  is the plasma width. This equation has a solution given in terms of first-order Bessel and Hankel functions which is given by,

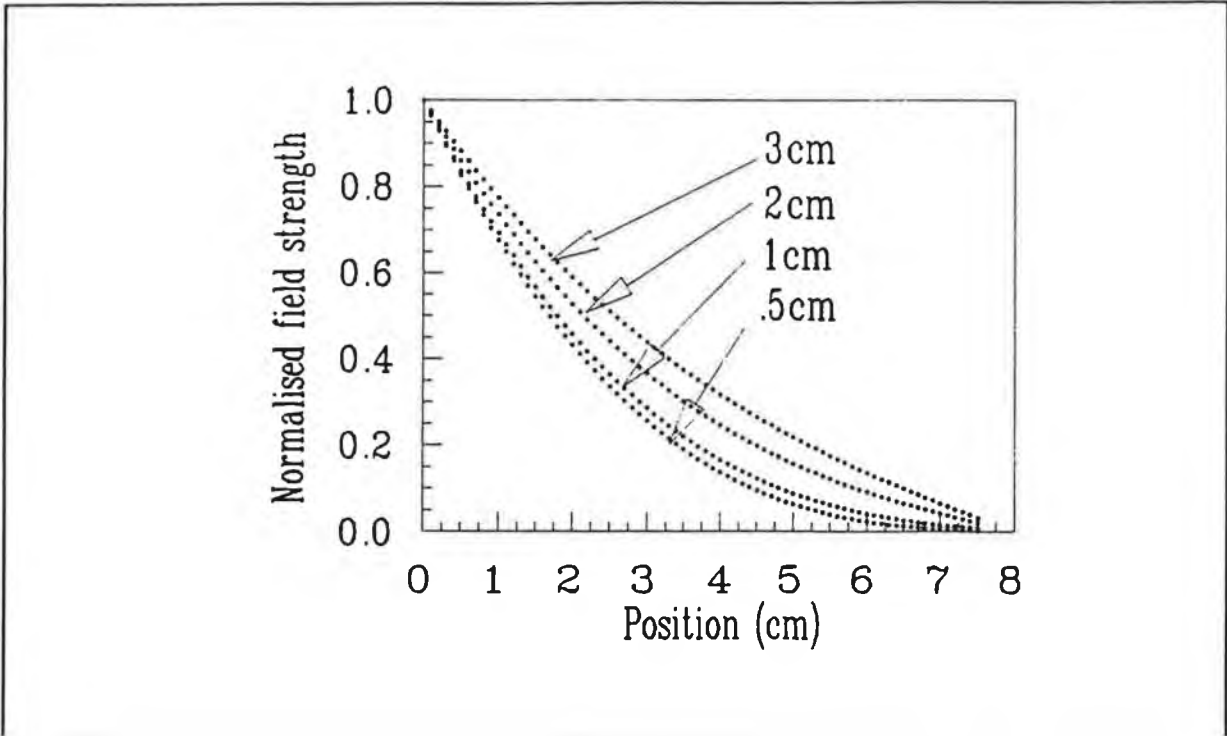


Figure 5.4. Plot of expected electric field profiles in a 20mTorr plasma at skin depths of 3cm, 2cm, 1cm and .5cm using equation 5.11.

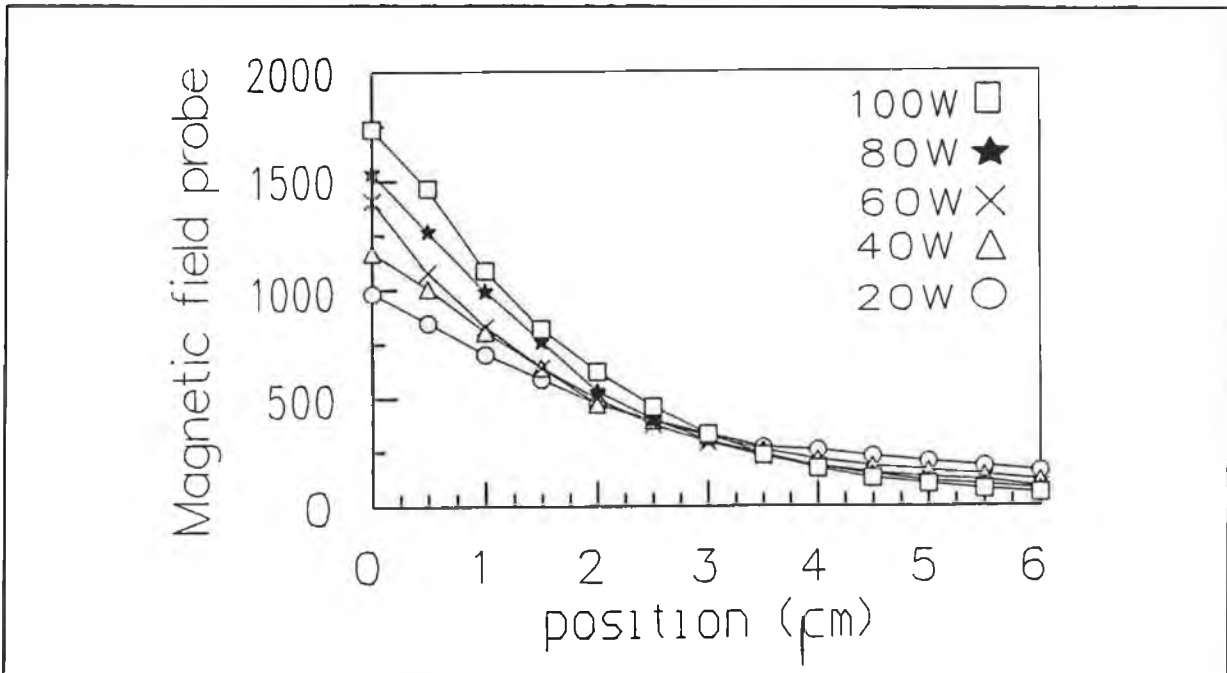


Figure 5.5. Plot of magnetic probe measurements taken at 5mTorr at powers from 20W to 100W.

$$E_0 = A J_1(\Gamma r) + A H_1^{(2)}(\Gamma r) \quad 5.11$$

where A is a constant depending on the boundary conditions of the situation i.e. the electric field is a maximum at the antenna and falls to zero at the chamber walls.  $\Gamma$  is given by,

$$\Gamma = \sqrt{\frac{-j 2 R^2}{\delta^2(1 + \nu/\omega)}} \quad 5.12$$

Figure 5.4 shows the solution to equation 5.10 at various values of skin depth for a 20mTorr plasma. One notices the more rapidly decreasing electric field across the discharge as the skin depth is reduced. Figure 5.5 shows actual magnetic probe measurements taken in a 5mTorr discharge at various discharge powers. At the higher powers there is a more rapid decrease in the field penetrating the plasma corresponding to a lower skin depth. This is due to the increased electron density occurring in the discharge at the higher powers (see equations 2.18 and 2.23).

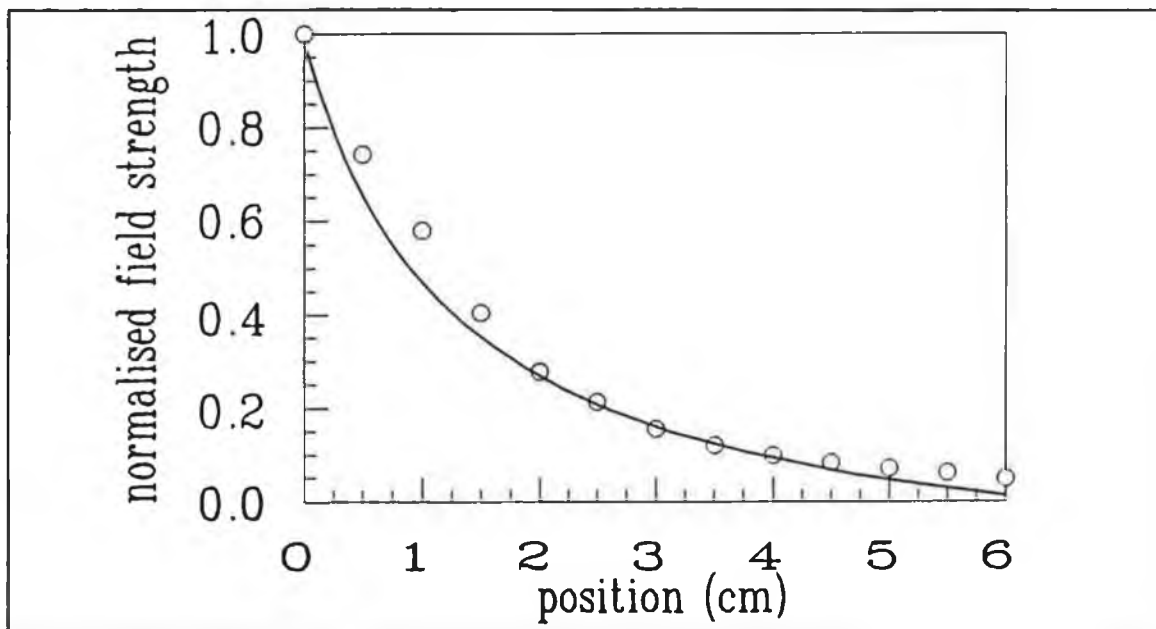


Figure 5.6. Plot of least-squares fit of measured data taken at 75W in a 20mTorr Argon plasma (circled points) to a equation 5.11. This analysis concludes a skin depth of 3.1cm.

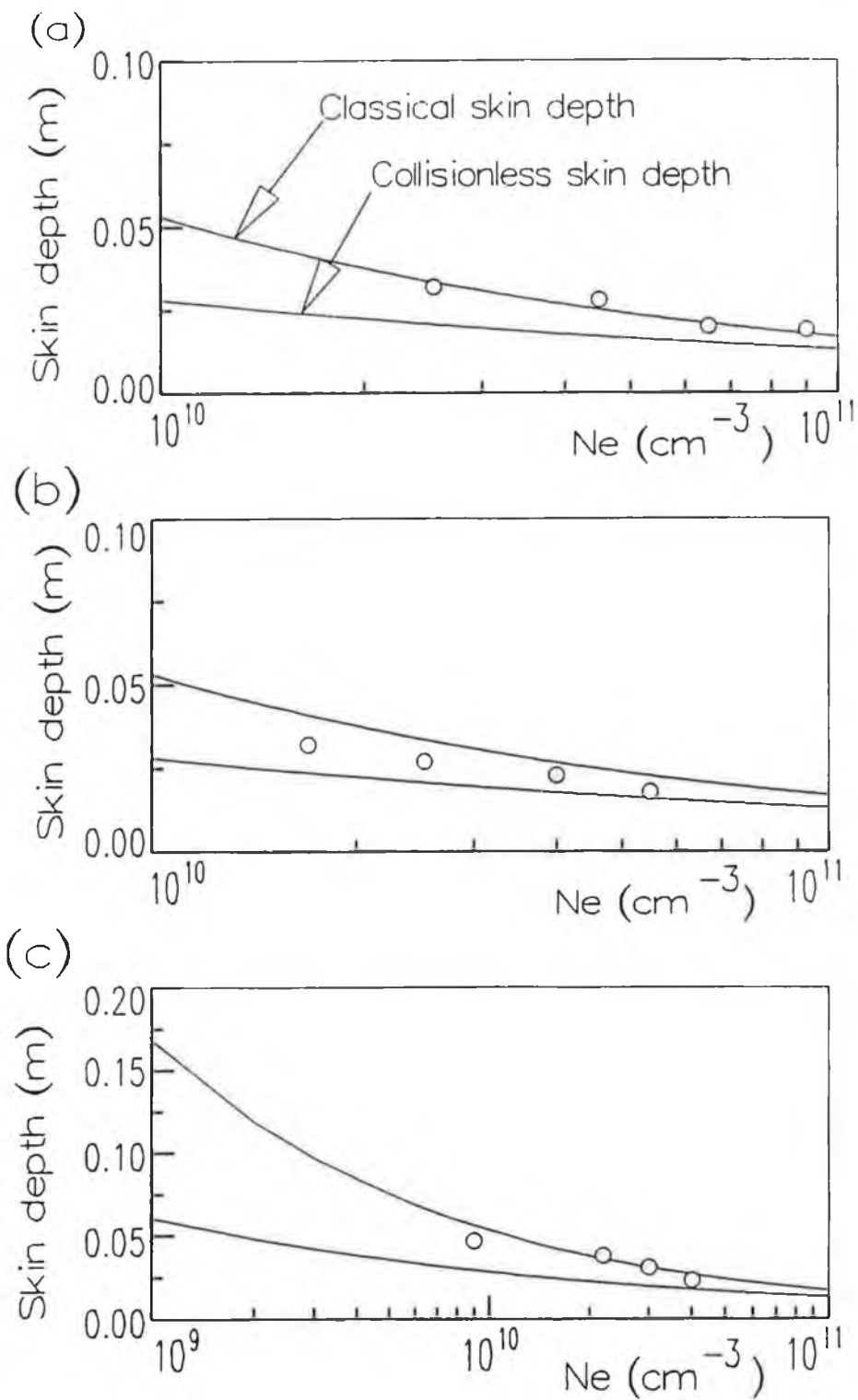


Figure 5.7. Measured skin depths with predicted classical and collisionless values at (a)5, (b)10 and (c)20mTorr.

One can determine the skin depth under particular conditions by finding a least-squares fit of the solution of equation 5.10 to actual probe measurements. One such fitting of the measurements taken in a 20mTorr 75W discharge is shown in figure 5.6 and was carried out using the computer package Mathematica™. This analysis shows the skin depth to be 3.1cm. The skin depth was calculated similarly at powers of 30W, 50W, 75W and 100W at pressures of 20mTorr, 10mTorr and 5mTorr and the results compared with the expected classical and collisionless skin depths in figure 5.7.

#### 5.4 Plasma resistance measurements.

Resistance measurements were taken following the procedure described in section 3.3.2. The pressure was varied from 1mTorr to 100mTorr with the plasma size being kept constant i.e. same plasma density. To keep the discharge at approximately a constant size the light output from the discharge was monitored using a monochromator. The monochromator was set to detect an Argon transition line and by keeping the light output constant the discharge was expected to be consistent. The actual resistance measurements taken are the load resistance (antenna plus plasma) per electron, thus ensuring comparable measurements at all pressures.

For comparison with predictions of the collisionless and Ohmic heating mechanisms, only the trends in the resistance values over a range of pressures were needed. To calculate the expected load resistance values under collisional Ohmic conditions at the range of pressures of interest the following procedure was followed. The power absorbed by the plasma under collisional conditions is given by,

$$P_{plasma} = \frac{1}{2} \int_V \sigma_R |\underline{E}|^2 dV \quad 5.13$$

where  $\sigma_R$  is the real part of the plasma conductivity and  $\underline{E}$  is the induced electric field in the plasma. As described by Faradays law one can relate the induced electric field to the current in the antenna using,

$$\underline{E} = -\frac{\partial A}{\partial t} \quad 5.14$$

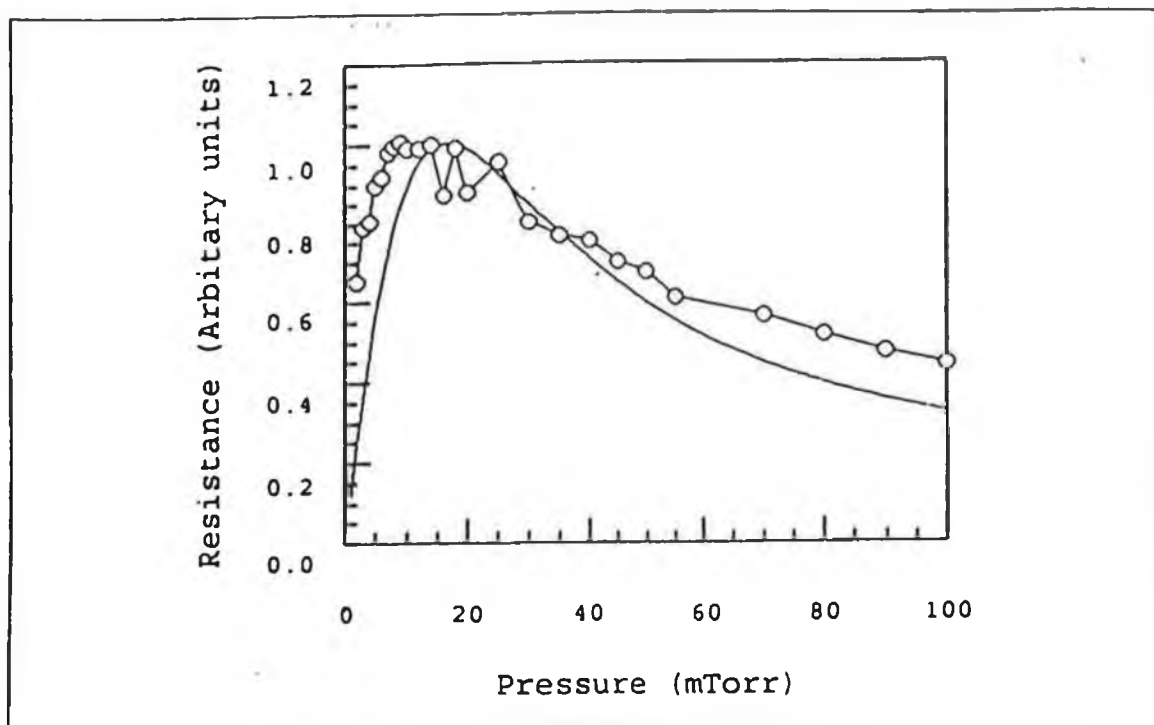


Figure 5.8. Argon resistance values with normalised predicted values from collisional theory.

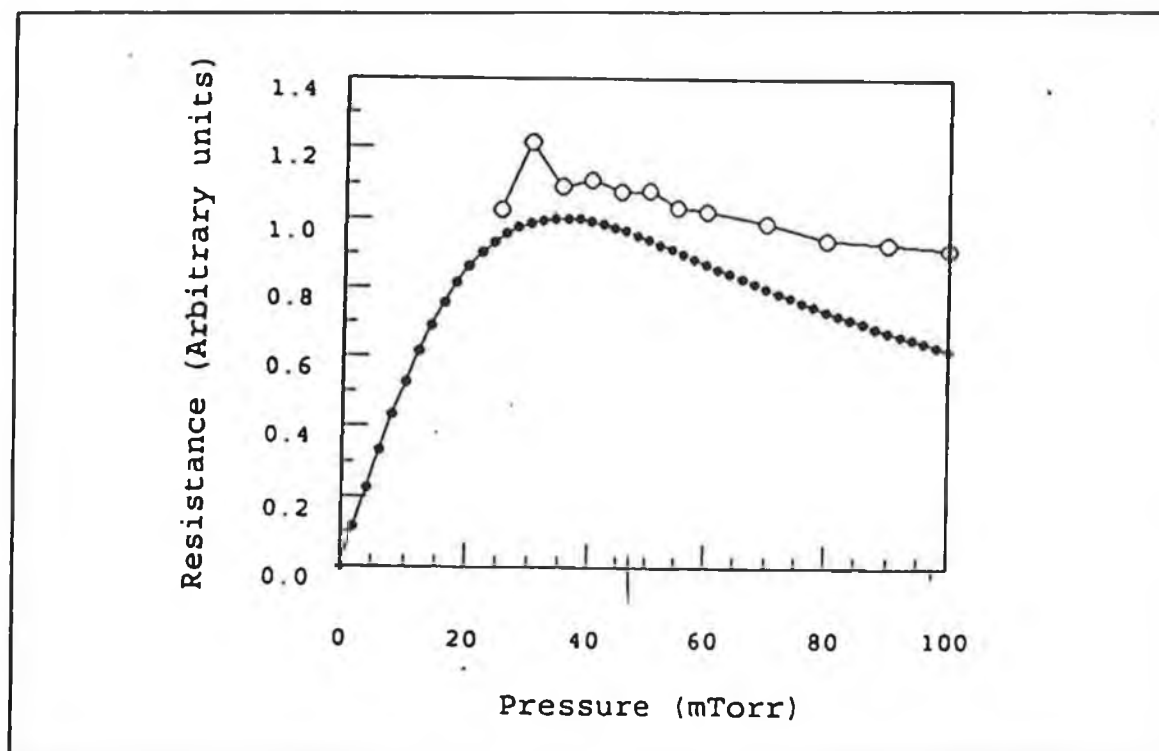


Figure 5.9 . Helium resistance values with normalised predicted values from collisional theory.

where the vector potential  $\underline{A}$  is given by,

$$\underline{A}(t) = \frac{\mu_0 I(t)}{4\pi} \int \frac{dl}{r} \quad 5.15$$

where  $I(t) = I_0 e^{-i\omega t}$  is the antenna current. From equation 5.14 one finds,

$$\underline{E} \propto -\omega I_{ant} \quad 5.16$$

The power absorbed by the load, plasma and antenna, can be written in terms of the current in the antenna,  $I_{ant}$ ,

$$P = \frac{1}{2} R I_{ant}^2 \quad 5.17$$

where  $R$  is the load resistance. Using equation 5.16 one can relate the load resistance in equation 5.17 to the plasma conductivity in equation 5.13,

$$R_{load} \propto \frac{n_e e^2}{m_e} \frac{\nu}{\nu^2 + \omega^2} \quad 5.18$$

By calculating values of the plasma conductivity over a range of collision frequencies one can predict the load resistance change with pressure.

Therefore to estimate the plasma resistance, the collision frequency,  $\nu$ , must be known. This can be calculated knowing the electron collision frequency and electron distribution function [6],

$$\nu = N \langle \sigma v \rangle = N \sqrt{\frac{2}{m_e}} \frac{\int_0^{\infty} \sigma(E) E f(E) dE}{\int_0^{\infty} \sqrt{E} f(E) dE} \quad 5.19$$

where  $N$  is the particle density,  $\sigma(E)$  is the electron collision cross section (a function of electron energy),  $f(E)$  the electron energy distribution function. The values of electron collision cross section are well known and in these measurements a Maxwellian electron energy distribution function is assumed.

Figure 5.8 shows measured resistance values over the pressure range 1mTorr to

100mTorr in Argon along with expected normalised resistance values calculated from equations 5.18 and 5.19. Both curves show similar trends. At low pressures the resistance values are low, then reach a peak at approximately 10mTorr and then decrease gradually as the pressure increases towards 100mTorr. Resistance measurements were also taken in Helium (figure 5.9). The measurements show quite a good agreement with the collisional resistance predictions down to 25mTorr. This is expected since the plasma is operating under collisional conditions at these pressures. It was difficult to maintain the plasma density at a constant level below 25mTorr. Even to strike a Helium plasma at pressures below 25mTorr was not easy, requiring high powers (>250W). A similar situation was found for Hydrogen, chapter 4, which was also difficult to fire at low pressures. This may be due to the low mass of the Helium ion which leads to greater ion losses to the chamber walls and thus larger power losses than with an Argon plasma. The lower electron collision cross section for Helium is also a factor. Power is less likely to be absorbed by the Helium plasma if the electron collision cross section is lower (figure 5.10).

These resistance measurements assume that the only factor affecting the load resistance is changes in the plasma resistance. The antenna is air cooled thereby reducing any increase in its resistance which may occur if the antenna heats up while the plasma is being fired.

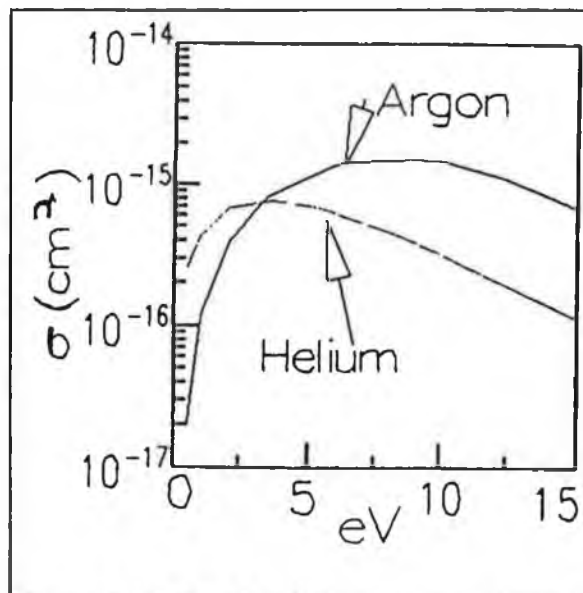


Figure 5.10. Total collision cross sections of Argon and Helium.

### 5.5 Discussion and conclusions.

Three types of measurement were taken in the investigation of low pressure heating in this ICP. Firstly, EEDF measurement in two directions for detection of the electron current driven by the induced electric field in the discharge, secondly,

measurement of the depth of penetration of the antenna electric field into the plasma and finally, resistance measurements. Using the data from these tests the validity of the proposed collisionless heating mechanism could be evaluated.

The collisionless heating mechanism is described in detail in section 2.4.3. An important feature of this collisionless heating process is that it is a warm plasma effect. In order to gain energy electrons must have sufficient velocity to pass within the induced electric field (the skin depth) in a time less than one RF cycle. Therefore one would expect to measure a population of electrons which have gained energy from the antenna electric field outside of the skin depth. Indeed since the plasma is collisionless ( $\omega > \nu$ ) at the pressures of interest (less than 20mTorr), one would expect to measure these electrons across the full width of the plasma.

The EEDF measurements were taken in two directions, facing along the induced electric field and the perpendicular to this field. The induced electric field is such that one would expect that the electrons to be preferentially heated in the azimuthal direction. The measurements taken in the longitudinal direction can therefore be assumed to correspond to the background plasma. The EEDF measurements show an obvious increase in the hot electron population ( $> 20\text{eV}$ ) in the azimuthal direction as opposed to the background plasma. This is not surprising, but what is unexpected is the fact that the energetic electron population drops off rapidly as one moves away from the antenna. In fact at both pressures, 2mTorr and 10mTorr, the heated electron population falls off within one skin depth (3.8cm at 2mTorr and 2.8cm at 10mTorr). Thus there is no evidence from these measurements of the hot electrons leaving the skin depth in less than one RF cycle. From the EEDF measurements it is difficult to determine whether there is a contribution of cooler electrons to the electron current in the plasma in the azimuthal direction.

The skin depth measurements were taken using a magnetic field probe which actually measures the time rate of change of the magnetic field. The results are in general between the classical and collisional skin depth predictions. The skin depth measurements were inconclusive in relation to the investigation of the low pressure heating mechanism.

The load resistance is another attribute of the discharge which is expected to deviate from classical, Ohmic, behaviour at low pressures. As shown in section 2.4.3. the collisionless heating mechanism predicts a finite resistance at low pressures whereas

under Ohmic heating the resistance becomes negligible at low pressures. Here the measurements presented show a plasma resistance in general agreement with the Ohmic resistance. There is an obvious steep fall in the resistance at low pressures which follows the collisional heating trend, however the the resistance is higher at lower pressures than predictions of the collisional model.

From the measurements taken some characteristics of ICP operation at low are clear. One aspect of the ICP operation was the fact that an Argon plasma could be readily sustained at low pressures. When Hydrogen (section 4.5) and Helium plasmas (section 5.4) were operated it was difficult if not impossible to sustain these plasmas at pressures less than 25mTorr in the case of Helium, and 50mTorr in the case of Hydrogen at the powers used. Of the three gasses used, Argon, Helium and Hydrogen the total scattering cross section of Argon is greater than that of the other gasses. Thus electrons are more likely to undergo collisions, transferring energy to other plasma species and thus power the plasma.

The EEDF measurements taken in the azimuthal direction show a drop off in the high energy electron populations within a few centimetres of the antenna which is unexpected behaviour in a collisionless plasma. The 30eV electron population in the 2mTorr plasma, for example, falls to a background level within four centimetres of the antenna, yet this would concur with a collision frequency over seven times the RF cycle. Clearly this is cannot be the case as at 2mTorr the collision frequency is less than on fifth of the RF driving frequency. One possible explanation for the rapid fall off in the high energy electron population moving away from the antenna is that the electrons follow paths around the antenna close to the plasma antenna interface. In this way electrons will effectively have a much greater mean free path before hitting the chamber wall. The electrons, if they are confined close to the antenna for a sufficient period, can undergo collisions. The relatively large collision cross section of Argon, particularly at high electron energies would further aid this process and the mean free path of the electron will be lower than for Helium or Hydrogen. After the electrons collide the lose their energy can move out of the azimuthal path around the antenna.

The above argument stresses the importance of collisions even when the ICP is operated at low pressures. Even though the electron collision frequency may be low, the electrons are confined within approximately one skin depth of the antenna until they

undergo a collision. The experimental evidence presented in this chapter does not clearly support the collisionless heating mechanism.

## References.

- [1] M. M. Turner. Phys. Rev. Lett. **71** (1993) 1844
- [2] V. A. Godyak, R. B. Piejak and B. M. Alexandrovich Plasma Sources Sci. Technol. **3** (1994) 169
- [3] P. Lorrain, D. P. Corson and F. Lorrain. "*Electromagnetic fields and waves*". (Freeman, 1988)
- [4] G. G. Lister and M. Cox. Plas. Sources Sci. Technol. **1** (1992) 67
- [5] J. Hopwood, C. R. Guernieri, S. J. Whitehair and J. J. Cuomo. J. Vac. Sci. Technol. A. **11** (1993) 152
- [6] B. E. Cherrington, "*Gaseous Electronics and Gas lasers*". (Pergamon Press)

## Chapter 6. Measurements of electron kinetics in an ICP.

### 6.1 Introduction.

This chapter focuses on measurements taken in the plasma pertaining to the kinetic models described in section 2.6. The local and non-local models each predict certain behaviour of the EEDF in the plasma. The local model anticipates an EEDF which mirrors the applied electric field, it is hottest where the electric field is a maximum [1,2]. The non-local model predicts an EEDF of total energy which is valid across the whole discharge [3,4]. The kinetic energies of individual electrons though, will change across the discharge as a result of the space-charge potential. The kinetic energy lost by the electrons traversing the space-charge potential is coupled by an increase in their potential energy, their total energy remains constant. Here EEDF's of total energy are presented as at the pressures of interest ( $< 10\text{mTorr}$ ) it is expected that the ICP will display non-local kinetics.

The ICP system, a central antenna in a cylindrical discharge chamber, results in anisotropies in the plasma due to the inhomogeneity of the applied RF field. There is a current of electrons close to the antenna in the azimuthal direction following the applied electric field. The disc probe described in section 5.1 allows one to look in a single direction and at any position between the plasma-antenna interface and the chamber wall. Pointed in the azimuthal direction the probe allows measurements to be taken in the current around the antenna, while measurements of the background plasma can be taken when the probe faces along the longitudinal direction. Radial EEDF measurements of total energy and space-charge potentials are taken in the two directions at various pressures and compared with the predictions of the kinetic models.

The EEDF's of total energy were extracted from EEDF measurements (of kinetic energy) by superimposing the measurements such that they show good agreement over most energies. It was found that the resulting EEDF's of total energies differed at the low energy end corresponding to the influence of the space charge potential on the low energy electrons. The energies at which the EEDF's of total energy go to zero are taken to coincide with the space charge potential energy at the position where the EEDF was taken.

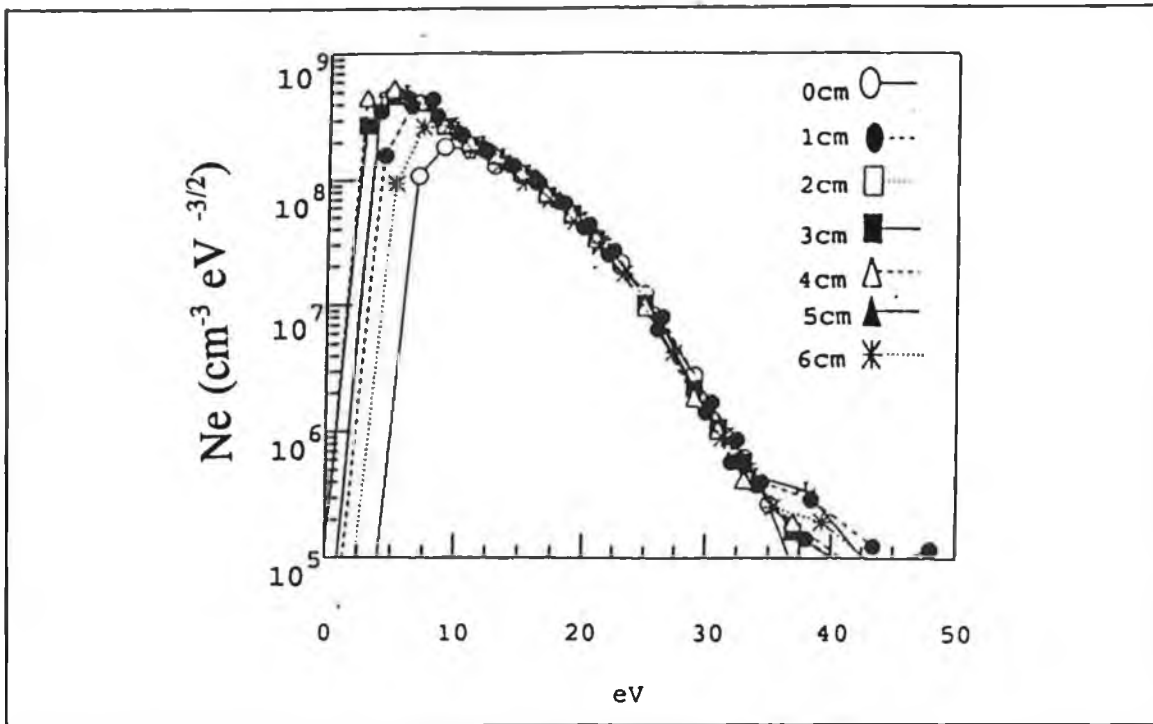


Figure 6.1. 3mTorr 100W EEDF measurements of total energy in the longitudinal direction.

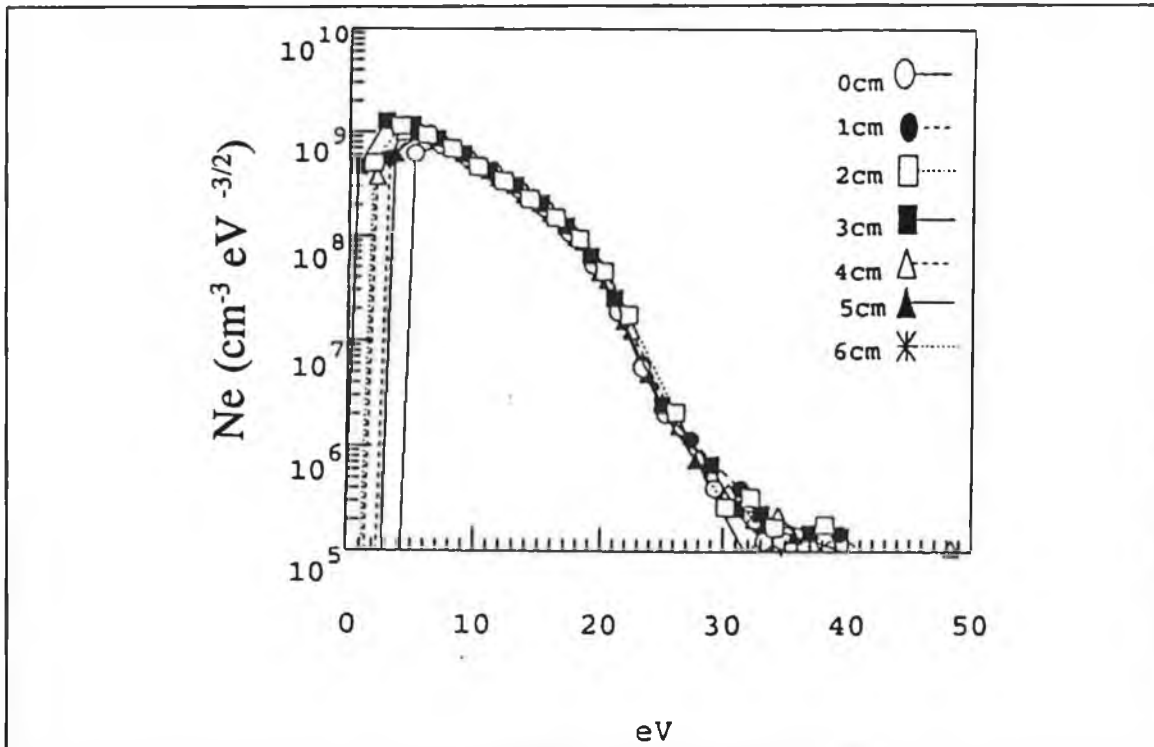


Figure 6.2. 10mTorr 100W EEDF measurements of total energy taken in the longitudinal direction.

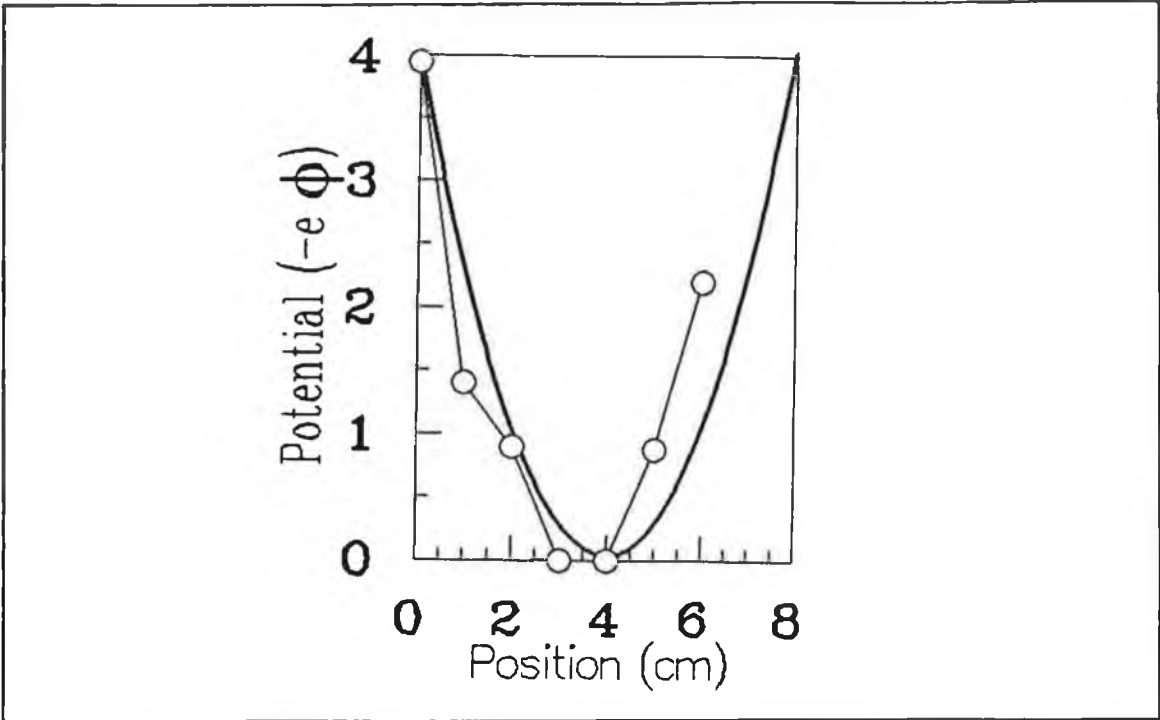


Figure 6.3. Measured and expected space-charge potential energy profiles,  $-\phi(z)$ , at 3mTorr in the longitudinal direction.

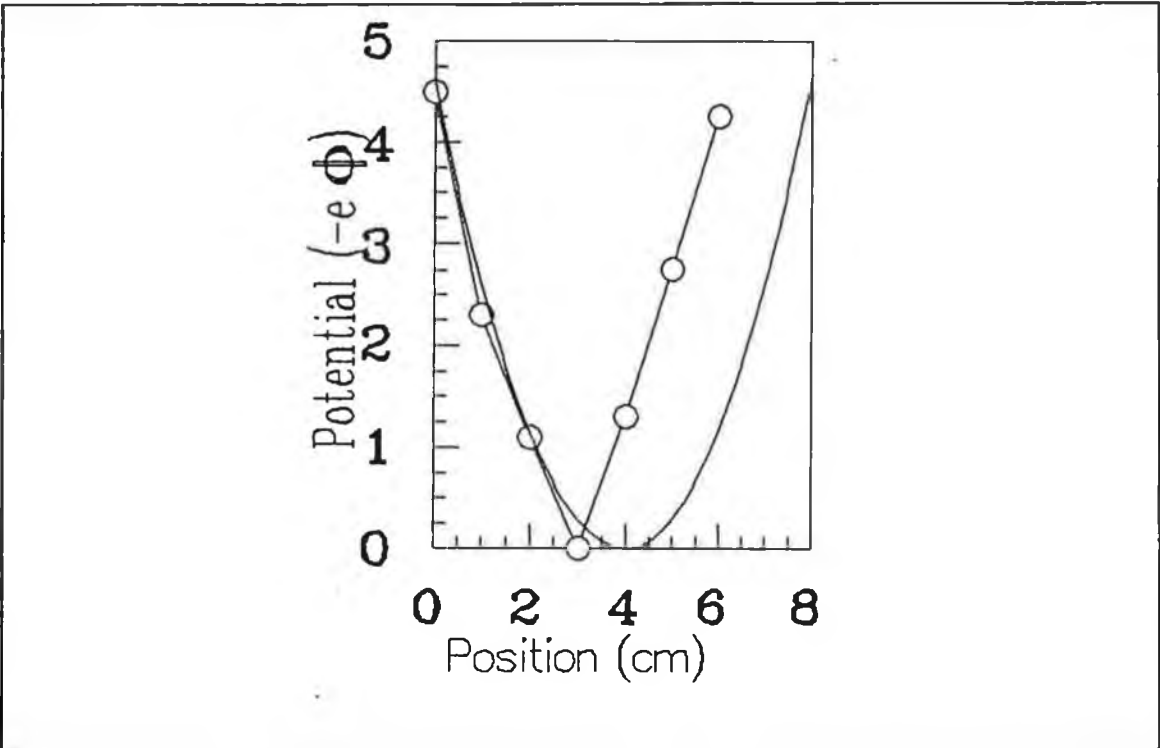


Figure 6.4. Measured and expected space-charge potential energy profiles,  $-\phi(z)$ , at 10mTorr in the longitudinal direction.

## 6.2 Results of measurements taken in the background plasma.

### 6.2.1 EEDF of total energy measurements in the background plasma.

Radial EEDF measurements of total energy were determined at 3mTorr and 10mTorr in a 100W Argon plasma (figure 6.1 and 6.2). The disc probe was positioned so as to face parallel to the antenna axis and sample only the background plasma. The probe was moved from the glass wall surrounding the antenna to 1.5cm from the chamber wall in 1cm steps.

Above 10eV the EEDF's show good agreement at all positions at both pressures. This means that for electrons with energies above 10eV the plasma is homogeneous. The electron energy gains and losses are the same across the width of the plasma. This region of the EEDF, above 10eV does not show any evidence of electron kinetics predicted by the local model. It is however consistent with the non-local model, where the energy relaxation length of electrons is greater than the plasma width. Above 30eV some distortion seems to appear on the EEDF's, but at the low densities being measured ( $.5 \times 10^5 \text{cm}^3$ ), this can be attributed to noise in the measuring circuitry.

The low energy region of the EEDF's ( $< 10\text{eV}$ ) at both pressures show interesting features. At the centre of the discharge (3-4cm from the glass wall surrounding the antenna), the EEDF's reveal a population of electrons at all energies. Moving away from this area there is a low energy cut-off below which electrons cannot be detected. As one moves to the periphery of the plasma the effect becomes more pronounced.

This effect is similar to that predicted by the non-local model. It results from the influence of the space-charge electric field on the low energy electrons. Electrons with total energies insufficient to overcome the space-charge potential barrier are trapped. When they approach a position in the plasma where the space-charge potential energy,  $-\phi(z)$ , is equivalent to their total energy, they lose all their kinetic energy and are reflected back towards the centre of the discharge where the space-charge potential energy is at a minimum. These low energy electrons will not be detected at the edge of the discharge, resulting in the low energy cut-off seen in the EEDF's.

At the centre of the discharge, where the electron potential energy due to the space-charge is zero, electrons of all energies are detected. The EEDF measured here includes electrons of all energies; the kinetic energy is a maximum and the potential

energy is zero.

### 6.2.2 Space-charge potential in longitudinal direction.

The space-charge potential profile was calculated by superimposing EEDF measurements of total energy on the EEDF taken at the centre of the discharge, and calculating the low energy cut-off at each position. The EEDF's were fitted so as to coincide in the energy region above 10eV. The low energy cut-off energy is equivalent to the space-charge potential at each position.

The expected form of the space-charge electric field may be determined from a consideration of the electron current density in the plasma. The electron current density is a measure of the number of electrons crossing a unit area in a conductor in unit time. In a plasma this is a function of electron production rate, or ionisation rate, at a given position in the plasma (the electrons produced at a position  $z$  in the plasma will contribute to a current at this point in the discharge). Since the ionisation rate is dependent on the energy of the electrons involved in the ionisation collisions, most of the electrons will be produced at the centre of the discharge where the space-charge electric field is a maximum. Therefore one can write,

$$J = n_e \langle \sigma u \rangle_i N 2 \pi z \quad 6.1$$

where  $u$  is the electron velocity,  $\langle \sigma u \rangle_i N$  is the ionisation collision frequency and  $z$  is the position in the plasma ( $z=0$  corresponds with the antenna-plasma interface and  $z=7.5\text{cm}$  corresponds with the chamber wall, the  $2\pi$  factor is included to account for the cylindrical geometry of the system).

One may also determine the current density in terms of the average electron velocity,  $\bar{u}$ ,

$$J = \bar{u} n_e e \quad 6.2$$

where the average electron velocity is related to the electron energy,  $kT_e$ , by,

$$\bar{u} = \sqrt{\frac{8 k T_e}{\pi m_e}} \quad 6.3$$

The electron energy may be related to the electric field when one considers the

energy balance in a discharge. Assuming a weakly ionised plasma where electron neutral collisions dominate and a dc space-charge field, the energy gained by an electron from the space-charge electric field per unit time is given by,

$$\epsilon_{gain} = \sigma E^2 = \frac{n_e e^2}{m \nu_m} E^2 \quad 6.4$$

where  $\nu_m$  is the collision frequency for momentum transfer collisions. The energy loss per unit time due to electron neutral collisions is given by,

$$\epsilon_{loss} = n_e \kappa \nu_m \frac{3k(T_e - T)}{2} \quad 6.5$$

where  $\kappa$  is the energy transfer coefficient for elastic collisions ( $2m_e/M$ ), and  $3k(T_e - T)/2$  is the average electron energy above the background neutral particle energy, described by a temperature  $T$ . Considering a steady plasma where electron energy losses and gains are equal, one finds,

$$n_e \kappa \nu_m \frac{3k(T_e - T)}{2} = \frac{n_e e^2}{m \nu_m} E^2 \quad 6.6$$

From this one can relate the electron temperature  $T_e$  to the electric field  $E$  by (assuming  $T_e \gg T$ ),

$$T_e = \frac{2e^2 E^2}{3km\kappa\nu_m^2} \quad 6.7$$

The electron neutral collision frequency is obviously related to the neutral density  $N$ , and therefore one may rewrite equation 6.7 as,

$$T_e = \frac{A E^2}{k N^2} \quad 6.8$$

where  $A$  takes account of the parameters in equation 6.7, and the relationship between electron neutral collision frequency and neutral density. Considering equations 6.2 and 6.8 one may rewrite the electron current as,

$$J = A n_e e k \frac{E}{N} \quad 6.9$$

Comparing equations 6.1 and 6.9 one finds,

$$A n_e e k \frac{E}{N} = n_e \langle \sigma v \rangle_i N^2 \pi z \quad 6.10$$

Thus one finds the space-charge electric field is dependent on z,

$$E = \frac{A \langle \sigma v \rangle N^2 \pi N^2}{e k} z \quad 6.11$$

The space-charge potential may be calculated at any position in the plasma by integrating equation 6.11 around a closed loop at a fixed distance, z, from the antenna,

$$\phi = \oint \frac{E \cdot dl}{c} \quad 6.12$$

Carrying out this integration on the electric field given in equation 6.12 one finds that the space-charge potential has a parabolic dependence with distance between the antenna-plasma interface and the chamber wall,

$$\phi = \alpha z^2 \quad 6.13$$

In the analysis of the measured space-charge potential profile, a parabolic fit is made to the data which is zero at the antenna-plasma interface and chamber wall, and a maximum at the centre of the discharge. The graphs presented, figures 6.3, 6.4, 6.7, 6.8, show the space-charge potential energy profile for electrons in the discharge i.e an inverted space-charge potential profile  $PE = -\phi(z)$ . The potential energy profiles show a zero potential energy at the centre of the discharge rising to a maximum at the discharge boundaries. This reflects the effect of the space-charge electric field retarding the migration of electrons from the plasma.

One may note however that there is a discrepancy in the space-charge potentials measured and those expected from theory. A possible reason for this difference may be a result of the geometry of the system. The cylindrical nature of the system means that the chamber wall has a greater surface area, thus electrons are more likely to be lost

there than at the glass wall. A second reason results from the electrical properties of the walls; one is a conductor the other is an insulator. At the metallic chamber wall the total electron and ion fluxes must be equal over the entire wall surface area, whereas at the glass wall they must be equal locally [7].

The observations made about electron kinetics in the background plasma are entirely reasonable at these pressures as the plasma is collisionless. One would expect the local-model to describe the plasma accurately as the mean free path for electron energy relaxation is greater than the plasma size at this pressure.

### **6.3 Results of measurements taken in the current (azimuthal) direction.**

#### **6.3.1 EEDF measurements of total energy in the azimuthal direction.**

EEDF measurements of total energy taken in the azimuthal direction show unusual characteristics for the low pressures at which the measurements were taken (figures 6.5 and 6.6). Unlike the background plasma measurements the EEDF's here do not all coincide above 10eV across the plasma. Instead above about 18eV the EEDF's begin to show differences. Near the glass wall surrounding the antenna there is a much greater population of high energy electrons at both pressures. Moving away the population of these high energy electrons drops off. It is only at a few centimetres from the glass wall that one can see any similarity in the shape of the EEDF's. This seems to be evidence of the electron kinetics predicted by the local model, at least for electrons with energies above the threshold for inelastic collisions, 14eV in Argon.

The reason for the difference between these EEDF's and those taken in the background plasma is that the induced electric field points in the azimuthal direction and electrons gain energy from the field in this direction only. The heating effect of the applied electric field seems to fall off with the skin depth, there is not much evidence of electron heating beyond 2-3cm (chapter 5).

The behaviour of the electrons with energies above 18eV is entirely consistent with the local model where the EEDF follows the strength of the local electric field; the EEDF has more hot electrons where the applied field is strongest. This is unusual behaviour since at these pressures one would have expected hot electrons at the antenna to be detected across the entire plasma as collisions are rare.

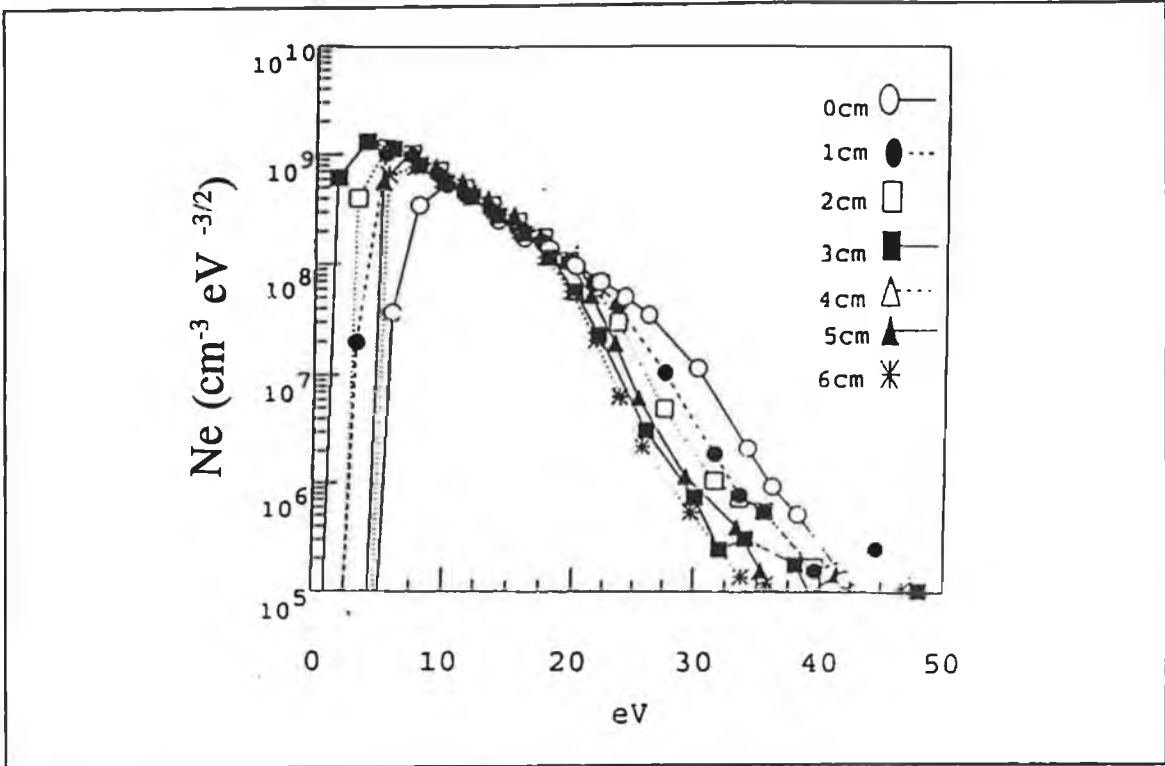


Figure 6.5. 3mTorr 100W EEDF measurements of total energy taken in the azimuthal direction.

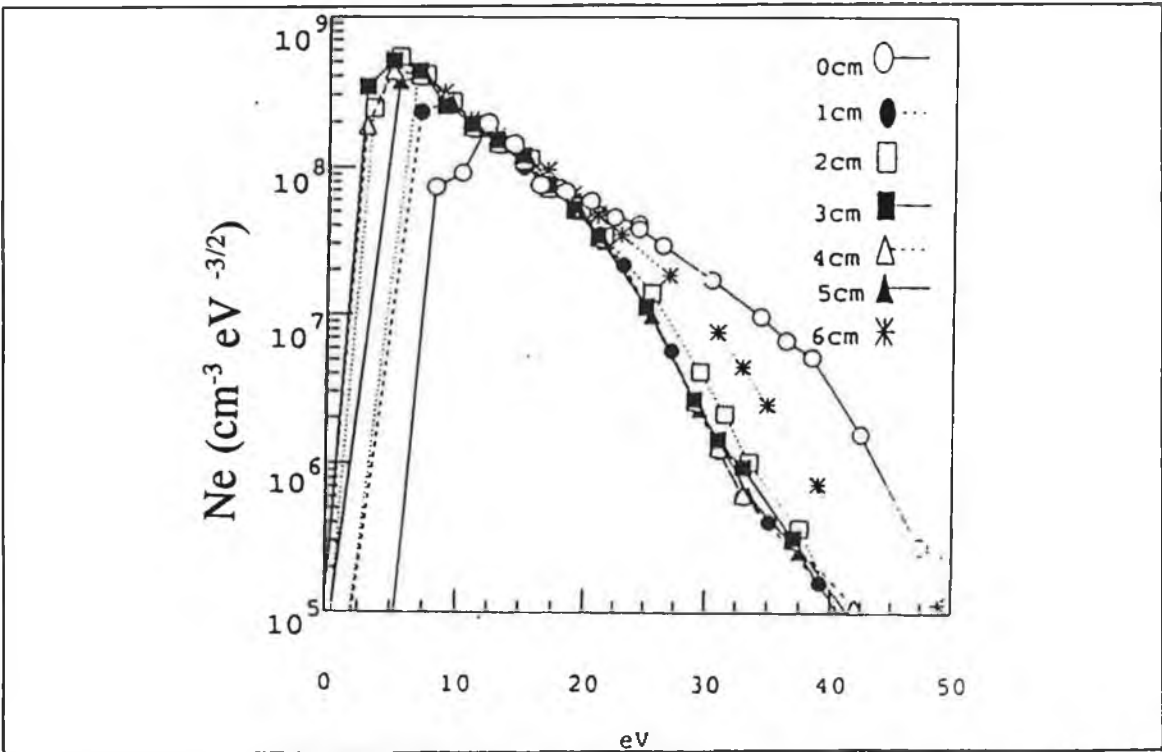


Figure 6.6. 10mTorr 100W EEDF measurements of total energy taken in the azimuthal direction.

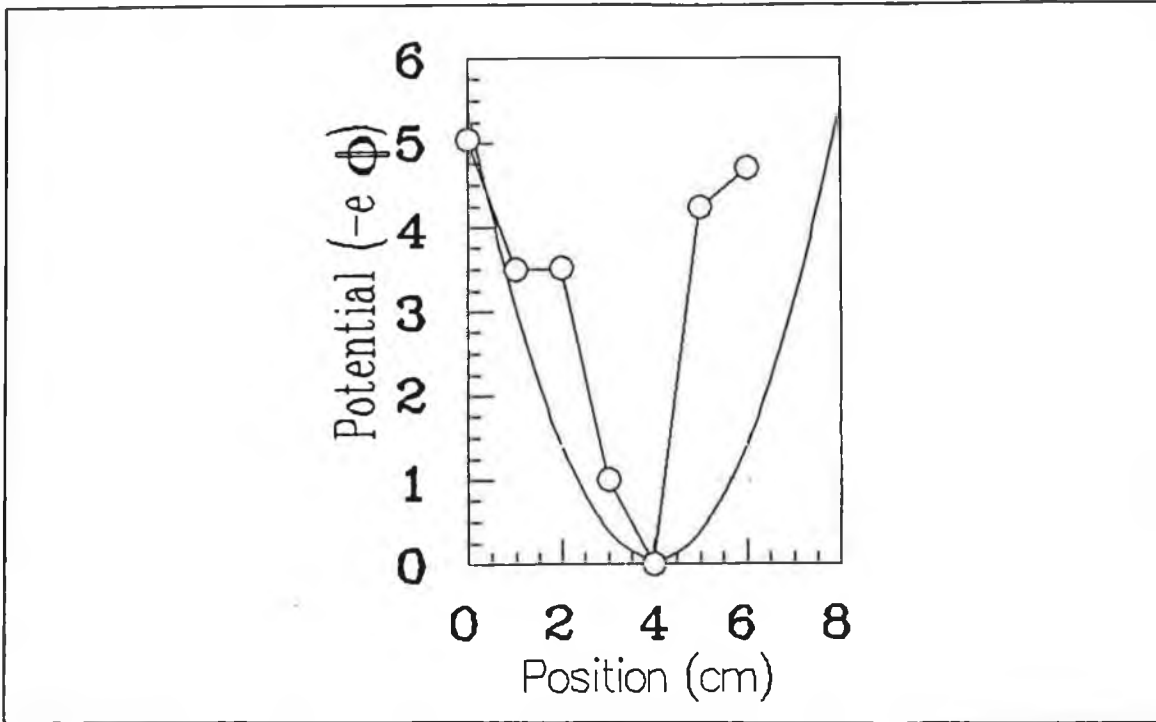


Figure 6.7. Measured and expected space-charge potential energy profiles,  $-\phi(z)$ , at 3mTorr and 100W in the azimuthal direction.

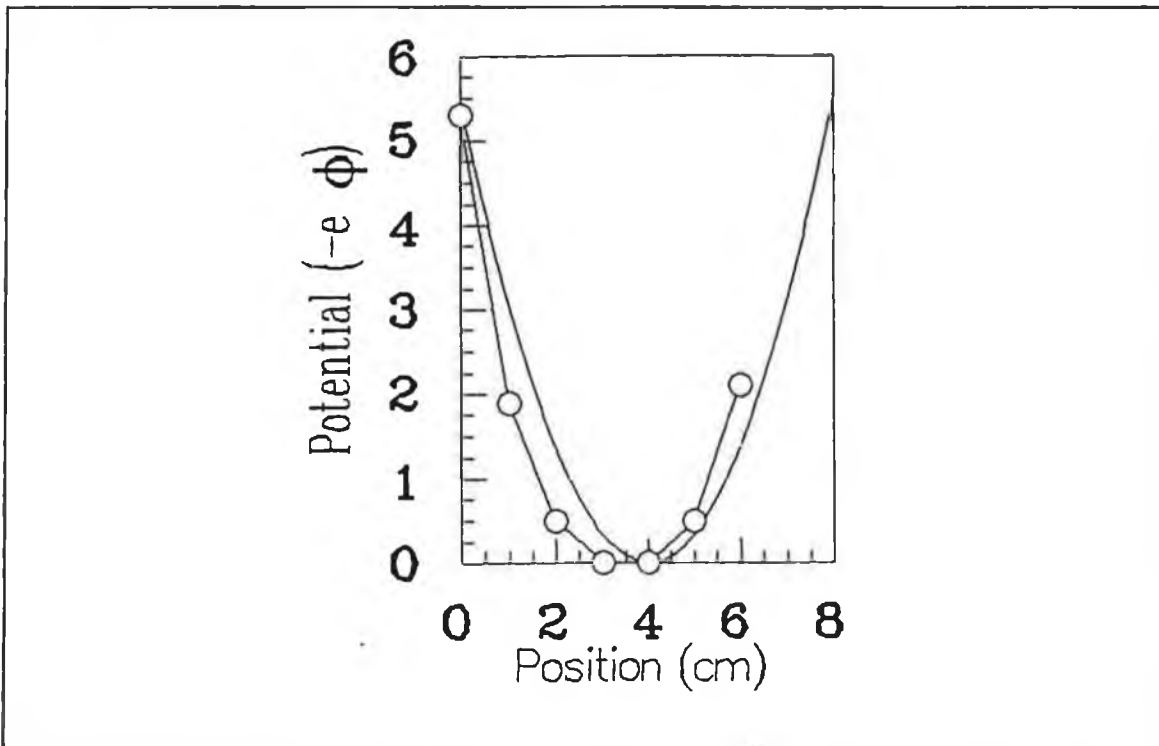


Figure 6.8. Measured and expected space-charge potential energy profiles,  $-\phi(z)$ , at 10mTorr and 100W in the azimuthal direction.

The low energy, ( $< 10\text{eV}$ ), end of the EEDF's show similar traits to EEDF's taken in the background plasma. At low energies the azimuthal measurements also show characteristics of non-local electron kinetics. They show the low energy cut-off of the low energy electrons due to the space-charge potential. The EEDF of total energy at the centre of the discharge shows populations of electrons at all energies since the potential energy of electrons is zero.

### **6.3.2 Space-charge potential measurements in azimuthal direction.**

The space-charge potential energy profiles for the electrons generally show the expected parabolic shape expected (figures 6.7 and 6.8). Compared with the background plasma measurements though, there are some slight differences. In the 3mTorr case the space potential seems to be greater in the azimuthal direction near the glass wall. This may be due to experimental error since the space-charge potential,  $\phi$ , is expected to be independent of direction.

### **6.4 Discussion of the local and non-local characteristics observed in the plasma in the azimuthal direction.**

The EEDF's measured in the azimuthal direction display local and non-local electron kinetics simultaneously. Similar behaviour of the EEDF was reported by Godyak and Piejak [8] in an Argon capacitively coupled plasma but at 300mTorr. They noted that low energy electrons displayed non-local electron kinetics while the hotter electrons ( $>$  the threshold energy for inelastic collisions, 14eV in Argon) demonstrated local electron kinetic characteristics.

These characteristics were explained in terms of the different behaviour of the high and low energy electron groups characterised by temperatures  $T_{\text{high}}$  and  $T_{\text{low}}$  respectively. The timescale for electrons to lose most of their energy and attain the temperature of the background neutral species is dependent on the electron energy and available energy loss mechanisms. For the low energy electrons, with energies less than the threshold energy required for inelastic collisions, the electrons can only lose energy through inefficient electron neutral collisions. The energy lost by an electron per second due to elastic, electron neutral collisions, is given by,

$$\Delta \epsilon = \frac{2 m_e}{M_n} \cdot v_{e-n} \cdot \epsilon_{initial} \quad 6.14$$

where the first term on the right hand side is the electron energy transfer coefficient  $\kappa$  (which is much less than one) and  $\epsilon_{initial} = 3kT_{el\text{ow}}/2$ . Thus the rate of electron energy loss per second for the low energy electrons,  $T_{el\text{ow}}$ , in a plasma of neutral background temperature  $T$  which is given by,

$$\frac{d\epsilon}{dt} = -n_e \kappa v_{e-n} \frac{3k(T_{el\text{ow}} - T)}{2} \quad 6.15$$

A solution to this equation is,

$$T_{el\text{ow}} = T + (T_{el\text{ow}} - T)_o \exp[-\kappa v_{e-n} t] \quad 6.16$$

where  $(T_{el\text{ow}} - T)_o$  is the initial difference between the electron and neutral gas temperature. The time it takes for an electron to attain the same temperature as the background neutral gas due to energy losses in elastic collisions is denoted by the energy relaxation time constant for the low energy electrons,  $\tau_{el\text{ow}}$ ,

$$\tau_{el\text{ow}} = \frac{1}{\kappa v_{e-n}} \quad 6.17$$

The high energy electrons,  $T_{ch\text{igh}}$ , have the possibility of undergoing inelastic collisions where most of their energy may be lost in a single collision. Thus the energy relaxation time constant is given by,

$$\tau_{ch\text{igh}} = \frac{1}{v_{inelastic}} \quad 6.18$$

where  $v_{inelastic}$  is the collision frequency due to all the inelastic processes available to the electrons. This time constant is much shorter than the low energy electron time constant.

Therefore in the actual plasma one can measure a rapid fall off in the populations of the high energy electrons across the discharge width since the time required for the high energy electron to lose most of its energy is less than the time required for the electron to traverse the plasma (this requires a sufficient gas pressure so that the inelastic collision frequency is high enough). In the case of the low energy electrons however, the

time required for the electrons to lose most of their energy is greater than the time required to traverse the plasma width.

This can explain the discharge kinetics of a plasma at 300mTorr, but here at 3mTorr and 10mTorr this argument cannot fully explain the phenomenon observed. As discussed in chapter 5, the azimuthal electric field heating the plasma may greatly influence the situation. The fact that the fast electron population falls off to the background level in approximately one skin depth suggests this may be the case.

As suggested in chapter 5, the electrons within the skin depth are heated by the RF field in the azimuthal direction and may actually be confined in a path around the antenna by the applied field itself. By confining the electrons in paths around the antenna, the plasma width seen by these electrons will be much greater than the actual plasma width. Therefore the hot electrons can undergo a collision before leaving the skin depth. A 30eV electron for example will travel almost 30cm in one RF cycle which is greater than its relaxation length at this energy. Once the hot electrons collide they leave the hot tail of the EEDF and join the bulk plasma.

## **6.5 Conclusions.**

Measurements of EEDF's were taken in two directions in a 100W plasma. Firstly in the longitudinal direction, parallel to the antenna axis. Measurements taken were consistent with non-local electron kinetics. The EEDF at any position in the plasma can be determined knowing the EEDF of total energy, found at the centre of the discharge, and the space-charge potential. At pressures of 3mTorr and 10mTorr these results are not unexpected.

The EEDF measurements taken in the azimuthal direction, the same direction as the induced electric field, show interesting results. Both local and non-local kinetics were observed. To the authors' knowledge this effect has not been observed in ICP's elsewhere although it was reported in a capacitive discharge, but at 300mTorr. Some possible explanations were put forward; the short mean free path for energy relaxation of hot electrons in Argon [8], and the possibility that electrons are trapped within the skin depth before undergoing collisions.

It is hoped that other workers will look in this area to see if the phenomenon is a characteristic of all ICP's operating at low pressures. Modelling of the discharge would

also help to determine the reason for this local/non-local behaviour of the plasma.

## References.

- [1] U. Kortshagen. J. Phys. D: Appl. Phys. 26 (1993) 1691.
- [2] A.B. Sa, C. M. Ferreira, S. Pasquires, C. Boise-leporte, P. Leprince and J. Marec. J. Appl. Phys. 70 (1991) 1691
- [3] V. I. Kolobov, D. F. Beale, L. J. Mahoney and A. E. Wendt. Appl. Phys. Lett. 65 (1994) 537.
- [4] U. Kortshagen and L. D. Tsendin. Appl. Phys. Lett. 65 (1994) 1355.
- [5] I. B. Bernstein and T. Holstein. Phys. Rev. 94 (1954) 1475.
- [6] S. C. Brown. *"Introduction to electrical discharges in gases"*. (Wiley. New York, London, Sydney. 1965)
- [7] U. Kortshagen, I. Pukropski and M. Zethoff. J. Appl. Phys. 76 (1994) 2048
- [8] V. A. Godyak and R. B. Piejak. Appl. Phys. Lett. 63 (1993) 3137.

## **Chapter 7. Conclusions and suggestions for further work.**

### **7.1 Summary of work and conclusions.**

A rigorous study of a low pressure ICP has been carried out. The work involved a characterisation of the discharge using Langmuir and magnetic field probes as well as an analysis of the electrical properties of the system. The experiment itself was designed and constructed in the laboratory and employed an 11 turn antenna placed along the central axis of the discharge chamber. The design allowed easy access for probes to the most intense area of the discharge near the antenna coil (section 4.2).

The initial intention of the project was to characterise the ICP and also investigate low pressure heating. The first findings were that the plasma produced was not purely inductive, especially at low powers and pressures. The switch between a low intensity capacitively dominated discharge, powered by the electrostatic field between neighbouring antenna loops, to a more intense inductively dominated discharge was noted (section 4.3).

The basic plasma parameters of electron and ion density, electron temperature, EEDF's, plasma and floating potentials were all measured as a function of power, pressure and position within an Argon discharge (chapter 4). The ICP was found to produce an efficient plasma with expected plasma potential trends (it is expected that the plasma potential decreases with increasing plasma density as the discharge becomes more efficient).

However when a Hydrogen discharge was attempted, it was found to be difficult to sustain at the pressures at which an Argon plasma was readily attainable ( $< 50\text{mTorr}$ , section 4.5). Magnets were placed around the chamber forming a multicusp magnetic field which acted to increase the electron confinement time and thus the probability of electron collisions. The efficiency of the discharge was therefore increased and a plasma could be sustained.

The investigation of low pressure ICP heating produced interesting and unexpected results, chapter 5. The collisionless heating mechanism described in section 2.4.3 directed the experiment to measure directional EEDF's, skin depths and plasma resistance. The directional Langmuir probe, shown in figure 5.1, was found to be a very useful diagnostic in this study as it allowed the plasma conditions in the direction of the

induced electric field and also the background plasma to be monitored independently. Instead of supporting the proposed heating mechanism, the results are inconclusive. From the experimental evidence it seems that electrons within the skin depth can gain energy from the induced electric field, but remain close to the antenna until they undergo a collision. The powered electrons are effectively confined in orbits around the antenna and therefore have increased mean free paths as they do not collide with the chamber walls. These suggestions are supported particularly by the directional EEDF measurements which show a rapid decline in powered electron populations in the azimuthal direction as one moves away from the antenna.

A survey of the electron kinetics within the plasma also showed interesting and unexpected results chapter 6. The directional probe proved to be ideal for this study. Results of measurements taken in the background plasma showed characteristics of non-local electron kinetics, behaviour entirely consistent with a low pressure ICP. Measurements taken in the azimuthal direction, following the induced RF electric field within the discharge showed characteristics of both local and non-local electron kinetics. The local effects manifested themselves as a drop in high energy electron population moving away from the power source. This is behaviour associated with a collisionally dominated discharge where electrons have short mean free paths.

### **7.1 Suggestions for future work.**

In the course of the project many questions about the behaviour of a low pressure ICP were answered, but in the end the experiments themselves pose many more questions. This in itself shows the success of the project as behaviour which was not expected was observed.

The investigation of the low pressure heating mechanism did not seem to support a collisionless mechanism, but as yet a definitive explanation has yet to be found. In order to arrive at a suitable explanation for the discharge behaviour encountered the experiments carried out here need to be carried out on other ICP systems. The results found here may only apply to this particular discharge geometry, a central antenna, for example. Computer modelling of the system would also help in the investigation of this aspect of ICP operation.

Electron kinetic measurements show more scope for further work. Again the simultaneous existence of both local and non-local electron kinetics requires further

study. The effects noted may be a characteristic of ICP's in general or just a consequence of the particular system being used here.

The use of a directional Langmuir probe proved to be invaluable in this work and it is hoped that workers in this area would employ this diagnostic technique to investigate the phenomena encountered here.